Cell-mediated Contraction & Induced Regeneration Of the Injured Peripheral Nerve

by

Eric C. Soller

S.M., Mechanical Engineering,
Massachusetts Institute of Technology, 2005

S.B., Mechanical Engineering,
Rose-Hulman Institute of Technology, 2003

Submitted to the Department of Mechanical Engineering in Partial Fulfillment of the Requirements for the Degree of

Doctor of Philosophy in Mechanical Engineering

at the

MASSACHUSETTS INSTITUTE OF TECHNOLOGY

June 2011

Signature of Author .....
Department of Mechanical Engineering
May 20, 2011

Certified by .....
Ioannis V. Yannas
Professor of Mechanical Engineering, Polymer Science, & Biological Engineering
Thesis Supervisor

Accepted by.....
Douglas P. Hardt
Professor of Mechanical Engineering
Chairman, Department Committee on Graduate Students

Cell-mediated Contraction & Induced Regeneration Of the Injured Peripheral Nerve

by

Eric C. Soller

Submitted to the Department of Mechanical Engineering on May 20, 2011
in Partial Fulfillment of the Requirements for the Degree of
Doctor of Philosophy in Mechanical Engineering

ABSTRACT

Cell-mediated mechanical forces drive closure of severe wounds in adult mammalian organs, including the sciatic nerve following neurotmesis. Without experimental intervention the defect closes rapidly via contraction of transected nerve stumps by a thick, cohesive capsule of myofibroblasts (MFB) and subsequent collagen synthesis (scar), leading to a painful neuroma. Despite considerable progress in regenerating injured peripheral nerves with biomaterials, adequate recovery is generally limited to inter-stump gap lengths of about 20-30 mm in humans. Observations of successful induced regeneration in adults coincide with reduced MFB formation, yet the direct effect of the MFB capsule on nerve regeneration is unknown. According to the pressure cuff theory, a transected peripheral nerve could heal by regeneration, rather than MFB-mediated contraction and scar formation, provided the MFB capsule size (and corresponding cellular forces applied) are reduced.

A well-characterized library of type I collagen tubular scaffolds with identical chemical composition and pore size, and varying degradation rate was used to evaluate the ability of a porous scaffold to block MFB contraction after injury in a demanding model of peripheral nerve regeneration in the adult rat. At 9 weeks post-neurotmesis, the MFB capsule thickness, δ, around the regenerating nerve was measured and the correlation with several quantitative measures of the quality of nerve regeneration, Q, was evaluated.

A negative, statistically significant association was observed between the contractile capsule thickness, δ, and the quality of axonal regeneration, Q, (consisting of measures of regenerate area, the number of myelinated fibers, and the number of large-diameter fibers) at 9 weeks post-sciatic neurotmesis. This constitutes the strongest evidence to date that capsules of contractile MFB antagonize induced regeneration of severely injured peripheral nerves in the adult mammal. Collagen devices of intermediate degradation rate minimized δ and maximized Q. Reduced contractile cell presence and disrupted organization inside moderately cross-linked scaffolds that consequently degraded at an intermediate rate, but not in highly cross-linked scaffolds that degraded at very low rate, support the hypothesis of cell escape from the wound (making use of scaffold permeability) as a mechanism for scaffold regenerative activity.

Thesis Supervisor: Ioannis V. Yannas
Title: Professor of Mechanical Engineering, Polymer Science, and Biological Engineering

This page was left blank intentionally.

Acknowledgements

I am grateful for the guidance, enthusiasm, and support of the following individuals, without whom this work would not have been possible.

Prof. Ioannis V. Yannas, my advisor and mentor

Prof. Myron Spector and Prof. Lorna Gibson, my doctoral committee members

Dr. Hu-Ping Hsu, a talented surgeon and friend

Drs. Soller (n=2), my parents

The Soller Boys (n=5)

Past & present members of the Yannas Lab for Regenerative Biomaterials, particularly Dimitrios Tzeranis

The many friends who made my time here in Cambridge truly enjoyable.

I dedicate this work to my grandfather James Camillo Flanagan, P.E., who first put me to work as an engineer some 15 years ago analyzing artesian water wells in Central Texas.

Eric Soller
Cambridge, MA

This page was left blank intentionally.

TABLE OF CONTENTS

LIST OF FIGURES

1

Course of the Nerves - Neck and Thorax
Charles Bell (1774-1842): A Series of Engravings, Explaining the Course of the Nerves

This page was left blank intentionally.

1

Introduction

1.1 A Clinical Need for Improved Peripheral Nerve Regeneration

Several hundred thousand individuals suffer from acute peripheral nervous system (PNS) injuries each year in the Unites States and Europe alone (Wiberg and Terenghi 2003). On the modern battlefield blast-related injuries now account for 65 % of all combat injuries (Affairs 2005). Advances in battlefield wound management have decreased significantly the lethality of war wounds but soldiers frequently present with traumatic wounds of the extremities and severe PNS lesions are prominent (Clark, Bair et al. 2007).

Failure to adequately treat severe injury to the peripheral nerve often results in partial or total paralysis of the affected limb. The practitioners of the field, surgeons and other health care professionals, clearly state that current treatments are inadequate: "Even after optimal surgical repair, functional outcome - especially sensory recovery - is disappointingly poor" (Wiberg and Terenghi 2003).

Neural engineering is an important and active area of research. The last thirty years have brought significant advances to the field including an enhanced pathophysiological understanding of the PNS response to acute injury, improved imaging and microsurgical techniques for diagnosis and treatment, and the clinical entry of the first FDA-approved biodegradable devices for peripheral nerve regeneration. Despite this progress, the traditional surgical methods of end-to-end anastomosis[1] and autografting[2] persist as gold standards in the treatment of severe

[1] Anastomosis: a coaptation of the cut ends (nerve stumps) via direct suturing

peripheral nerve defects over short and long gaps, respectively. These techniques have numerous drawbacks including a limited supply of donor nerves and donor site morbidity (in the case of autografts), surgical complexity, and a relatively poor functional outcome. The clinical need for improved strategies for PNS regeneration, particularly across long gaps, remains.

1.2 Irreversible Injury in Skin and Peripheral Nerves

The complex inflammatory response of the adult mammal to injury is increasingly elucidated by on-going research at the cellular and molecular level. Although the formation of an accurate mechanistic perspective of wound healing is essential both in understanding the effect of current clinical treatment and in the development of emergent therapies, an examination of the macroscopic outcome of healing also provides a uniquely valuable viewpoint. An introductory phenomenological discussion of spontaneous wound healing at the tissue level provides a framework that forms a focus for future discussion of detailed cellular/molecular mechanisms and facilitates the derivation of concepts and rules of induced regeneration that may conceivably apply to almost any organ in the body.

1.2.1. Macroscopic Outcomes of Wound Healing: Repair vs. *Regeneration*

When exposed to injury, in the form of either acute trauma or chronic insult, the organism mounts a spontaneous wound healing process that typically closes the discontinuity in organ mass caused by the injury in a matter of days. Two macroscopic outcomes to injury have been observed experimentally, regeneration and repair. These fundamentally different processes are clearly distinguished by the identity of tissue present in the final state, i.e., the tissue that has been displaced or synthesized to close the injury. In the early mammalian fetus and in many species of amphibians, wound healing is largely reversible and proceeds via spontaneous regeneration, a process that restores the structure and physiological function through synthesis of the missing organ

---

[2] Auto-grafting: the transplantation of donor nerve from another part of the body to bridge the gap between nerve stumps

structures (Yannas 2001). Certain adult urodeles exhibit an impressive capacity for spontaneous regeneration: replacement of an amputated appendage occurs by direct outgrowth of the severed cross-section (epimorphic regeneration), a reversible process (Goss 1992).

In clear contrast, severe injury to normal adult mammalian tissue typically results in an irreversible healing response. Spontaneous healing of severe skin wounds proceeds via repair, in which the wound closes with a combination of tissue deformation and translation (collectively referred to as contraction) and synthesis of a nonphysiological tissue (scar) in place of the normally functioning tissue that has been injured *(1)*. By replacing the lost organ mass with scar, the injured organ is condemned whereas the organism is spared as a result of the healing process. The immediate consequence of irreversible injury is a loss of normal organ function. On a broader scale skin injury may have additional detrimental effects, such as loss of mobility and lack of social accept- ance following formation of disfiguring scars from burns. It appears that nearly all adult mammalian organs can be injured irreversibly, the extent of irreversibility seems to depend both on the identity of the tissue injured and the severity of the injury (Yannas 2001).

1.2.2. Regenerative Similarity of the Tissue Triad

Standard pathology texts describe three generic tissue types that comprise the majority of organs in the body: epithelia, basement membrane, and stroma (Yannas 2001; (Burkitt H.G. 1993; Martinez-Hernandez 1998); **Fig. 1.1**). Collectively, we will refer to these three tissue types as the tissue triad. This classification provides a useful framework for comparing the regenerative capacity of specific tissue types from one organ to another. The composition of each member of the triad is markedly different. Epithelial tissue forms a completely cellular covering on every surface, tube, and cavity in the body, performing a wide array of vital functions including protection, secretion, absorption, and filtration. As epithelial tissue is devoid of extracellular matrix (ECM) and blood vessels, it is sustained by the diffusion of nutrients from the underlying vascular connective tissue, or stroma. With the exception of the liver, epithelia is separated from the underlying stroma by the basement membrane (basal lamina), a very thin, noncellular tissue layer, comprising exclusively ECM. The stroma is a connective tissue layer that is vascularized, containing both cells and ECM.

The skin, as one example, consists of the epidermis (epithelia) attached to the basement membrane and the underlying dermis (stroma). Considerable evidence from peripheral nerve studies indicates that Schwann cells function as epithelial cells

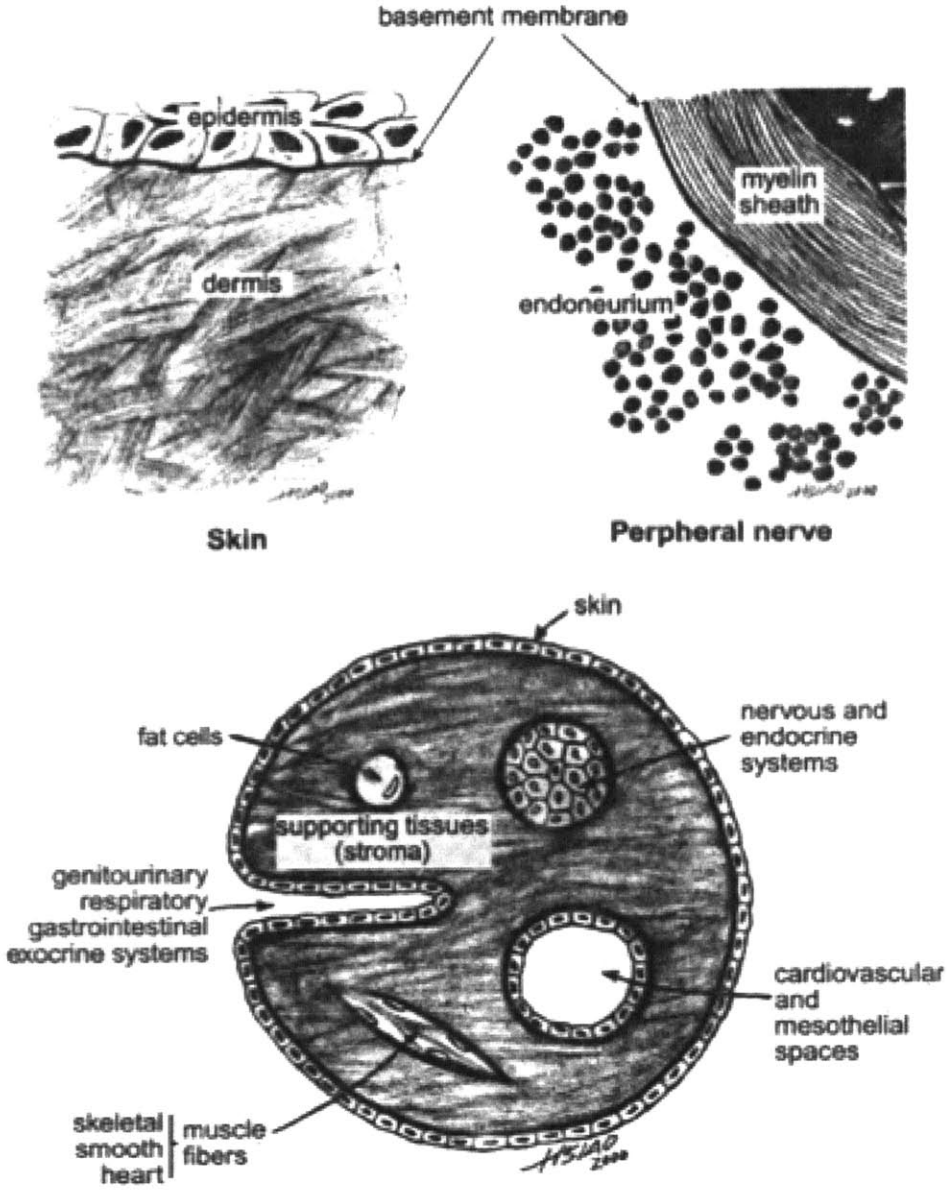

FIG. 1.1 THE TISSUE TRIAD STRUCTURE IN SKIN AND PERIPHERAL NERVES. The basement membrane (basal lamina), a thin noncellular layer consisting of extracellular matrix, separates the cellular, nonvascular epithelia (epidermis, myelin sheath) from the stroma (dermis, endoneurium) which contains cells, ECM, and blood vessels. Epithelia and basement membrane regenerate spontaneously; stroma does not. (Bottom) The tissue triad layers in mammalian anatomy. Stromal tissues include bone, cartilage, and their associated cell types as well as elastin and collagen. Epithelial tissues are those that line the genitourinary, respiratory, and gastrointestinal tracts as well as surfaces of the mesothelial cells in body cavities, and include muscle fibers, fat cells, and endothelial cells in the cardiovascular system. (Yannas 2001).

following synthesis of a completely cellular layer (myelin sheath) around axons. Nerve fibers (Schwann cell-axon units) are attached to a basement membrane that separates them from the outlying endoneurial stroma, a tissue consisting of vascularized ECM. Further evidence for the epithelial nature of the myelin sheath comes from the observed polarity of Schwann cells that is very similar to that of keratinocytes (KC), the epithelial cells that form the epidermis in skin. In each case, one epithelial cell surface is firmly attached to a basement membrane and another is part of the epithelial tissue, endowed in each case with function unique to the respective organ, which characterizes the epidermis (in the case of skin) or the nerve fiber insulation of peripheral nerves (Bunge, Bunge et al. 1989). Tissues that are "regeneratively similar" appear in different organs yet share a common spontaneous healing response, be it regeneration or repair. The spontaneous healing behavior of each layer of the tissue triad in skin and peripheral nerves is well documented and will be briefly reviewed. The response of the peripheral nerve to severe injury will be discussed in more detail later in this chapter.

Partial or full-thickness injury to the epithelial layer of either of the two organs (the epidermis in skin and myelin sheath in peripheral nerves, respectively) results in spontaneous regeneration of the injured tissue by remaining epithelial cells in the defect (provided the stroma is still intact to facilitate epithelial cell spreading) (Yannas 2001; (Haber, Hanna et al. 1985; Ikeda, Oda et al. 1989; Stenn 1992; Fu and Gordon 1997). Following nerve crushing with myelin disruption but with no injury to the endoneurium, the myelin sheath regenerates spontaneously and no contraction is observed. Similarly, epidermal excision is a reversible injury that closes exclusively by spontaneous regeneration rather than contraction. The epidermis in skin and the myelin sheath in peripheral nerves exhibit spontaneous regeneration, a reversible healing response leading to a full recovery of structure and function, and are therefore regeneratively similar (Yannas 2001). Injuries that interrupt the continuity of the basement membrane in both organs also exhibit spontaneous regeneration by epithelial cells; basement membranes are regeneratively similar in the two organs. However, when a wound is severe enough to cause injury to the stroma of either organ (the dermis in skin or the endoneurial stroma in peripheral nerves), the organism achieves wound closure by a combination of contraction and scar synthesis (irreversible healing response) (Uitto J. 1996). The dermis and non-neuronal peripheral nervous tissue heal

by repair; because they are both non-regenerative they are considered to be regeneratively similar.

In summary, when the spontaneous regenerative capacity of corresponding tissue types in skin and peripheral nerves is directly compared, a useful similarity emerges (Yannas 2001). Epithelia and basement membrane are regeneratively similar tissue layers, exhibiting a reversible healing response even in the case of severe injury. Likewise, the stroma in both organs is distinctly non-regenerative. Hence, the central objective of induced organ regeneration is synthesis of the non-regenerative stroma.

1.3 Experimental Considerations

1.3.1 Importance of an Anatomically Well-Defined Defect

The appropriate experimental volume for studies of induced organ regeneration is the anatomically well-defined defect (Yannas 2001). As discussed earlier of the differential regenerative capacity of the various tissue triad layers calls for an experimental injury that is free of non-regenerative tissue. In this manner, the effects of an exogenous regenerative agent on the potential synthesis of non-regenerative tissue can be evaluated without ambiguity.

In addition, the experimental volume should also have well-defined anatomical boundaries to reduce contributions from extraneous healing processes occurring elsewhere in the organ (e.g., caused by collateral damage during the surgical procedure) and to improve the reproducibility of the surgical protocol from one animal to the next as well as between independent laboratories. The treatment of the defect should include prevention of loss of extravascular tissue fluid (exudate), which contains important growth factors and regulators that are crucial both to regeneration and to repair. Inability to prevent exudate loss from the injured site radically affects the outcome of both spontaneous and induced healing processes in both skin and peripheral nerves (Winter 1972) (de Medinaceli, Wyatt et al. 1983) (Terzis 1987) Physical containment is also necessary to prevent detrimental extraneous processes, such as bacterial infection in skin, from interfering with the outcome of the healing response.

For studies of induced regeneration in skin, the most widely used well-defined defect is the dermis-free full thickness wound in the rodent or swine. In the case of

peripheral nerves, the tubulated, fully-transected peripheral nerve in the rat or mouse has been studied extensively (Yannas 2001). Both the introduction of various grafts or sheet-like covers to skin defects and tubulation to transected nerves using a variety of materials typically impart significant activity that either assists or hinders regeneration; their use must be controlled carefully.

1.3.2 Synthetic Protocol: In Vitro or In Vivo?

A detailed comparison of the synthetic regeneration processes carried out in vitro and in vivo shows that in studies of skin and peripheral nerves, various protocols for in vitro synthesis have so far resulted largely in the formation of epithelia and the associated basement membrane but not the physiological stroma. In contrast, several protocols conducted in vivo have yielded not only the physiological epithelia and basement membrane, but a near-physiological stroma as well. The following section highlights these observed cases of induced regeneration.

1.4 Overview of Induced Organ Regeneration

1.4.1. Empirical Evidence

Studies that started in the early 1970s in the Fibers and Polymers Laboratory at Massachusetts Institute of Technology have shown that the adult mammal can be induced to regenerate selected organs that have been accidentally lost or excised. In every case it had been established previously that the excised adult organ in question does not regenerate spontaneously; that is, in the absence of experimental intervention, the adult excised site generally closed spontaneously by contraction and scar formation rather than by regeneration. The organs in question were induced to regenerate partially with the aid of certain insoluble substrates (scaffolds) that were optionally seeded with cells.

The most extensive data on induced organ regeneration are available with skin and peripheral nerves (see ref. 1 for a detailed review). Data with other organs from the work of several investigators were presented in a recent volume (Yannas 2005). We review below the induced organ regeneration data obtained in our laboratory.

The three anatomical sites which were induced to regenerate partially were: 1) full-thickness skin wounds, with epidermis and dermis completely excised, in the adult guinea pig, adult swine and adult human; 2) full-thickness excision of the conjunctiva, with complete excision of the stroma, in the adult rabbit; 3) the fully transected rat sciatic nerve, with stumps initially separated by a gap of 15 mm (later 22 mm and recently 30 mm). A summary of induced regeneration data for the constitutive tissues of each organ is presented in **Table 1**.

Table 1
Constitutive Tissues of Skin, Peripheral Nerves, and Conjunctiva That Were Induced to Regenerate in Adults

Organ	Regeneration observed	Regeneration observed	Regeneration not studied
Skin (guinea pig, swine, human) *(1)*	Keratinized epidermis, basement membrane, dermis, nerve endings, blood vessels	Appendages (e.g., hair follicles, sweat glands)	
Peripheral nerve (mouse, rat, cat, monkey, human)	Myelin sheath, nerve fibers (large and small diameter), blood vessels, endoneurial stroma?		Endoneurial stroma? perineurium
Conjunctiva (rabbit)	Epithelia, conjunctival stroma		Basement membrane

TABLE 1.1 CONSTITUTIVE TISSUES OF SKIN, PERIPHERAL NERVES, AND CONJUNCTIVA THAT WERE INDUCED TO REGENERATE IN ADULTS. (Adapted from Yannas , 2001).

Observations of induced regeneration in adults made over the years have been tested repeatedly by morphological and functional tests, as follows: (A) confirmation of partial regeneration of skin (including both a dermis and an epidermis but lacking skin organelles) was made by histological, immunohistochemical, ultrastructural and functional studies (Burke, Yannas et al. 1981; Yannas, Burke et al. 1981; Yannas, Burke et al. 1982; Yannas, Lee et al. 1989; Murphy, Orgill et al. 1990; Compton, Butler et al. 1998; Butler, Yannas et al. 1999); (B) confirmation of regeneration of the conjunctiva (including the conjunctival stroma) was made using histological data

(Hsu, Spilker et al. 2000); (C) confirmation of regeneration of peripheral nerves was made using both morphological and functional (electrophysiological and neurological) data (Yannas 1985 ; Yannas I.V. 1987; Chang A. 1990; Chang 1992; Chamberlain, Yannas et al. 1998; Chamberlain, Yannas et al. 1998; Chamberlain, Yannas et al. 2000; Chamberlain, Yannas et al. 2000; Spilker 2000).

The available evidence in the above studies strongly supports the conclusion that these severely injured anatomical sites did not close by contraction and scar formation.

Nevertheless, induced regeneration observed to date is described as 'partial' since perfectly physiological organs have not yet been regenerated. Regenerated skin was histologically and functionally different from scar and identical to physiological skin in almost all respects, including a physiological epidermis, well-formed basement membrane, well-formed capillary loops at the rete ridges of the dermal-epidermal junction, nerve endings with confirmed tactile and heat-cold feeling, and a physiological dermis; however, the regenerate lacked certain organelles (hair follicles, sweat glands, etc.). Evidence for the induced regeneration of partial skin is presented in **Fig. 1.2**. The supportive data for induced regeneration of peripheral nerves is presented in **Fig. 1.3**.

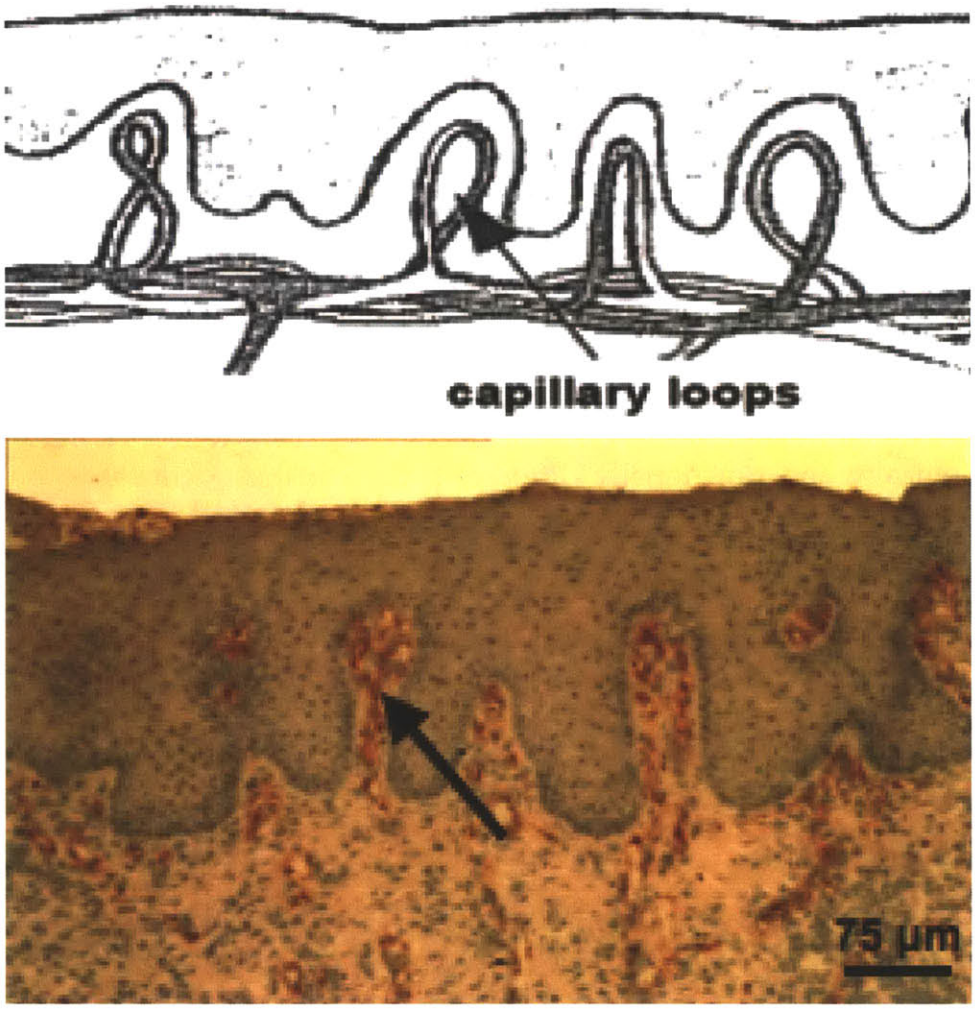

FIG.1.2. EVIDENCE FOR INDUCED REGENERATION OF SKIN. The dermal-epidermal junction for normal skin is represented schematically (top) and contrasted with that of partially regenerated skin in the swine, following grafting with the keratinocyte-seeded dermal regeneration template scaffold (bottom). The new skin is not scar, as evidenced by the presence of rete ridges and capillary loops inside the ridges. (Top, from Burkitt HG, Young B, Heath JW. Wheater's Functional Histology. Edinburgh, Scotland: Churchill Livingstone; 1993. Bottom, from Compton, Butler et al, *J Invest Dermatol*. 1998).

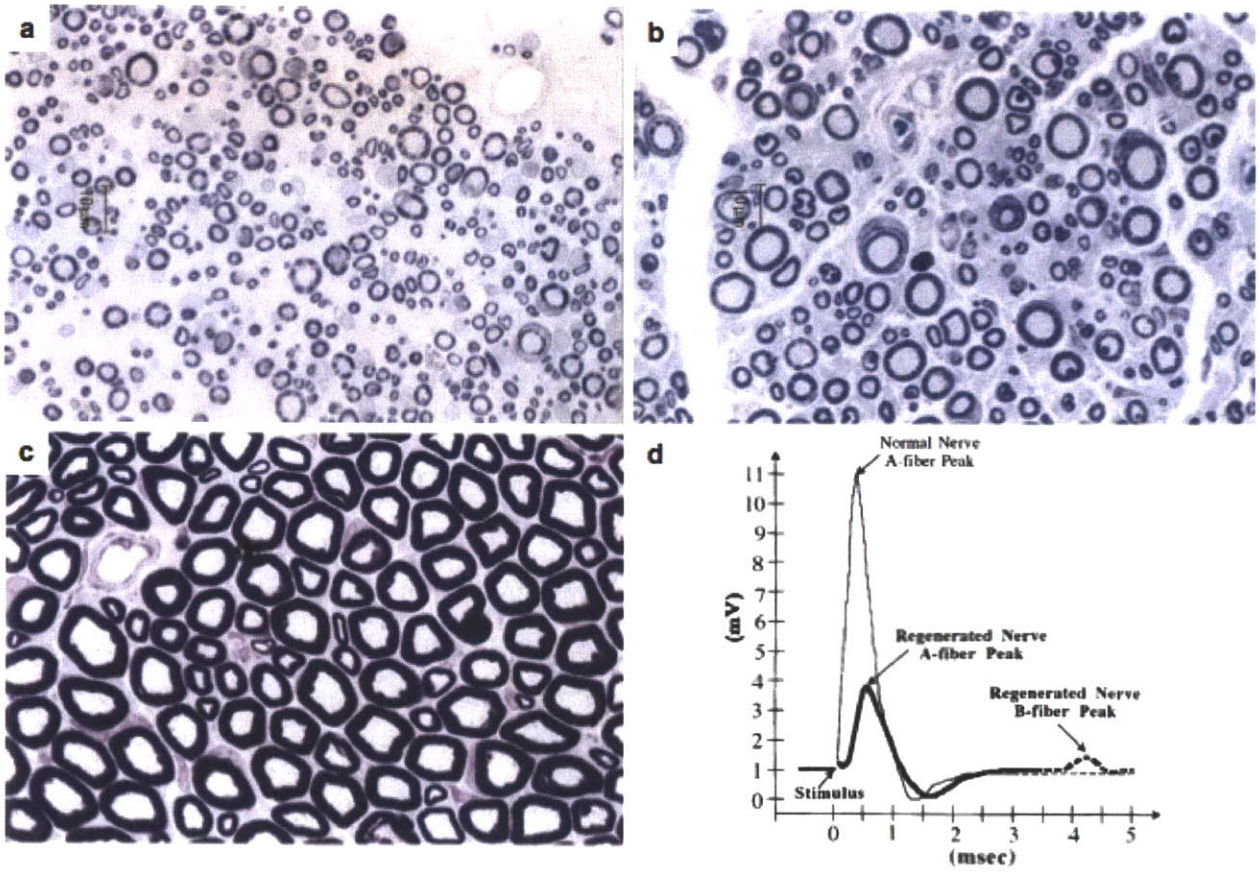

FIG. 1.3. EVIDENCE FOR INDUCED REGENERATION OF PERIPHERAL NERVES. Histological micrographs of nerve tissue postfixed with osmium tetroxide and stained with toluidine blue, scale bars, 10 μm. (a) Tissue regenerated through the midportion of a matrix-filled large-pore collagen (LC/M) implant at 30 weeks. Note the large number of axons in this cross-section with the majority of axons being small in diameter. The largest axons have diameters of approximately 7 μm. Many Schwann cells are visible with some actively participating in myelination. The blood vessel that is visible in this micrograph was characteristic of the caliber of most vessels present in the regenerated tissue. (b) Tissue regenerated through the midportion of a LC/M implant at 60 weeks. Compared to 30 weeks, the axons are much larger (diameters up to 12 μm) and have thicker myelin sheaths. Also, fewer small diameter axons are visible. Few nonmyelinating Schwann cells are visible at 60 weeks. (c) Normal nerve tissue from the level of the lesion is shown as a control. Note the number of large diameter fibers and the thickness of the myelin sheaths compared to the regenerated nerves. (d) Typical oscilloscope tracings of A-fiber and B-fiber com- pound nerve action potentials for normal sciatic nerve and nerve regenerated through a LC/M implant at 60 weeks postimplantation. The A-fiber peak for the regenerated nerve has a significantly smaller amplitude than the normal nerve control. This was typical of all regenerated groups. In contrast, the conduction velocity of the regenerated nerve, although significantly slower than normal, was approaching normal values. The latency is measured along the x-axis from the stimulus to the peak and then combined with the constant distance between electrodes to determine conduction velocity. The dashed line indicating the B-fiber peak has been added on to the tracing for reference. Note that the normal nerve tracing has no visible B-fiber peak. In the regenerated nerves, the B-fiber peak was similar and visible in all groups. Adapted from Chamberlain et al, 2000.

1.4.2. The Defect Closure Rule

Careful review of the literature suggests that not more than three distinct processes are used to close an anatomically well-defined defect (dermis-free defect) in skin wounds, contraction originating from the edges of the defect, scar formation by stromal fibroblasts (followed by epithelialization of scar), and regeneration.

Continuous kinetic data are rarely available in regeneration experiments and often difficult to compare from one study to another. One approach to studying the regenerative activity of exogenous agents on the healing process is to establish two standardized configuration states and to evaluate the total change that is caused during this fixed period in the healing process. In the absence of kinetic data, the defect closure rule bridges the gap by presenting a quantitative
description of the healing process through comparison of snapshots of the initial and final stages of wounding. The initial state of configuration is the anatomical description of the recently generated defect, characterized by the loss of structural continuity in one or more tissues, the beginning of exudate flow, and the loss of physiological homeostatic control of the organ. As defect healing progresses, the original area, $A0$, eventually diminishes spontaneously because of one or more of the three processes mentioned above. The area of the closed defect (the closed wound) comprises tissues that result either from contraction (fractional amount, $\%C$), scar formation ($\%S$), or regeneration ($\%R$). The configuration of the final state can be described by the following simple relation:

$$C + S + R = 100 \qquad (1)$$

Eq. 1 states that the defect closure in any organ can be described by only three outcomes: contraction, scar formation (neuroma or fibrosis), and regeneration (partial or total).

For the idealized case of early fetal wound healing (spontaneous regeneration), con- traction and scarring is absent (C, $S = 0$) and

$$R = 100 \qquad \text{(regeneration)}$$

For normal defect closure in adult mammals in response to irreversible injury

(repair), regeneration is absent ($R = 0$) and

$$C + S = 100 \quad \text{(repair)}$$

The literature describes several assays to determine the configuration of the final state (recently closed defect) *(1)*. Functional assays can be used to qualitatively identify the physiological nature of the tissue and assist in providing a quantitative measure of its incidence in the final state in terms of the numerical values of these three quantities (C, S, or R?). The defect closure rule may be interpreted as a conservation principle: provided that the magnitude of two individual terms (C and S for example) has been determined, the magnitude of the remaining process may be calculated. Defect closure data are expressed using the following convention: [$\%C$, $\%S$, $\%R$].

The defect closure rule is useful in evaluating the activity of unknown reactants as inductive agents of regeneration. This quantitative description of the structure and function of the injured organ at its final state has shed interesting light on the relationship between the characteristic elements of the adult healing response (contraction or scar synthesis, or both) and regeneration.

1.4.3 Prevalence of Contraction During Spontaneous Healing

In the skin, the defect closure rule has been used to approximate data on the configuration of the final state following spontaneous healing of the anatomically well-defined defect (dermis-free defect) in several species. In all cases, it was ensured that the contribution of regeneration to defect closure was negligible ($R = 0$). Skin contraction was measured directly as the reduction in initial wound surface area by inward (centripetal) movement of skin from the margins of the wound. Scar formation was studied qualitatively by histology or quantitatively by use of laser light scattering (to measure the average degree of collagen fiber orientation). Values for the percentage of initial defect area closed by epithelialized scar (S) were determined using the simplified defect closure rule for repair ($S = 100 - C$).

The contribution of the various methods of defect closure in anatomically well-defined defects is species dependent. In rodents, in which the integument is mobile, contraction is by far the main engine of closure of skin wounds, whereas scar formation has been shown to be quantitatively much less important.

The spontaneous healing of a full-thickness skin wound in the guinea pig is

charac- teristic of several rodents and lagomorphs (rabbits), and results in the following final state configuration: [91, 9, 0] (Yannas, Burke et al 1982). In general, $C >> S$ and defect closure for adult rodents and rabbits reduces to C approx 100. Alternatively, the approximation of the final state is expressed as [100, 0, 0].

Human integument is tethered more securely onto subcutaneous tissues and contraction and scar formation contribute approximately equally to wound closure. Experimentally, the spontaneous healing of full-thickness skin defects in the humans ($R = 0$) results in a final state represented by [37, 63, 0] (Ramirez A.T. 1969).

In the absence of direct quantitative observations, histological analysis was used to describe the closure of the fully transected peripheral nerve in the adult rat. Spontaneous healing results in reduction of the initial area of cross-sections of nerve trunks by 95% with neuroma formation (neural scar) accounting for the remaining 5%. The resulting estimation of the final state configuration is [95, 5, 0] (Chamberlain, Yannas et al, 2000).

The contraction of a wide array of organs in response to trauma is well documented in both animals and humans, yet these reports are almost exclusively of a qualitative nature (Holmes and Z. 1942; Weiss 1944; Weiss 1944 ; Kiviat 1973 ; Peacock Jr 1984 ; Dahners 1986; Wilson 1988; Sunderland 1990; Rudolph 1992; Krishnan K.G. 2000; Levine D. 2000; Cornelissen A.M. 2000 ; Delaere P.R. 2001; Zeinoun T. 2001 ; Ivarsen A. 2003; Bulut T. 2004; Wong T.T.L. 2004; Chou T.D. 2004 ; Oppenheimer and Hinman 1955; Unterhauser FN 2004; Schmidt M.R. (2004)). With very few exceptions the sole organ in which contraction has been studied systematically to date is the skin. Despite the dearth of widespread quantitative data, the prevalence of contraction must not be overlooked; it appears to be a critical outcome of the spontaneous healing response throughout the adult organism.

1.4.4 Antagonistic Relation Between Contraction and Regeneration

The characteristic elements of the adult healing response (contraction or scar synthesis, or both) must be controlled in order for induced regeneration to occur. Extensive data, including empirical data on the final state of the defect in response to various reactants, suggest that during healing of a severe injury, contraction antagonizes regeneration (Yannas 2001).

Induced regeneration of skin, a peripheral nerve trunk, and the conjunctival

stroma was accompanied in each case by direct observation of a significant reduction in contraction as a mode of defect closure. Conjunctival and peripheral nerve regeneration studies were guided by earlier studies of skin regeneration. Partial skin was first induced to regenerate in the adult guinea pig. The spontaneous healing behavior of the untreated dermis-free defect in this organism resulted in a final configuration of [91, 9, 0]. Grafting an identical well-defined skin defect with a highly porous polymer of type-I collagen and chondroitin 6-sulfate (referred to as a DRT) (**Fig. 1.4A**), abolished scar synthesis and led to the regeneration of a small mass of dermis and subsequent synthesis of an overlying epidermis within the defect. In the context of the defect closure rule, the regenerative activity of the DRT on the configuration of the final state was as follows:

$$[92, 8, 0] \rightarrow [89, 0, 11] \qquad \text{(DRT)}.$$

In addition, the DRT led to a significant delay in wound contraction over 25 days *(40,41)*.

When a DRT seeded with KC was grafted into an identical defect, the result was more pronounced (**Fig 1.4B-D**):

$$[91, 9, 0] \rightarrow [28, 0, 72] \qquad \text{(DRT + KC)}.$$

KC-seeded DRTs accomplished rapid wound closure through partial regeneration of skin (simultaneous synthesis of a physiological dermis and epidermis, described earlier), and completely arrested contraction at 35–40 days (Yannas, Burke et al. 1982).

The cell-free DRT that induces partial skin regeneration comprises the regenerative component of the two-layer device (Integra DRT®) approved by the Food and Drug Administration (FDA) for restoration of a physiological epidermis and dermis in patients suffering from severe burns as well as those undergoing plastic and reconstructive surgery of the skin, as described in an early study (Burkey, Yannas et al, 1981) and reviewed recently (Yannas, Orgill et al. 2011). Growth factors (Greenhalgh, H. et al. 1990; Puolakkainen, D.R. et al. 1995), epidermal cell suspensions, and cell sheets (Billingham and J. 1952) exhibited negligible regenerative activity when added to full-thickness skin wounds in other rodent models. These reactants did not significantly alter the configuration of the final state or the extent of contraction delay. Similarly, a

number of synthetic polymer scaffolds (Cooper, F. et al. 1991 ; Hansbrough, L. et al. 1993) failed to induce physiological dermis (or skin) regeneration. These observations focus attention on the mechanism of scaffold regenerative activity, to be discussed later.

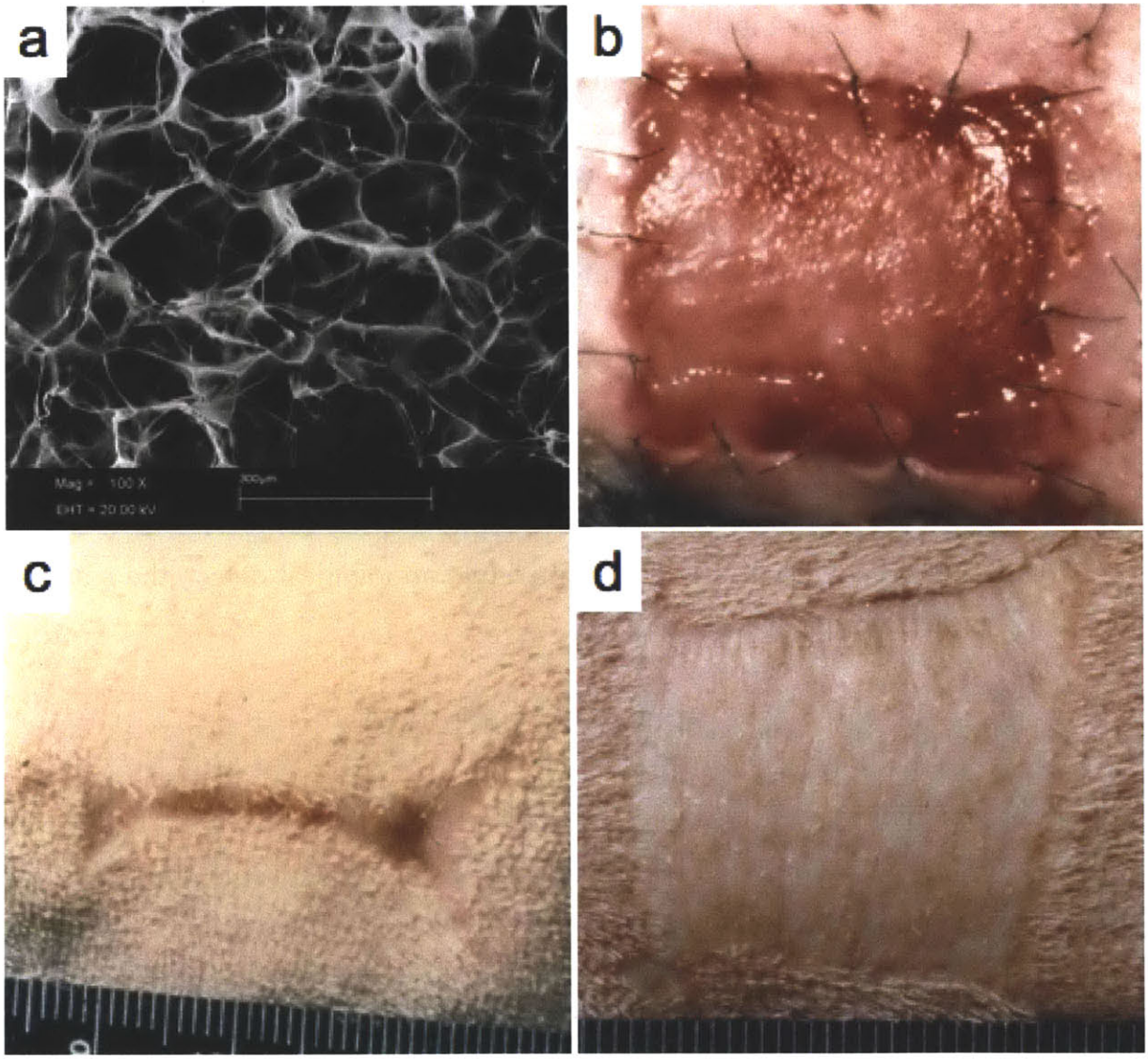

FIG. 1.4. INDUCED REGENERATION OF SKIN COINCIDES WITH SIGNIFICANT REDUCTION OF CONTRACTION AS A MODE OF WOUND CLOSURE IN THE ADULT GUINEA PIG. a) SEM micrograph of an active collagen-glycosaminoglycan (CG) scaffold (also known as dermal regeneration template or DRT). b) A full-thickness (dermis-free) skin wound is grafted with CG scaffold and seeded with keratinocytes (KC). c) An inactive KC-seeded scaffold leads to contraction and scar formation. d) An active scaffold (dermal regeneration template or DRT) seeded with KC alters the defect closure by blocking macroscopic contraction dramatically and leads to simultaneous synthesis of epidermis and dermis. The new tissue formed is skin, not scar. SEM micrograph: E. Soller, 2008. B-D adapted from Yannas et al, 1989 *PNAS*.

Quantitative studies of induced regeneration of peripheral nerves were conducted

in the adult rat. The spontaneous healing behavior of the untreated transected peripheral nerve in this organism resulted in a final configuration that was estimated using histological analysis to be [95, 5, 0]. Insertion of the fully transected nerve stumps into a silicone tube filled with a collagen-based regeneration template (referred to as a Nerve Regeneration Template or NRT) resulted in reduced contraction (as determined by histological analysis of cross-sectional areas of regenerates) and partial regeneration over an unprecedented gap length (Chamberlain, Yannas et al, 2000; Chamberlain, Yannas et al, 2000). Contraction was abolished and the quality of regeneration improved significantly when the NRT was used in con- junction with a degradable collagen tube. In the context of the defect closure rule, the regenerative activity of the NRT in each experimental configuration can be evaluated by inspecting the characteristics of the final state, as follows (the arrow indicates the change observed following use of the scaffold):

$$[95, 5, 0] \rightarrow [53, 0, 47] \qquad \text{(NRT in silicone tube)},$$
$$[95, 5, 0] \rightarrow [0, 0, 100] \qquad \text{(NRT in collagen tube)}.$$

The relative importance of each method of defect closure (*C*, *S*, and *R*) changes during animal development. A sharp change occurs during the fetal–adult transition in mammals (roughly during the third trimester of gestation), in which contraction replaces regeneration as the dominant method of closure (Mast, J.M. et al. 1992 ; Lorenz and Adzick 1993 ; Martin 1996). Similarly, as amphibian development progresses, contraction becomes a more prominent method of wound closure, as regeneration recedes and scar formation becomes more evident (Stocum 1995; Yannas, J. et al. 1996).

Although scar has been widely considered the key barrier to regeneration in adults, quantitative study reveals that contraction is the dominant mode of spontaneous closure in skin and peripheral nerve defects. Studies of induced regeneration in skin, peripheral nerves using analogs of the ECM indicate that scar formation is a process that is secondary to contraction: in studies of induced regeneration in these organs, when contraction was even slightly inhibited, scar formation was totally abolished (Yannas 2001).

[92, 8, 0] → [89, 0, 11] (DRT)
[91, 9, 0] → [28, 0, 72] (skin, DRT + KC)
[95, 5, 0] → [53, 0, 47] (peripheral nerve, NRT in silicone tube),
[95, 5, 0] → [0, 0, 100] (peripheral nerve, NRT in collagen tube).

Suppression of contraction in certain cases of impaired healing, for example, following use of pharmacological agents, such as steroids, or application of devices, for example, use of mechanical splints or full-thickness skin grafts, was not accompanied by regeneration, indicating that suppression of contraction alone did not suffice to induce regeneration (Yannas 2001).

The available evidence supports the theory that selectively suppressed contraction in adult defects is required, but not sufficient to induce regeneration of skin and peripheral nerves. This can be expressed in the context of the defect closure (Eq. 1) rule as follows:

$$\Delta R>0 \text{ and } S\rightarrow 0 \text{ if } \Delta C<0 \qquad (2)$$

This condition describes an antagonistic relationship between contraction and regeneration in the closure of a defect. It suggests that successful induced regeneration strategies consist of reactants that block contraction without blocking other aspects of the healing process.

1.4.5. Repair: Mechanism of Contraction

Similarities in the mechanistic hypotheses for inducing regeneration of skin and peripheral nerves originate in their common response to irreversible injury. Both organs spontaneously respond to injury by recruiting contractile cells that, if not properly suppressed, drive closure of the defect by contraction and scar synthesis rather than by regeneration. Contraction of skin defects starts from a cell cluster at the edge of the defect and later extends across the entire defect area. In peripheral nerves, contraction primarily results from the activity of a circumstantial sheath of contractile cells.

The well-documented, macroscopic contraction that drives the closure of skin defects finds its origin at the cellular scale, arising from the individual contribution of contractile forces generated by differentiated myofibroblasts (MFB) (Rudolph, Abraham et al. 1978; Frangos 1993; Racine-Samson, Rockey et al. 1997; Freyman, I.V. et al. 2001; Freyman, Yannas et al. 2001; Desmouliere, Chaponnier et al. 2005) *(75,77–83)*. The

current consensus is that MFBs present in the granulation tissue following skin wounding derive directly from fibroblasts and comprise an intermediate, contractile, cellular phenotype between the fibroblast and the smooth muscle cell (Zeinoun, Nammour et al, 2001). There is also evidence that undifferentiated fibroblasts may contribute to macroscopic contraction by applying traction to the ECM very soon after coming into contact with it (Dahners, Banes et al 1986; (Davison, McCaffrey et al. 1999; Ehrlich, Keefer et al. 1999 ; Ehrlich, Gabbiani et al. 2002) In response to external tension, fibroblasts exert sustained isometric force on their surrounding environment via a rho/rho-kinase-mediated, actomyosin contractile apparatus (Kimura, Ito et al. 1996; Amano, Chihara et al. 1997; Hall 1998; Tomasek, Vaughan et al. 2006). This three-dimensional, transcellular structure consists of bundles of actin and nonmuscle myosin microfilaments called "stress fibers." Of the many ultrastructural and biochemical factors that distinguish MFBs from their fibroblast precursors, the most useful operational distinction of MFB differentiation is expression of the α-smooth muscle actin (SMA) phenotype (Desmouliere, Chaponnier et al, 2005). Stress fibers of immature MFBs (called proto-MFBs) contain only β- and γ-cytoplasmic actins. Additionally, differentiated MFBs exhibit stress fibers typically arranged parallel to the long axis of the cell, nuclei which consistently show multiple indentations or deep folds, and two cell-matrix adhesion macromolecules (vinculin and fibronectin) (Serini, Bochaton-Piallat et al. 1998; Dugina, Fontao et al. 2001)

Simplistically, the myofibroblast differentiation process can be described as a positive feedback loop that requires the concurrent action of at least three factors: the cytokine transforming growth factor (TGF)- β1, the presence of mechanical tension, and the ED-A splice variant of cellular fibronectin (an ECM component) **(Fig. 1.5).** Fibroblasts respond to the development of mechanical tension by upregulating TGF- β1 production and expressing the α-SMA isoform; in turn, α-SMA expression strengthens the contractile apparatus and increases tension development (Tomasek, Gabbiani et al. 2002)Desmouliere, Chaponnier et al, 2005). Recent work suggests that mature myofibroblasts in skin granulation tissue link their cytoskeletons together using cadherin proteins, which allow them to generate even higher levels of force to drive wound closure (Hinz, Pittet et al. 2004).

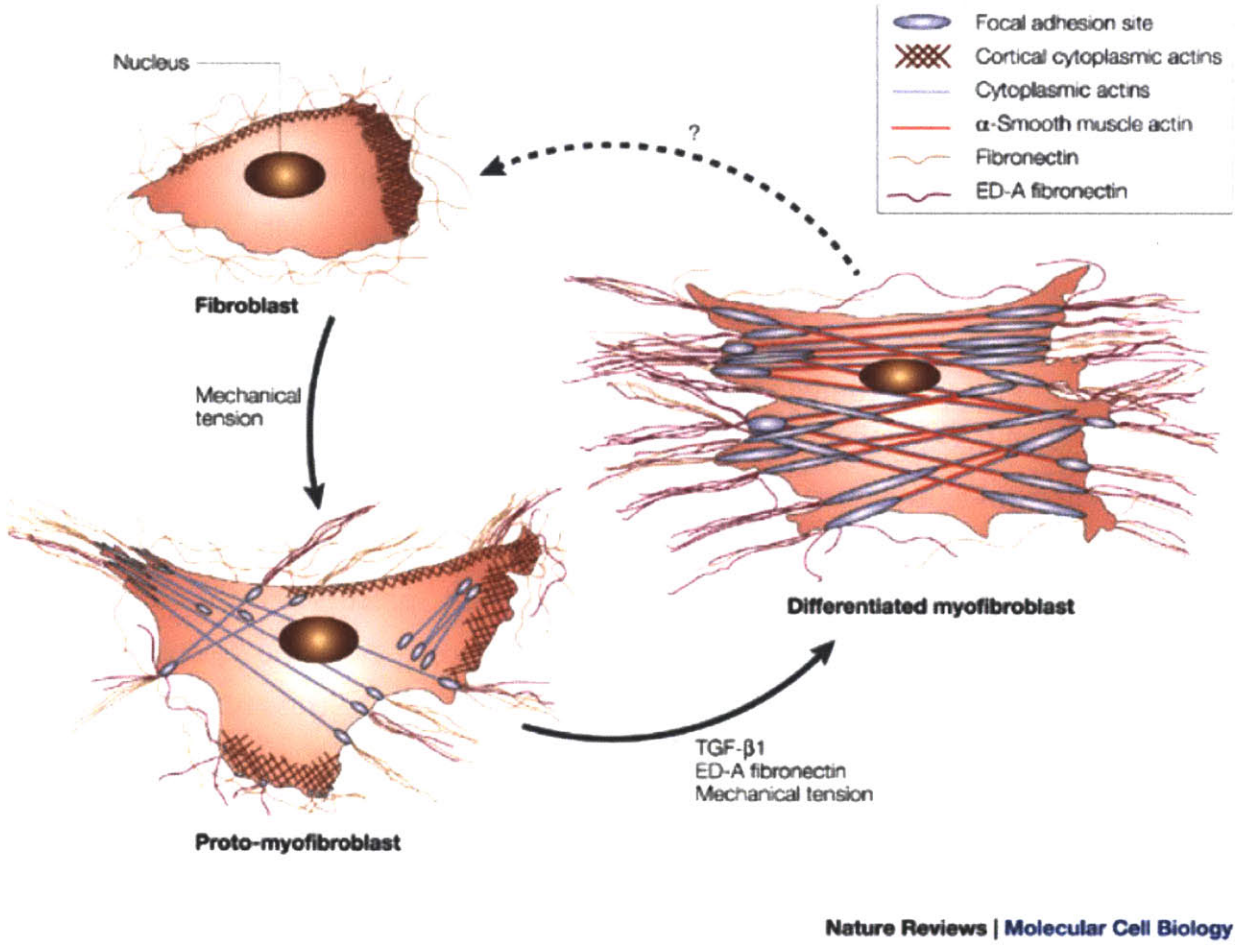

FIG. 1.5. THE TWO-STAGE MODEL OF MYOFIBROBLAST DIFFERENTIATION. Under normal conditions *in vivo* fibroblasts have a quiescent phenotype and do not express stress fibers or focal adhesions with the extracellular matrix (ECM). Mechanical tension prompts differentiation into proto-myofibroblasts, which form cytoplasmic actin-containing stress fibers terminating in fibronexus adhesion complexes. Proto-myofibroblasts express the ED-A splice variant of cellular fibronectin and are capable of generating contractile force.Transforming growth factor beta-1(TGF-β1)increases the expression of ED-A fibronectin. Both factors, in the presence of mechanical stress, promote the modulation of proto-myofibroblasts into differentiated myofibroblasts that are characterized by de novo expression of the contractile filament protein α-smooth muscle actin (α-SMA) in more extensively developed stress fibers and by large fibronexus adhesion complexes *in vivo* or supermature focal adhesions *in vitro*. Functionally, differentiated myofibroblasts generate greater contractile force than proto-myofibroblasts and exhibit a higher level of organization of extracellular fibronectin into fibrils. Reproduced from Tomasek, Gabbiani et al. 2002.

1.4.6. Structural Determinants of Scaffold Regenerative Activity

Scaffolds that induce regeneration of partial skin possess a highly specific structure that is distinctly different in pore structure and degradation rate from scaffolds that regenerate peripheral nerves (Yannas, 2001). The nature and duration of

the contractile response as well as the structure of the two organs differ greatly as do the values for several of the structural parameters of the early scaffolds that were used to control contraction and induce regeneration in each organ. The scaffolds have a common ligand identity due to an identical chemical composition (type I collagen/GAG, 98/2 w/w ratio) yet they differ in average pore diameter (higher in the case of the DRT), the pore channel orientation (axial for the nerve guide, random for the DRT), and degradation rate (a higher average molecular weight between cross-links, *Mc* [kDa] in the nerve guide leads to faster degradation).

In skin wounds, the mechanism of induced regeneration has been elucidated through careful modulation of the DRT's structural properties that impart contraction blocking activity. DRTs that actively block contraction in skin wounds (and induce regeneration) have structural properties that seem to accomplish three main processes: 1) reduction in MFB number present in the wound, possibly due to inhibition of TGF-β synthesis, leading to downregulation of myofibroblast recruitment; 2) blocking orientation of myofibroblast (MFB) axes in the plane of the defect where macroscopic contraction is observed and 3) ensuring that DRT degradation time is sufficiently long to ensure that contraction blocking persists for the duration of the interim myofibroblast contractile response but not so long as to interfere with key regenerative processes.

1) *Apparent downregulation of TGF-β synthesis.* The quaternary structure of collagen fibers is a requirement for the aggregation of platelets, an early component of the wound response. Platelet aggregation initiates a cascade of events that include the release of the cytokine TGF-β1, one of the main inductors of the myofibroblast phenotype. Collagen fibers in the DRT maintain their tertiary (triple helical) structure but are practically free of banding (due to treatment with acetic acid during scaffold preparation). Collagen that has been treated in this manner during scaffold preparation loses its quaternary structure, although it maintains its triple helical structure, and has been shown not to aggregate plaetelets *in vitro* (Sylvester et a., 1989). DRT apparently, therefore, disrupts platelet aggregation that normally takes place in contact with native collagen fibers within the defect, reducing production of TGF-β1, and the recruitment of contractile myofibroblasts to the wound site (Yannas 1997).

2) *Blocking orientation of MFB axes in the plane of the wound as well as MFB-MFB binding.* Contraction of wound edges appears to require orientation of MFB axes in the

plane of the wound as well as MFB-MFB binding and MFB-ECM binding. MFB binding on the extensive surface of the highly porous 3D scaffold inhibits such orientation as well as inhibiting MFB-MFB and MFB-ECM binding. It is suggested that these mechanisms are additionally responsible for contraction blocking by the scaffold. According to this suggested mechanism contraction blocking requires extensive MFB binding onto a sufficiently large scaffold surface, which must take place via specific integrin-ligand interactions. Fibroblasts normally bind onto a specific GFOGER ligand on a collagen surface via the $\alpha1\beta1$ and $\alpha2\beta1$ integrins (Knight 2000). When other structural properties are held constant, the ligand density of a scaffold increases with decreasing average pore size (since the specific surface area of the scaffold available for attachment is thereby increased). An appropriately high ligand density appears to be necessary to disrupt extensive MFB-ECM binding responsible for the onset of macroscopic contraction in skin wounds (**Fig. 1.6**).

When myofibroblasts bind to specific DRT integrins that are distributed evenly in a three-dimensional, interconnecting porous network, the axes of the MFB contractile apparatus becomes disoriented. At the cellular level, the randomized configuration of the preferential contractile axes that individual myofibroblasts adopt in the presence of DRT leads to approximate cancellation of the macroscopic mechanical forces that lead to two-dimensional contraction and scar synthesis in ungrafted skin wounds. When the pore diameter of DRT is increased much beyond the level of 120 μm, the contraction-blocking activity of the scaffold is lost, probably because the effective DRT ligand density drops to a value that does not provide sufficient binding of myofibroblasts. (Yannas 2001; Yannas, Lee et al, 1989, **Fig. 1.7**). Similarly, a minimal average pore size exists that is necessary to ensure MFB migration inside the scaffold in order to enable MFB binding on the scaffold surface. According to this interpretation if the pore size is too small, MFB does not infiltrate the scaffold, MFB-DRT ligand bonds do not form, and MFB contractile activity is not cancelled (Yannas, Lee et al, 1989). Experimentally, the highly planar orientation of myofibroblast axes that is characteristic of the spontaneous contractile response in ungrafted skin wounds is negligible in the presence of DRT (Troxel 1994).

3) *Duration of DRT in an undegraded state over the entire contraction process.* It is known that the regenerative activity of the scaffold depends sensitively on its

degradation rate during skin regeneration (Yannas, Burke et al. 1980) as well as during regeneration in the PNS (Harley, Spilker et al. 2004). To explain the data it has been hypothesized that the DRT is required to undergo a process of *isomorphous tissue replacement*, in which the regenerate (dermis or nerve tissue) is synthesized at a rate which is of the same order as the rate of degradation of the DRT (Yannas, Burke et al. 1980; Harley, Spilker et al., 2004). The requirement for an optimal scaffold duration may reflect the need to have the scaffold persist in an undegraded (insoluble) state over a period that matches the length of the contraction process in skin wounds and nerve wounds, thereby ensuring that the contraction blocking activity is operative when it matters. In skin wounds the optimal half-life of degradation (t_b) for DRT *in vivo* is 14 days, roughly matching the irreversible contraction response in ungrafted wounds (t_h) (Yannas, Burke et al, 1982) . In peripheral nerve wounds the optimal degradation half-life is about 2 weeks, again matching roughly the half-life for the healing process in the transected nerve stump (Harley, Spilker et al, 2004). When the scaffold degraded at a slower rate ($t_b >>$ 14 days), the persisting DRT appeared to interfere with synthesis of the regenerate and scar formed around the scaffold. When the half-life of the DRT was significantly lower than the half-life of the contractile response ($t_b <<$ 14 days) the DRT had little effect on blocking contraction or scar synthesis and regeneration was not observed (Yannas, Lee et al, 1989) , **Fig. 1.7**.

In summary, DRT dramatically blocks contraction while inducing skin regeneration. Scaffolds with similar structure to DRT that do not block contraction also do not induce regeneration. There is evidence that DRT prevents recruitment of MFB and formation of oriented structures of MFB, two processes that characterize spontaneous healing in the adult mammal, over the duration of the normal contraction process.

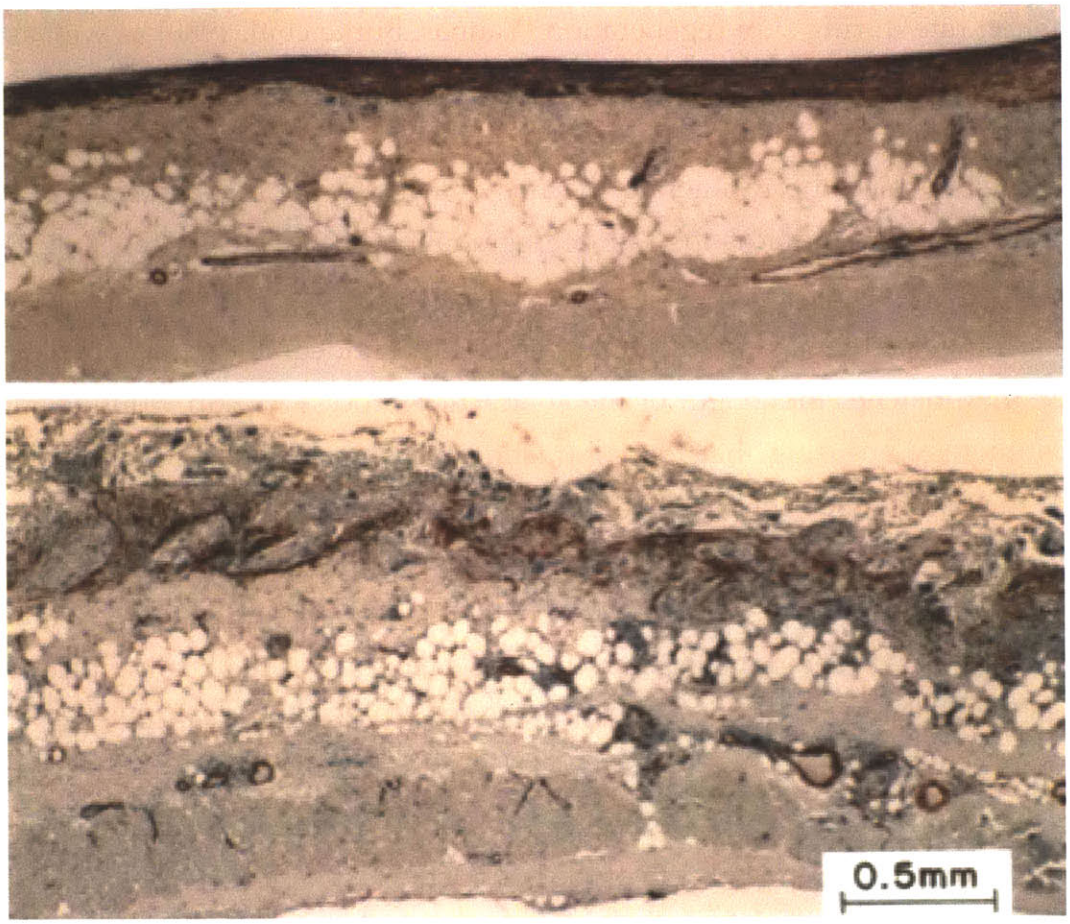

FIG. 1.6. HISTOLOGICAL CONTRAST BETWEEN UNGRAFTED AND GRAFTED FULL-THICKNESS SKIN WOUND IN THE GUINEA PIG. The ungrafted wound is contracting vigorously at day 10 after injury (above), whereas the wound grafted with the unseeded dermal regeneration template shows no contraction at the same time following injury (below). The tissue sections were stained with an antibody against α-smooth muscle actin (red), a protein that is synthesized when fibroblasts differentiate to the myofibroblast, the contractile phenotype. In the grafted wound, the myofibroblast density is reduced to approximately 20 percent of its level in the ungrafted wound; also, the long (contractile) axes of myofibroblasts become randomly oriented in space in the presence of the scaffold (Murphy et al., 1990). The result is blocking of wound contraction, a prerequisite for induced regeneration. Adapted from (Yannas 2005) *J R Soc Interface.*

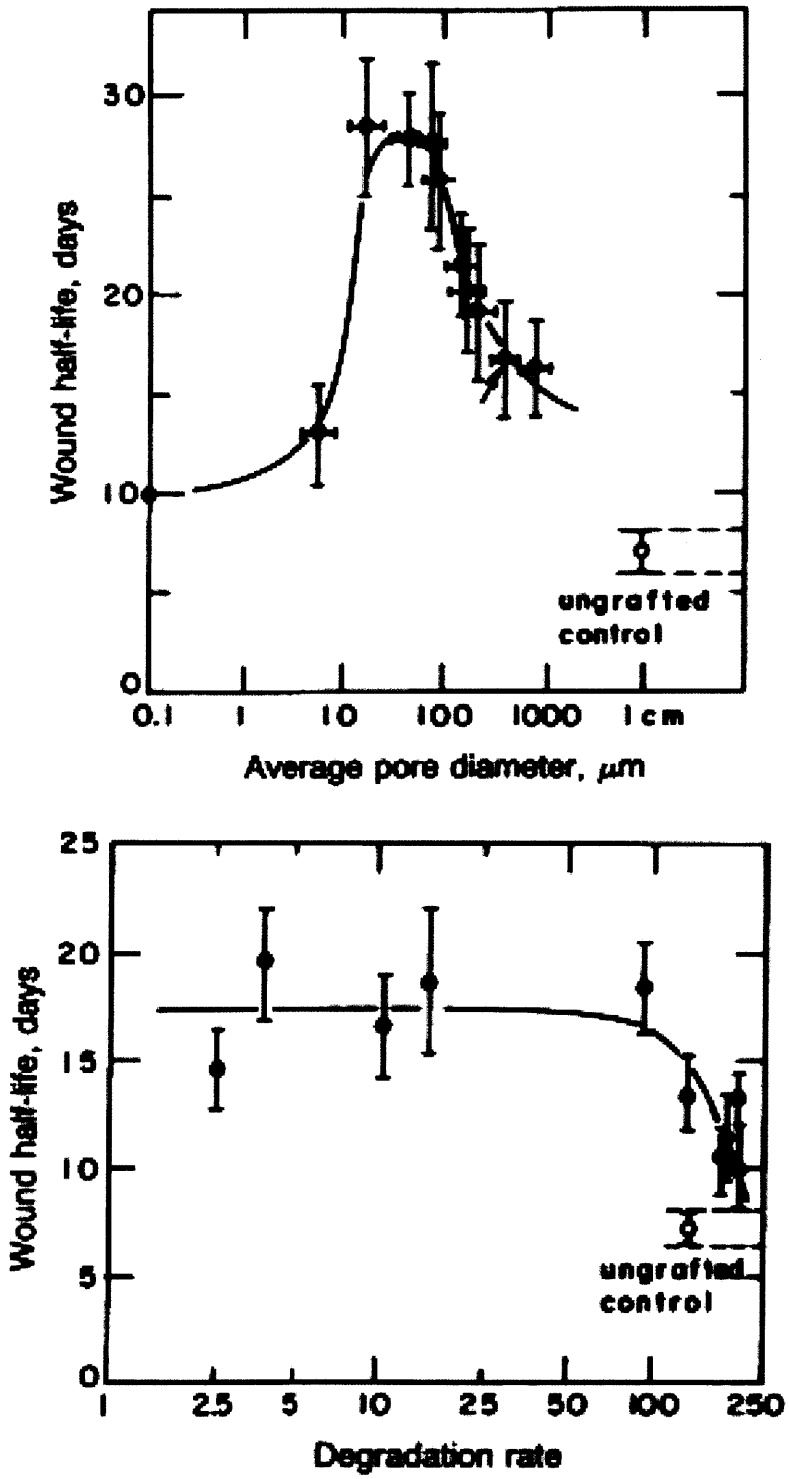

FIG. 1.7. STRUCTURAL DETERMINANTS OF SCAFFOLD CONTRACTION-BLOCKING ACTIVITY IN SKIN. TOP: Variation of the skin wound half-life (the time required for a wound to contract to 50% of the original area) with the average pore diameter of CG copolymer used as the graft. BOTTOM: Variation of the skin wound half-life with degradation rate R of CG copolymer used as the graft. The degradation rate is in empirical units, which are defined in the text. Adapted from Yannas et al, 1989 *PNAS*.

1.5 The Peripheral Nervous System (PNS): A Model Organ for Induced Regeneration Studies

1.5.1. Structure and Function

The peripheral nervous system (PNS) consists of all the nerves and ganglia in the body residing outside of the brain and spinal cord (**Fig. 1.8**). The PNS is a network resembling the vasculature that connects the central nervous system (CNS) to the limbs and organs of the body, permitting the vital transduction of motor and sensory signals.

The PNS is further classified into somatic and autonomic components. The somatic nervous system (SNS) regulates body functions that are under conscious control including the voluntary control of all skeletal muscles as well as the sensory reception of external stimuli in the skin and sensory organs. The autonomic nervous system (ANS) is an unconscious control system that mediates a wide variety of visceral functions including heart rate, digestion, respiratory rate, perspiration, micturition, and sexual arousal.

The peripheral nerve is a considered a discrete organ of the PNS and contains parenchymal (neuronal) and stromal (connective) tissue elements.

1.5.1.1 Parenchymal Components

Each PN is composed of numerous nerve fibers which are often covered in lipid-based material called myelin, although nerve fibers may be unmyelinated or myelinated. A nerve fiber consists of a neuronal cell body, or axon, which generates and conducts the action potentials necessary for signal transduction. Nerve fibers are classified into three general types (types A, B and C) based on their conduction velocity, size and degree of myelination. Schwann cells (SCs) are special support cells that play important roles in normal PN development (Atanasoski, Boentert et al. 2008), maintenance, and regeneration (Yannas 2001). SCs may be myelinating or non-myelinating. They also act as phagocytes to clear cellular debris following severe injury to the axons.

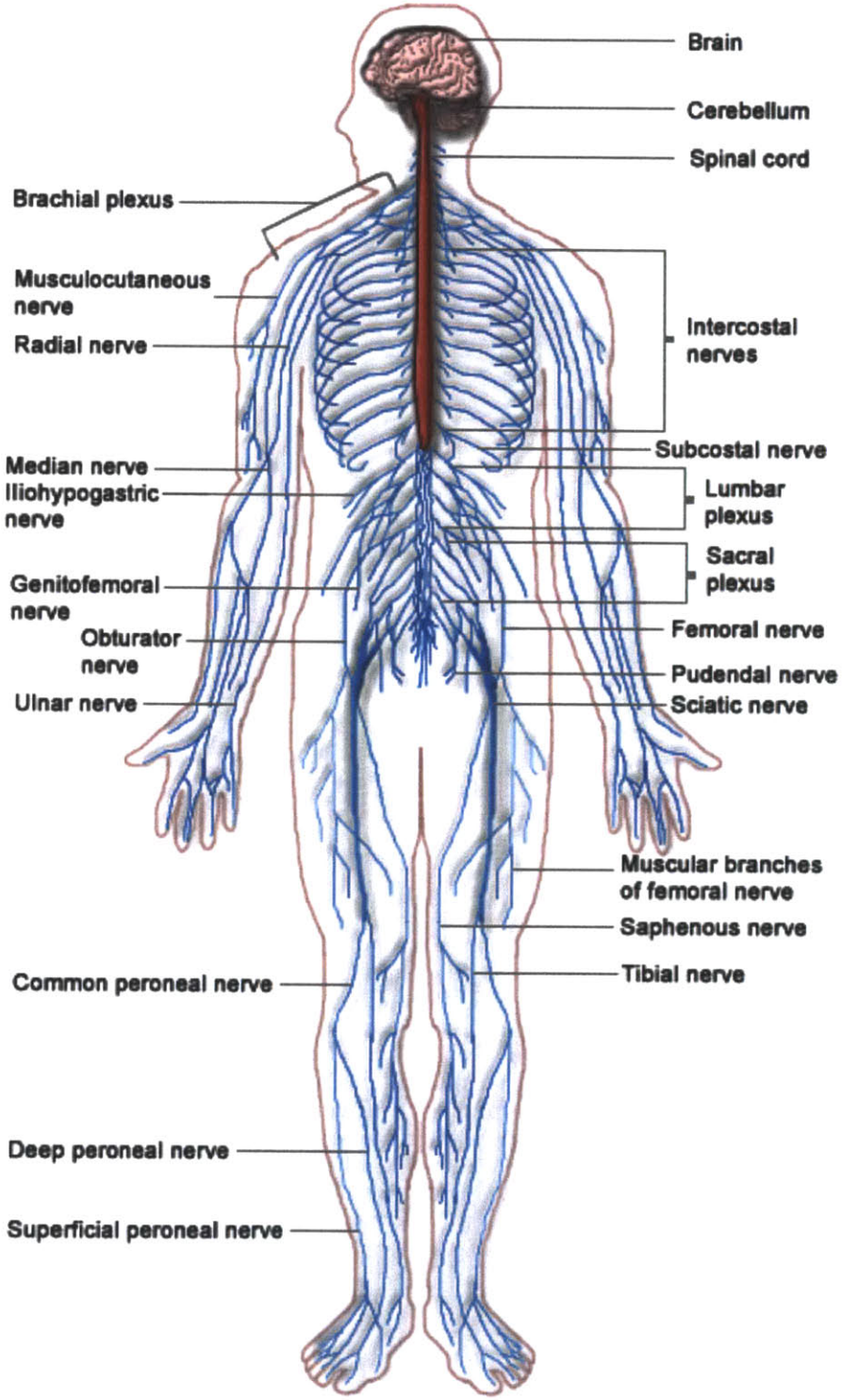

FIG. 1.8. THE HUMAN NERVOUS SYSTEM. The peripheral nervous system (PNS, blue) consists of all nerves and ganglia in the human body outside of the central nervous system (CNS, brain and spinal cord, shown in red, *Wikipedia* 2011).

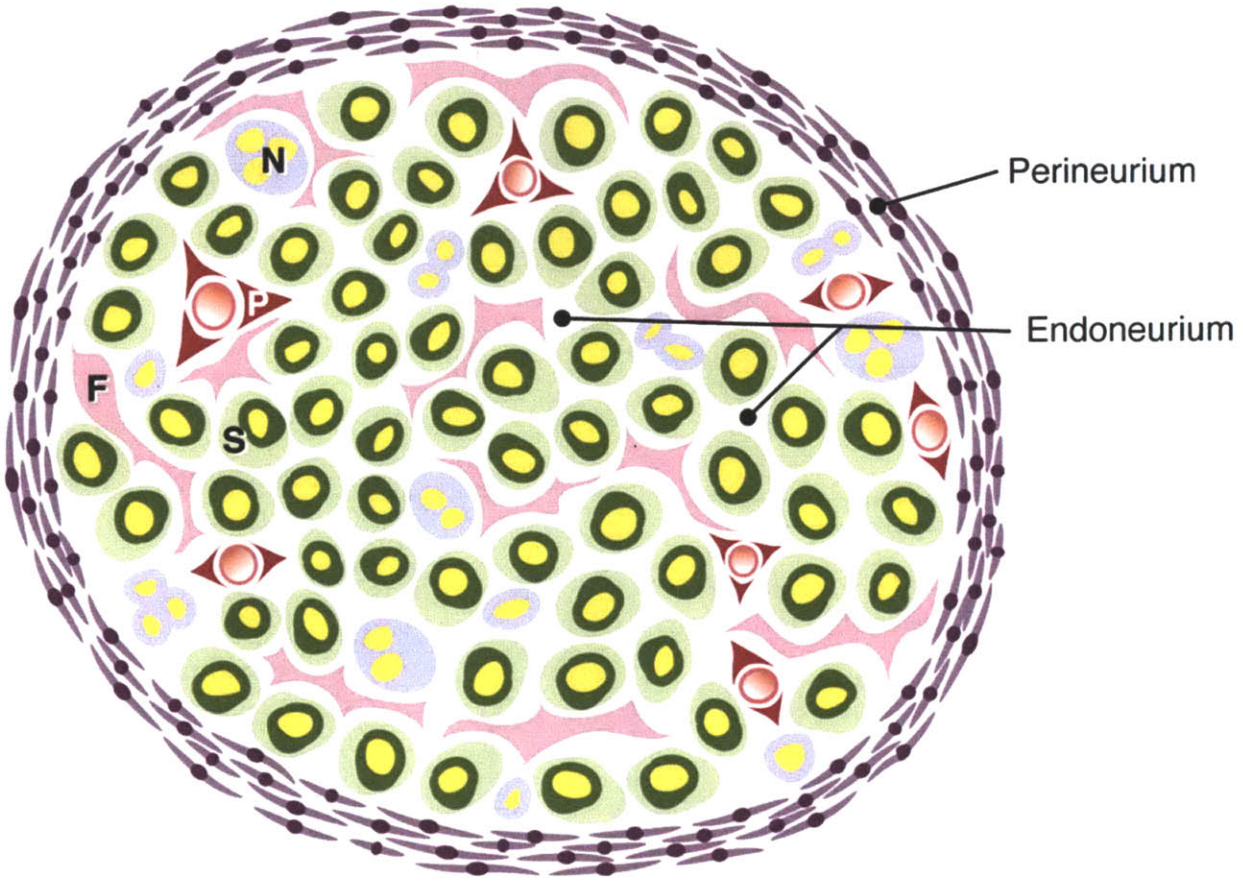

FIG. 1.9. NORMAL PERIPHERAL NERVE ANATOMY. Perineurial cells form a sheath around the nerve called the perineurium (purple), which functions as a mechanical barrier between the endoneurial environment and the epineurial environment. The endoneurium contains Schwann cells that myelinate axons (S; green cells surrounding yellow axons), non-myelinating Schwann cells that are associated with multiple axons (N; blue cells), endoneurial fibroblasts (F; pink cells), and pericytes (P; red) that surround small blood vessels. A single layer of endothelial cells also surrounds the blood vessels (not shown). Perineurial cells are identified by characteristic flattened morphology and circumferential orientation at the periphery of the nerve bundle. Pericytes are distinguished by their expression of SMA. Schwann cells are distinguished by their association with axons, their expression of glial markers such as S100β, and their basal lamina. Endoneurial fibroblasts lack a basal lamina, often have long interdigitating processes, are not associated with axons, and fail to express SMA or S100β *in vivo* under normal conditions. (Joseph, Mukouyama et al. 2004). Note: figure not to scale. Normal adult Lewis rat sciatic nerve contains 4500 myelinated fibers of about 8.5 μm average diameter.

1.5.1.2 Stroma

The biochemical nature and morphology of the nonneuronal components of the PNS have been studied in detail (Thomas 1963; Gamble and Eames 1964; Burkel 1966; Landon 1976; Jessen and Mirsky 1999; Kerns 2008).

The stroma of the PN consists of vascularized connective tissue structures that organize the axons (Flores, Lavernia et al. 2000) and provide the flexibility and strength that protects them from mechanical and chemical insults (Flores, Lavernia et al, 2000; Jessen and Mirsky 1999; Kerns 2008). The stroma consists of three main connective tissue structures: the endoneurium, the perineurium and the epineurium (**Fig. 1.9**).

The endoneurium is the innermost connective tissue structure that surrounds the ScC-axon (nerve fiber) units. It consists of a loose mesh of collagen and other extracellular matrix molecules (Jessen and Mirsky 1999; Kerns 2008) as well as fibroblasts and microvessels surrounded by pericytes.

The endoneurium contains many nerve fibers that together form a fascicle that is surrounded by the perineurium. Peripheral nerves in the human body are typically multi-fascicular. The perineurium can be thought of as a "cellular tube" or wall surrounding the endoneurium. It is composed of one or more layers of flattened perineurial cells (epitheloid, myofibroblasts) that are covered by a basal lamina. Under normal conditions, perineurial cells are joined by gap junctions and form tight, impermeable connections with each other (Jessen and Mirsky 1999; Kerns 2008). This organization forms a blood-nerve barrier (BNB), protecting the delicate axonal structures within the endoneurium from large molecule and/or cell infiltration (Parmantier, Lynn et al. 1999).

The developmental origin of glial cells (perineurial cells, pericytes, and endoneurial fibroblasts) in the peripheral nerve is not known and is subject to debate. The origin of perineurial cells in particular is unclear. They do not seem to arise from the neural crest (Bunge, Williams et al. 1980) as other peripheral glia do (Jessen and Mirsky 2005) and may have a mesodermal origin (Bunge, Wood et al. 1989). Pericytes are most likely mesodermally-derived and the embryonic origin of endoneurial fibroblasts is unknown.

1.5.2. Regenerative Microenvironment After Neurotmesis

The normal function of the PNS relies on both the structural integrity of and the interaction between axons, Schwann cells and connective sheaths. Unlike the brain and spinal cord, the PNS lacks the protection of mineralized tissue (skull or spine) as well as the blood-brain barrier. This leaves the organ system particularly vulnerable to both mechanical and chemical injury.

Here, the specific response of the transected (neurotomized) peripheral nerve in the presence of the nerve guide is described in more detail. The seminal studies of Williams et al. (Williams, Longo et al. 1983; Williams 1984; Williams, Powell et al. 1984; Williams and Varon 1985; Muller, Williams et al. 1987; Williams, Danielsen et al. 1987) describe the regenerative response of a transected nerve in a biodurable (non-degradable) silicone tube across a 10 mm gap in detail. After transection and a period described as Wallerian degeneration in which macrophages digest myelin debris, a fibrin cable forms between the nerve stumps which facilitates the migration of various cell types into the gap. Bands of Bünger (basement membrane tubes) are formed by Schwann cells which migrate from these tubes in the proximal stump towards the distal stump along with regenerating axons, remyelinating them, and eventually reconnecting these axons with their distal counterparts to reinnervate muscles and/or other downstream organs. The regenerated nerve continues to mature over months to years, increasing in both average axon diameter and conduction velocity. The temporal progress of these events is as follows:

Day 1: the chamber fills with exudate (fluid) from the proximal and distal stumps

Days 2-6: An acellular fibrinous matrix forms between the two stumps

Days 7-14: Cells migrate into the matrix from both stumps. The first cells to migrate are perineurial-like cells at the circumferential part of the matrix, followed by Schwann cells and endothelial cells.

Days 15 to 21: Axons grow from the proximal stump at 1-2 mm per day. Eventually they enter the distal stump around 21 days with myelination following after a 5 day delay. Eventually the axons reinnervate the downstream organs.

1.6. Theories of Peripheral Nerve Regeneration & The Pressure Cuff Theory

One of the challenges neural engineers face in devising strategies for bridging the nerve gap is the difficulty of comparing experimental configurations that vary widely in methodology including, but not limited, to the nerve guide structural and chemical properties, the identity and concentrations of fillers used (exogenous cells, polymer substrates, growth factors, etc), the animal model (mouse, rat, monkey, etc), and the gap length (5 – 30 mm, typically) ((J, Jansen et al. 2004; Chen, Yu et al. 2007; Deumens, Bozkurt et al. 2010).

A useful data reduction tool has been established to aid the investigator. The critical gap length, or L_c, is defined as the gap length for a particular configuration at which the probability of nerve stump reconnection is 50% (Yannas 2001). The critical gap length is a useful normalized measure of regenerative activity and allows powerful analysis of a wealth of experimental data.

The variable regenerative activity of nerve guides is attributed speculatively to their formation and maintenance of concentration gradients of neurotrophic factors between the stumps (Longo, Hayman et al. 1984; Lundborg, Dahlin et al. 1994), physical guidance cues provided by tracks of solid or semisolid surfaces for cells to migrate between the stumps (Fu and Gordon 1997), or enhanced neovascularization of the immature regenerate (Kemp, Syed et al. 2009).

However, investigation of regeneration mechanisms based on normalized data (Harley, Spilker et al. 2004; Zhang and Yannas 2005; Yannas, Zhang et al. 2007) suggests axonal regeneration is downregulated by experimental configurations that permit formation of a contractile cell (myofibroblast) capsule around the regenerating nerve that appears to restrict growth of a nerve trunk by application of circumferential mechanical forces (pressure cuff theory) and enhanced by configurations that favor syntheiss of linear columns of Schwann cells surrounded by basement membrane (Bands of Büngner) that serve as tracks for oriented axon elongation. It has been proposed that these two processes work competitively in the regulation of nerve regeneration in the nerve chamber model.

The pressure cuff theory (Chamberlain, Yannas et al. 1998; Chamberlain, Yannas et al. 2000; Yannas 2001, Harley, Spilker et al. 2004; Zhang and Yannas 2005; Yannas, Zhang et al. 2007) has been described previously using a simple, linear elastic continuum mechanics model that relates MFB capsule thickness, δ, and the diameter of the nerve regenerate. (Brau 2002). In this analysis, a first pass approximation was made: the magnitude of the circumferential hoop stress exerted by the MFB capsule on the regenerating nerve is proportional to the MFB capsule thickness, δ.

There is no available data describing the effect of the contractile capsule formation on the outcome of peripheral nerve regeneration after severe injury.

1.7. Research Goal

There is strong evidence that cell-mediated mechanical forces close wounds in adults by contraction and scar formation. There is also considerable evidence, uncovered in this laboratory, that healing in adults can proceed by regeneration, rather than by contraction and scar formation, if these forces are cancelled out by appropriate methods. What exactly constitutes appropriate methods of cancellation is not quite understood today.

This thesis aims to shed light on this question. It represents the first systematic attempt to provide a quantitative link between MFB-mediated contraction and quality of regeneration of the transected peripheral nerve.

1.7.1 Experimental Approach

The experimental approach is to control the MFB capsular thickness, δ, around the regenerating nerve stumps in a dose-dependent manner using two disparate contraction-blocking strategies and to evaluate the correlation of capsular MFB thickness with measures of the quality of peripheral nerve regeneration, Q.

Two contraction-blocking strategies (one a solid-state scaffold surface, the other a diffusible small molecule,) are studied in this work. A well-characterized library of collagen-based tubular scaffolds with highly specific chemical composition, pore size,

and degradation rate and a specific pharmacological inhibitor of cell-mediated contraction are used to study *in vivo* the influence of tissue-scale contraction by force-generating myofibroblasts (MFBs) on the quality of peripheral nerve regeneration across 15 mm gaps following complete transection of the sciatic nerve.

1.7.2 Significance

Despite significant progress to date in inducing regeneration in transected peripheral nerves, recovery from peripheral nerve injury using the nerve chamber model is imperfect and generally limited to gap lengths of about 20 mm. Current research in regenerative medicine, including peripheral nerves, focuses on the formation of new tissue in severely damaged organs, including the specific differentiation of precursor cells (e.g. stem cells, endothelial cells), the synthesis of ECM, and the extension of injured tissues/cells (e.g. axons). However, most research overlooks the importance of the contraction of the injured organ by a capsule of contractile cells located around the injured organ, which forms early (within 3 weeks) in the wound healing process (Yannas 2001). This is important to note as all successful attempts of inducing regeneration in adult organs to date coincide with reduced/delayed formation of contractile cell capsule. There are no published data on the direct effect of the capsule on the formation of the new organ tissue. Furthermore, even though much research focuses on developing biomaterials or small molecules that can induce regeneration in nerves, there are very few systematic ways to guide their design or to compare their performance in vivo both at the tissue and the molecular level.

The contribution of the proposed research is to provide solid evidence that the contraction of the injured organ is a "first-order" part of the wound healing process in transected nerves, and where possible, to provide quantitative guidelines for the design and evaluation of regenerative medicine products.

For the first time, this work will provide the field of peripheral nerve regeneration with a quantitative link between an overlooked but important mechanical phenomenon (contraction of nerve stumps by a contractile cell capsule that forms around the injured organ) and the quality of new tissue formation in injured nerves.

The proposed research may have a significant impact on the fields of regenerative medicine (in the PNS as well as other organs) and biomaterials. It supports

the hypothesis that suppression of the spontaneous organ contraction is a necessary condition for the successful formation of new nerve tissue, and suggests new directions for preparation, design and comparison of biomaterials used in regenerative medicine. shift the way bioengineers prepare, design and compare their biomaterials. The long-term objective of the work is to develop better biomaterials that could induce more complete regeneration in more severely wounded nerves, and provide guidelines for the development of biomaterials that can induce regeneration in a wider variety of organs.

1.7.3. Innovation/Major Findings

The novel contributions and major findings of this work are:

1. A negative, statistically significant association was observed between the contractile capsule thickness, δ and quality of regeneration metrics (total myelinated area, number of myelinated axons, number of large diameter axons) at the midpoint of the gap, 9 weeks post-neurotmesis Chapter 2).
2. Collagen devices of intermediate degradation rate minimize the thickness of the capsule that normally surrounds healing nerves and yield higher quality regenerates (measured by number of myelinated axons, number of large-diameter axons, N-ratio, and mean axon diameter) at the midpoint of a 15 mm gap, 9 weeks post sciatic-neurotmesis in a rat model (Chapter 2)
3. Novel methodology was developed to study continuously-delivered soluble factors in the nerve chamber model (Chapter 3).

1.7.4. Thesis Organization

The remainder of this work is organized in three parts. Chapter 2 contains a study of solid-state, insoluble regulators of cell-mediated contraction ("scaffolds") that vary in degradation rate in an animal model of peripheral nerve regeneration. Chapter 3 contains the results of a pilot study of a soluble, small-molecule inhibitor of cell-mediated contraction on the early response to nerve injury. Chapter 4 contains conclusions.

Portions of this chapter were published previously as "Induced Regeneration of Skin and Peripheral Nerves" in The Diabetic Foot, Springer, 2nd edition, 2006; and to be published (3rd edition), 2011.

Literature Cited

Affairs, D. o. V. (2005). Polytrauma Rehabilitation Procedures. D. o. V. Affairs. Washington, DC. 1172.1: 1.

Amano, M., K. Chihara, et al. (1997). "Formation of actin stress fibers and focal adhesions enhanced by Rho-kinase. ." Science. 275(5304): 1308-1311.

Atanasoski, S., M. Boentert, et al. (2008). "Postnatal Schwann cell proliferation but not myelination is strictly and uniquely dependent on cyclin-dependent kinase 4 (cdk4)." Mol Cell Neurosci 37(3): 519-527.

Billingham, R. E. and R. J. (1952). "Transplantation studies on sheets of pure epidermal epithelium and epidermal cell suspensions. ." Brit. J. Plast. Surg 5: 25-36.

Brau, R. R. (2002). Mechanisms of Peripheral Nerve Regeneration and Neuroma Formation. Cambridge, MA, Massachusetts Institute of Technology. M. Eng.

Bulut T., B. Y., Yanar H., Yamaner S., Balik E., Solakoglu S., and Koser M. (2004). "The effects of beta-aminopropionitrile on colonic anastomosis in rats. ." J Invest Surg. 17(4): 211-219.

Bunge, M. B., R. P. Bunge, et al. (1989). "Role of Peripheral-Nerve Extracellular-Matrix in Schwann-Cell Function and in Neurite Regeneration." Developmental Neuroscience 11(4-5): 348-360.

Bunge, M. B., A. K. Williams, et al. (1980). "Comparison of nerve cell and nerve cell plus Schwann cell cultures, with particular emphasis on basal lamina and collagen formation." J Cell Biol 84(1): 184-202.

Bunge, M. B., P. M. Wood, et al. (1989). "Perineurium originates from fibroblasts: demonstration in vitro with a retroviral marker." Science 243(4888): 229-231.

Burke, J. F., I. V. Yannas, et al. (1981). "Successful use of a physiologically acceptable artificial skin in the treatment of extensive burn injury." Ann Surg 194(4): 413-428.

Burkel, W. E. (1966). "Relation of Perineurium Blood Vessels and Reticular Fibers to Tissue Space in Peripheral Nerve." Journal of Cell Biology 31(2): A18-&.

Burkitt H.G., Y. B., Heath J.W., Kilgore, J. (1993). Wheater's Functional Histology. Edinburgh, Churchill Livingstone.

Butler, C. E., I. V. Yannas, et al. (1999). "Comparison of cultured and uncultured keratinocytes seeded into a collagen-GAG matrix for skin replacements." Br J Plast Surg 52(2): 127-132.

Chamberlain, L. J., I. V. Yannas, et al. (1998). "Early peripheral nerve healing in collagen and silicone tube implants: myofibroblasts and the cellular response." Biomaterials 19(15): 1393-1403.

Chamberlain, L. J., I. V. Yannas, et al. (2000). "Connective tissue response to tubular implants for peripheral nerve regeneration: the role of myofibroblasts." J Comp Neurol 417(4): 415-430.

Chamberlain, L. J., I. V. Yannas, et al. (1998). "Collagen-GAG substrate enhances the quality of nerve regeneration through collagen tubes up to level of autograft." Exp Neurol 154(2): 315-329.

Chamberlain, L. J., I. V. Yannas, et al. (2000). "Near-terminus axonal structure and function following rat sciatic nerve regeneration through a collagen-GAG matrix in a ten-millimeter gap." J Neurosci Res 60(5): 666-677.

Chang A., Y. I. V., Perutz S., Loree H., Sethi R.R., Krarup C., Norregaard T.V., Zervas N.T., and Silver J. (1990). Electrophysiological study of recovery of peripheral nerves regenerated by a collagen-glycosaminoglycan copolymer matrix. Progress in biomedical polymers. a. D. R. L. Gebeelin C.G. New York, Plenum: 107-119.

Chang, A. S.-P., and Yannas I. V. (1992). Peripheral nerve regeneration. Neuroscience Year. B. a. A. G. Smith. Boston, MA, Birkhauser.

Chen, Z. L., W. M. Yu, et al. (2007). "Peripheral regeneration." Annu Rev Neurosci 30: 209-233.

Chou T.D., L. W. T., Chen S.L., Lee C.H., Chen S.G., Chen T.M., and Wang H.J. (2004). "Split calvarial bone graft for chemical burn-associated nasal augmentation. ." Burns. 30(4): 380-385.

Clark, M. E., M. J. Bair, et al. (2007). "Pain and combat injuries in soldiers returning from Operations Enduring Freedom and Iraqi Freedom: implications for research and practice." J Rehabil Res Dev 44(2): 179-194.

Compton, C. C., C. E. Butler, et al. (1998). "Organized skin structure is regenerated in vivo from collagen-GAG matrices seeded with autologous keratinocytes." J Invest Dermatol 110(6): 908-916.

Cooper, M. L., H. J. F., et al. (1991). "In vivo optimization of a living dermal substitute employing cultured human fibroblasts on a biodegradable polyglycolic acid or polyglactin mesh. ." Biomaterials 12: 243-248.

Cornelissen A.M., M. J. C., Von den Hoff J.W., and Kuijpers-Jagtman A.M. (2000). "Local injection of IFN-gamma reduces the number of myofibroblasts and the collagen content in palatal wounds. ." J Dent Res. 79(10): 1782-1788.

Dahners, L. E., Banes A. J., and Burridge K. W. T. (1986). "The relationship of actin to ligament contraction. ." Clin. Orthop. 210: 246-251.

Davison, S. P., T. V. McCaffrey, et al. (1999). "Improved nerve regeneration with neutralization of transforming growth factor-beta1. ." Laryngoscope. 109: 631-635.

de Medinaceli, L., R. J. Wyatt, et al. (1983). "Peripheral nerve reconnection: mechanical, thermal, and ionic conditions that promote the return of function." Exp Neurol 81(2): 469-487.

Delaere P.R., H. J., Hermans R., and Van Den Hof B. (2001). "Prefabrication of composite tissue for improved tracheal reconstruction." Ann Otol Rhinol Laryngol 110(9): 849-860.

Desmouliere, A., C. Chaponnier, et al. (2005). "Tissue repair, contraction, and the myofibroblast. ." Wound Repair Regen. 13(1): 7-12.

Deumens, R., A. Bozkurt, et al. (2010). "Repairing injured peripheral nerves: Bridging the gap." Prog Neurobiol 92(3): 245-276.

Dugina, V., L. Fontao, et al. (2001). "Focal adhesion features during myofibroblast differentiation are controlled by intracellular and extracellular forces." J. Cell Sci. 114: 3285-3296.

Ehrlich, H. P., G. Gabbiani, et al. (2002). "Cell coupling modulates the contraction of fibroblast-populated collagen lattices. ." J Cell Physiol 184: 86-92.

Ehrlich, H. P., K. A. Keefer, et al. (1999). "Vanadate and the absence of myofibroblasts in wound contraction. ." Arch Surg. 134: 494-501.

Flores, A. J., C. J. Lavernia, et al. (2000). "Anatomy and physiology of peripheral nerve injury and repair." Am J Orthop (Belle Mead NJ) 29(3): 167-173.

Frangos, J. (1993). Physical Forces and the Mammalian Cell. New York, NY, Academic Press.

Freyman, T. M., Y. I.V., et al. (2001). "Micromechanics of fibroblast contraction of a collagen-GAG matrix." Exp Cell Res. 269: 140-153.

Freyman, T. M., I. V. Yannas, et al. (2001). "Fibroblast contraction of a collagen-GAG matrix." Biomaterials 22: 2883-2891.

Fu, S. Y. and T. Gordon (1997). "The cellular and molecular basis of peripheral nerve regeneration." Mol Neurobiol 14(1-2): 67-116.

Gamble, N. J. and R. A. Eames (1964). "Electron Microscopy of Connective Tissues of Normal + Degenerated Human Peripheral Nerves." Journal of Anatomy 98(3): 478-&.

Goss, R. J. (1992). Regeneration versus repair. Wound Healing: Biochemical and Clinical Aspects D. R. F. Cohen I.K., Lindblad W.J. Philadelphia, PA, Saunders: 20-39.

Greenhalgh, D. G., S. K. H., et al. (1990). "PDGF and FGF stimulate wound healing in the genetically diabetic mouse." Am. J. Pathol. 136: 1235-1246.

Haber, R. M., W. Hanna, et al. (1985). "Cicatricial junctional epidermolysis bullosa." J Am Acad Dermatol 12(5 Pt 1): 836-844.

Hall, A. (1998). " Rho GTPases and the actin cytoskeleton. ." Science. 279(5350): 509-514.

Hansbrough, J. F., M. J. L., et al. (1993). "Composite grafts of human keratinocytes grown on a polyglactin mesh-cultured fibroblast dermal substitute function as a bilayer skin replacement in full-thickness wounds on athymic mice. ." J. Burn Care Rehab. 14: 485-494.

Harley, B. A., M. H. Spilker, et al. (2004). "Optimal degradation rate for collagen chambers used for regeneration of peripheral nerves over long gaps." Cells Tissues Organs 176(1-3): 153-165.

Hinz, B., P. Pittet, et al. (2004). "Myofibroblast development is characterized by specific cell-cell adherens junctions. ." MBoC. 15(9): 4310-4320.

Holmes, W. and Y. J. Z. (1942). "Nerve regeneration after immediate and delayed suture." J. Anat. 77: 63-96.

Hsu, W. C., M. H. Spilker, et al. (2000). "Inhibition of conjunctival scarring and contraction by a porous collagen-glycosaminoglycan implant." Invest Ophthalmol Vis Sci 41(9): 2404-2411.

Ikeda, K., Y. Oda, et al. (1989). "Isolated Schwann cells can synthesize the basement membrane in vivo." J Electron Microsc (Tokyo) 38(4): 230-234.

Ivarsen A., L. T., and Moller-Pedersen T. (2003). "Characterisation of corneal fibrotic wound repair at the LASIK flap margin. ." Br J Ophthalmol. 87(10): 1272-1278.

J, I. J.-P., K. Jansen, et al. (2004). "Transection of peripheral nerves, bridging strategies and effect evaluation." Biomaterials 25(9): 1583-1592.

Jessen, K. R. and R. Mirsky (1999). "Schwann cells and their precursors emerge as major regulators of nerve development." Trends Neurosci 22(9): 402-410.

Jessen, K. R. and R. Mirsky (2005). "The origin and development of glial cells in peripheral nerves." Nat Rev Neurosci 6(9): 671-682.

Joseph, N. M., Y. S. Mukouyama, et al. (2004). "Neural crest stem cells undergo multilineage differentiation in developing peripheral nerves to generate endoneurial fibroblasts in addition to Schwann cells." Development 131(22): 5599-5612.

Kemp, S. W., S. Syed, et al. (2009). "Collagen nerve conduits promote enhanced axonal regeneration, schwann cell association, and neovascularization compared to silicone conduits." Tissue Eng Part A 15(8): 1975-1988.

Kerns, J. M. (2008). "The microstructure of peripheral nerves." Tech. REg. Anesth. Pain Manag. 12: 127-133.

Kimura, K., M. Ito, et al. (1996). "Regulation of myosin phosphatase by Rho and Rho-associated kinase (Rho-kinase). ." Science 273(5272): 245-248.

Kiviat, M. D., Ross R., and Ansell J. S. (1973). "Smooth muscle regeneration in the ureter." Am. J. Pathol. 72: 403-416.

Knight, C. G., Morton, L. F., Peachey, A. R., Tuckwell, D. S., Farndale, R. W. & Barnes, M. J. (2000). "The collagen-binding A-domains of integrins a1b1 and a2b1 recognize the same specific amino acid sequence, GFOGER, in native (triple-helical) collagens." J. Biol. Chem. 275: 35–40.

Krishnan K.G., W. P. A., Muller A., Grevers G., and Steiger H.J. (2000). "Closure of recurrent frontal skull base defects with vascularized flaps -- a technical case report. ." Acta Neurochir (Wien). 142(12): 1353-1358.

Landon, D. N. (1976). The PN. London, Chapman and Hall.

Levine D., R. D. C., Milner T.A., Breuss J.M., Fallon J.T., and Schnapp L.M. (2000). "Expression of the integrin alpha8beta1 during pulmonary and hepatic fibrosis. ." Am J Pathol. 156 (6): 1927-1935.

Longo, F. M., E. G. Hayman, et al. (1984). "Neurite-promoting factors and extracellular matrix components accumulating in vivo within nerve regeneration chambers." Brain Res 309(1): 105-117.

Lorenz, H. P. and N. S. Adzick (1993). "Scarless skin wound repair in the fetus. ." West J. Med. 159: 350-355.

Lundborg, G., L. Dahlin, et al. (1994). "Trophism, tropism, and specificity in nerve regeneration." J Reconstr Microsurg 10(5): 345-354.

Martin, P. (1996). "Wound healing: Aiming for perfect skin regeneration." Science 276: 75-81.

Martinez-Hernandez, A. (1998). Repair, regeneration, and fibrosis. Pathology. F. J. L. Rubin E. Philadelphia, PA, J.B. Lippincott-Raven: 66--95.

Mast, B. A., N. J.M., et al. (1992). Tissue repair in the mammalian fetus, . Wound Healing: Biochemical and Clinical Aspects, . I. K. Cohen, Diegelmann R. F. and Lindblad W. J. Philadelphia, PA, W. B. Saunders Company.

Muller, H., L. R. Williams, et al. (1987). "Nerve regeneration chamber: evaluation of exogenous agents applied by multiple injections." Brain Res 413(2): 320-326.

Murphy, G. F., D. P. Orgill, et al. (1990). "Partial dermal regeneration is induced by biodegradable collagen-glycosaminoglycan grafts." Lab Invest 62(3): 305-313.

Oppenheimer, R. and J. F. Hinman (1955). "Ureteral regeneration: Contracture vs. hyperplasia of smooth muscle." J. Urol. 74: 476-484.

Parmantier, E., B. Lynn, et al. (1999). "Schwann cell-derived Desert hedgehog controls the development of peripheral nerve sheaths." Neuron 23(4): 713-724.

Peacock Jr, E. E. (1984). Wound healing and wound care. Principles of Surgery S. I. Schwartz, G. T. Shires, F. C. Spencer and Storer E. H. New York, NY, McGraw-Hill.

Puolakkainen, P. A., T. D.R., et al. (1995). "The enhancement in wound healing by transforming growth factor-□1 (TGF- □1) depends on the topical delivery system." J. Surg. Res. 58(321-329).

Racine-Samson, L., D. C. Rockey, et al. (1997). "The role of alpha1beta1 integrin in wound contraction. A quantitative analysis of liver myofibroblasts in vivo and in primary culture." J. Biol. Chem. 272: 30911-30917.

Ramirez A.T., S. H. S., Schwartz M.S., Mooty J., Pearson E., and Raben M.S. (1969). Surg Gynecol Obstet. 128(2): 283-293.

Rudolph, R., J. Abraham, et al. (1978). "Myofibroblasts and free silicon around breast implants. ." Plast. Reconstr. Surg. 62: 185-196.

Rudolph, R., Van de Berg J., and Ehrlich P. (1992). Wound contraction and scar contracture Wound Healing: Biochemical and Clinical Aspects. I. K. Cohen, Diegelmann R. F. and Lindblad W. J. . Philadelphia, PA, W. B. Saunders Company: 96-114.

Schmidt M.R., M. M., Kristiansen S.B., Andersen H.R., and Falk E. ((2004)). "The natural history of collagen and alpha-actin expression after coronary angioplasty. ." Cardiovasc Pathol 13(5): 260-267.

Serini, G., M.-L. Bochaton-Piallat, et al. (1998). "The fibronectin domain ED-A is crucial for myofibroblastic phenotype induction by transforming growth factor-beta1." J. Cell Biol. 142: 873-881.

Spilker, M. H. (2000). Peripheral nerve regeneration through tubular devices. . Cambridge, MA., Massachusetts Institute of Technology, . Ph.D.

Stenn, K. S. a. M. R. (1992). Epithelialization. Wound Healing: Biochemical and Clinical Aspects. D. R. F. Cohen I.K., Lindblad W.J. Philadelphia, PA, Saunders: 115--127.

Stocum, D. L. (1995). Wound Repair, Regeneration and Artificial Tissues. Austin, TX, R.G. Landes Co.

Sunderland, S. (1990). "The Anatomy and Pathology of Nerve Injury. ." Muscle & Nerve 13(771-784).

Terzis, J. K. (1987). Microreconstruction of Nerve Injuries. Philadelphia, PA. , W.B. Saunders.

Thomas, P. K. (1963). "The connective tissue of peripheral nerve: an electron microscope study." J Anat 97: 35-44.

Tomasek, J. J., G. Gabbiani, et al. (2002). "Myofibroblasts and mechano-regulation of connective tissue remodelling." Nat Rev Mol Cell Biol 3(5): 349-363.

Tomasek, J. J., M. B. Vaughan, et al. (2006). "Contraction of myofibroblasts in granulation tissue is dependent on Rho/Rho kinase/myosin light chain phosphatase activity." Wound Repair Regen 14(3): 313-320.

Troxel, K. (1994). Delay of skin wound contraction by porous collagen-GAG matrices. Cambridge, MA, Massachusetts Institute of Technology, . PhD.

Uitto J., M. A., and McGrath J. (1996). The dermal-epidermal basement membrane zone in cutaneous wound healing. The Molecular and Cellular Biology of Wound Repair. R. A. F. Clark. New York, Plenum: 513--560.

Unterhauser FN, B. U., Zeichen J., and Weiler A. (2004). "Alpha-smooth muscle actin containing contractile fibroblastic cells in human knee arthrofibrosis tissue. ." Arch Orthop Trauma Surg 124(9): 585-591.

Weiss, P. (1944). "The technology of nerve regeneration: A review. Sutureless tabulation and related methods of nerve repair." J. Neurosurg. 1: 400-450.

Weiss, P. a. T. A. C. (1944). "Further experimental evidence against "neurotropism" in nerve regeneration. ." J. Exp. Zool. 95: 233-257.

Wiberg, M. and G. Terenghi (2003). "Will it be possible to produce peripheral nerves?" Surg Technol Int 11: 303-310.

Wikipedia. (2011). "The Human Nervous System." Retrieved April 24, 2011, from **http://en.wikipedia.org/wiki/File:Nervous_system_diagram.png**.

Williams, H. B. (1984). "The painful stump neuroma and its treatment." Clin Plast Surg 11(1): 79-84.

Williams, L. R., N. Danielsen, et al. (1987). "Exogenous matrix precursors promote functional nerve regeneration across a 15-mm gap within a silicone chamber in the rat." J Comp Neurol 264(2): 284-290.

Williams, L. R., F. M. Longo, et al. (1983). "Spatial-temporal progress of peripheral nerve regeneration within a silicone chamber: parameters for a bioassay." J Comp Neurol 218(4): 460-470.

Williams, L. R., H. C. Powell, et al. (1984). "Competence of nerve tissue as distal insert promoting nerve regeneration in a silicone chamber." Brain Res 293(2): 201-211.

Williams, L. R. and S. Varon (1985). "Modification of fibrin matrix formation in situ enhances nerve regeneration in silicone chambers." J Comp Neurol 231(2): 209-220.

Wilson, C. J. a. D. L. E. (1988). "An examination of the mechanism of ligament contracture. ." Clin. Orthop. 227: 286-291.

Winter, G. D. (1972). Epidermal regeneration studied in the domestic pig. Epidermal Wound Healing. H. L. a. R. D. T. Maibach. Chicago, IL, Year Book Medical Publishers: 71--112.

Wong T.T.L., D. J. T., Crowston J.G., and Khaw P.T. (2004). " MMP inhibition prevents human lens epithelial cell migration and contraction of the lens capsule. ." Br J Ophthalmol 88(7): 868-872.

Yannas I.V., O. D. P., Silver J., Norregaard T.V., Zervas N.T., Schoene W.C. (1987). Regeneration of sciatic nerve across 15mm gap by use of a polymeric template. Advances in Biomedical Polymers. C. Gebelein. New York, Plenum Publishing Corporation: 1-9.

Yannas, I. V. (1997). "Models of organ regeneration processes induced by templates. ." Ann. N. Y. Acad. Sci. 831: 280-293.

Yannas, I. V. (2001). Tissue and organ regeneration in adults. New York, Springer.

Yannas, I. V. (2005). Regenerative Medicine II: preclinical and clinical applications, Springer.

Yannas, I. V. (2005). "Similarities and differences between induced organ regeneration in adults and early foetal regeneration." J R Soc Interface 2(5): 403-417.

Yannas, I. V., J. F. Burke, et al. (1980). "Design of an artificial skin II: Control of chemical composition. ." J. Biomed. Mater. Res. 14: 107-131.

Yannas, I. V., J. F. Burke, et al. (1982). "Wound tissue can utilize a polymeric template to synthesize a functional extension of skin." Science 215(4529): 174-176.

Yannas, I. V., J. F. Burke, et al. (1981). "Prompt, long-term functional replacement of skin." Trans Am Soc Artif Intern Organs 27: 19-23.

Yannas, I. V., C. J., et al. (1996). "Wound contraction and scar synthesis during development of the amphibian Rana catesbeiana. ." Wound Rep. Reg. 4: 31-41.

Yannas, I. V., E. Lee, et al. (1989). "Synthesis and characterization of a model extracellular matrix that induces partial regeneration of adult mammalian skin." Proc Natl Acad Sci U S A 86(3): 933-937.

Yannas, I. V., Orgill D.P., Silver J., Norregaard T.V., Zervas N.T., and Schoene W.C. (1985). "Polymeric template facilitates regeneration of sciatic nerve across 15 mm gap. ." Trans. Soc. Biomater. 8: 146.

Yannas, I. V., D. P. Orgill, et al. (2011). "Template for skin regeneration." Plast Reconstr Surg 127 Suppl 1: 60S-70S.

Yannas, I. V., M. Zhang, et al. (2007). "Standardized criterion to analyze and directly compare various materials and models for peripheral nerve regeneration." J Biomater Sci Polym Ed 18(8): 943-966.

Zeinoun T., N., S., Sourov, N., and Luomanen, M (2001). " Myofibroblasts in healing laser excision wounds." Lasers Surg. Med. 28(1): 74-79.

Zhang, M. and I. V. Yannas (2005). "Peripheral nerve regeneration." Adv Biochem Eng Biotechnol 94: 67-89.

2

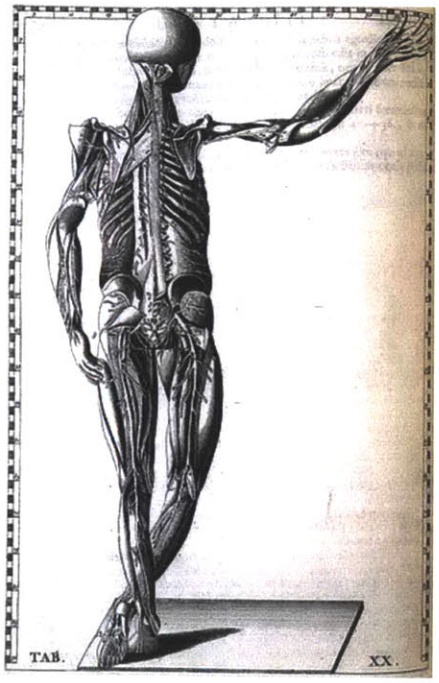

Peripheral Nervous System

Tabulae anatomicae clarissimi viri, 1722.

Bartolomeo Eustachi (1520?-1574)

2

Cell-mediated Contraction Impairs Axonal Regeneration After Sciatic Neurotmesis

2.1 Introduction

Cell-mediated mechanical forces drive acute closure of severe wounds in adult mammalian organs, including the sciatic nerve following neurotmesis. A thick, cohesive capsule of myofibroblasts (MFBs) expressing the contractile α-smooth muscle actin (α-SMA) isoform spontaneously forms around the perimeter of non-tubulated nerve stumps in the first 1-3 weeks after injury (Chamberlain, Yannas et al. 2000). These cells express the same phenotype implicated in pathological contracture, organ fibrosis, and the driving force in wound closure of spontaneously healing skin wounds (Yannas 2001; Tomasek, Gabbiani et al. 2002; Hinz 2007). The defect closes rapidly in the absence of experimental intervention via a combination of cell-mediated compression of the nerve stumps (contraction) and collagen synthesis (scar formation) (Chamberlain, Yannas et al. 2000), often leading to a painful neuroma (Foltan, Klima et al. 2008).

While the autograft remains the clinical gold standard in treatment of limb paralysis following severe trauma across long gaps, the nerve chamber model (Lundborg, Longo et al. 1982) has dominated the experimental study of PN regeneration in animal models in recent years. Transected nerve stumps, when inserted into non-neural conduits, or nerve guides, are capable of axonal recovery across gaps lengths of up to about 15 mm in the rat single anastomosis model. The earliest nerve guides were made of biodurable (non-degradable) silicone (Williams, Longo et al. 1983) and lead to nerves of relatively poor quality with thick contractile capsules of MFBs (50 cell layers thick). Inserting the stumps of a transected nerve into degradable type I collagen conduit yields both a better quality regenerate and a thinner contractile capsule (~1 cell layer thick) (Chamberlain, Yannas et al. 2000).

State-of-the art research in neural engineering utilizes biodegradable tubes made of synthetic and/or naturally-occurring polymers with a wide-range of chemical compositions, porosities, and degradation rates, used alone or with various cell types as well as with bound or diffusible regulators (Jiang, Lim et al. 2010), all of which exhibit a wide range of regenerative activity.

The variable regenerative activity of nerve guides is often attributed to their ability to form or maintain concentration gradients of neurotrophic factors between the stumps, physical guidance cues provided by tracks of solid or semisolid surfaces for cells to migrate between the stumps, or enhanced neovascularization of the immature regenerate (Chen, Yu et al. 2007; Deumens, Bozkurt et al. 2010).

Analysis of regeneration mechanisms using normalized data from numerous experimental studies using the nerve chamber model suggests that axonal regeneration is downregulated by experimental configurations that permit formation of a contractile cell (myofibroblast) capsule around the regenerating nerve that appears to restrict growth of a nerve trunk by application of circumferential mechanical forces (pressure cuff theory) and enhanced by configurations that favor synthesis of bands of Büngner, linear columns of Schwann cells and basement membrane that serve as tracks for oriented axon elongation (Zhang and Yannas 2005; Yannas, Zhang et al. 2007). There is little information describing the effect of the contractile capsule formation on axonal regeneration outcome.

Previously a homologous series of collagen-based nerve guides varying in degradation rate (but identical in other structural and chemical properties) led to the identification of an optimal scaffold degradation rate resulting in a maximum quality of axonal regeneration after sciatic neurotmesis at 9 weeks (Harley, Spilker et al, 2004). In the present work we provide for the first time a quantitative link between contraction of nerve stumps by a contractile capsule and the outcome of axonal regeneration using a similar well-characterized homologous series of collagen-based nerve guides, a demanding model of PN regeneration, and histomorphometry.

2.1.1 Project Goal & Major Findings

The goal of this study was to evaluate the quantitative effect of capsule thickness, δ, on the quality of regeneration, Q. A homologous series of type I collagen nerve

conduits was used that varies in degradation rate in a demanding model of peripheral nerve regeneration (rat sciatic neurotmesis, 15 mm gap).

The study finds that collagen tubes of intermediate degradation rate minimize capsule thickness, δ, while maximizing histomorphometric quality of regeneration, Q. A negative, statistically significant correlation exists between capsule thickness and several Q metrics, including myelinated area, number of myelinated fibers, and number of large-diameter myelinated fibers (A-fibers).

2.2 Materials and Methods

2.2.1 Synthesis and Characterization of a Homologous Series of Collagen Tubes that Vary in Degradation Rate

Collagen Tube Synthesis

A homologous series of 5 % solid content (w/w) type I collagen nerve conduits were prepared as described previously (Harley, Spilker et al, 2004). Briefly, 0.25 g of type I microfibrillar collagen (Integra Life Sciences, Plainsboro, NJ) was solubilized in 0.5 *M* acetic acid solution and mixed well via syringes and a connecting luer lock adapter until a homogenous slurry was achieved. The end of the syringe was sealed to prevent moisture loss and the collagen fibers were left to swell at room temperature for 3 hours.

Following swelling, the mixture was degassed via centrifugation for 1 hour at 4500 rpm. The degassed suspension was injected into a custom-designed, two-leaf Teflon and stainless steel mold with 6 circular lanes of approximately X mm diameter (for schematic see **Appendix B.1**). Teflon-coated stainless steel mandrels were inserted carefully into the slurry-filled mold and end caps were used to center the mandrels in the lanes. The slurry and mold were placed in an industrial freeze dryer (VirTis) pre-cooled to -40 °C and frozen for 1 hour at atmospheric pressure before the mold was removed from the freeze dryer and the frozen tubes were separated from the mold. The tubes were re-inserted into the machine and sublimated for 17 hours at 0 °C and 100 mTorr.

Following sublimation, all collagen tubes were removed from the freeze dryer and stored in a dessicator in sealed aluminum foil packets, protected from light.

Collagen tubes were inspected macroscopically for quality (including the uniformity of wall thickness, the uniformity of surface topography, and the absence of large pore defects) and acceptable samples were cut to the desired length for implantation (21 mm) using a no. 15 scalpel under sterile conditions. Detailed procedures for the fabrication of collagen tubes are found in **Appendix B.1**.

Cross-linking Treatments

A homologous series of type I collagen tubes was made using identical cross-linking treatments from a previous study (Harley, Spilker et al, 2004). To generate a homologous series of collagen tubes that vary in degradation rate, 21 mm-long, 5% (w/w) type I collagen tubes were subjected to either dehydrothermal (DHT) cross-linking treatment or to the hetero-bifunctional coupling agent 1-ethyl-3-(3-dimethylaminopropyl) carbodiimide (EDAC) in the presence of the N-hydroxysuccinimide (NHS) catalyst as follows (Harley, Spilker et al, 2004).

Group	Cross-linking Treatment	Duration	Temperature
A	None	N/A	N/A
B	DHT	24 hrs	90 ° C
C	DHT	48 hrs	90 ° C
D	DHT	48 hrs	120 ° C
E	EDAC/NHS	3.5 hrs	24 ° C

Table 2.1 Cross-linking Treatments for Homologous Series of Collagen Tubes. Degree of cross-linking increases from A-E.

Cross-linking is the process of chemically joining two or more molecules via a covalent bond. Dehydrothermal treatment (DHT) is a condensation reaction between carboxylic group (or hydroxyl group) and the primary amino group of the lysyl residue. EDAC covalently binds the collagen to collagen via nucleophilic attack of primary amines on the highly reactive lysine residues on collagen. Briefly, for DHT the freeze-dried tubes were placed under vacuum (50 mTorr at the specified conditions (**Table**

2.1). The EDAC process was carried out on the scaffolds according to previously described methods (Harley, Spilker et al, 2004). A 5:2:1 ratio of EDAC: NHS: COOH (1-ethyl-3-(3-dimethylaminopropyl) carbodimide: N-hydroxysuccinimide: carboxylic acid) was used for the current study. Briefly, the scaffolds were hydrated in deionized water and the required amount of EDAC/NHS solution was then mixed into the deionized water and the scaffold was maintained in this solution for 3.5 hrs. Tubes were then rinsed in PBS three times for 30 min each. Prior to implantation, tubes not sterilized via DHT were rinsed in 70% ethanol as described previously (Harley, Spilker et al, 2004). Detailed procedures for the cross-linking of collagen tubes may be found in **Appendix B.2**.

2.2.2 Tube Characterization

Scanning electron microscopy (SEM; Leo VP438 SEM Leo Electron Microscopy Inc., Thornwood, NY) was used to study the pore structure of the homologous series of collagen tubes. Specimens of tube 5 mm in length were cut at random locations in the scaffolds using a # 11 scalpel and these samples were cut in half along the length to permit visualization of the pore distribution in the tube wall. Specimens were mounted on an aluminum holder using conductive tape; the specimens were not gold coated. A backscattered electron detector was used under variable pressure mode to obtain the images.

The degradation rate of the cross-linked type I collagen nerve conduits was determined by a colorimetric procedure after incubating 5 mm long samples of the cross-linked tubes for 2 hr at 37 deg C in a 0.1 mg/mL solution of bacterial type I collagenase from Clostridium histolyticum (210 u/mg, #S6B8578, Worthington) in a buffer (ph 7.4), a modification of an existing method (Sigma-Aldrich 1996). Previous studies have shown that the use of bacterial collagenase as an *in vitro* empirical screening method provides a rank ordering of collagen implants according to degradation rate that agrees well with *in vivo* observations (Yannas, Burke et al. 1975; Yannas, Lee et al. 1989). Detailed procedures for the *in vitro* characterization of collagen tubes may be found in **Appendix B.3.**

2.2.3 Animal Model

NIH guidelines for the care and use of laboratory animals (NIH Publication No. 85-23 Rev. 1985) were observed. Twenty adult female Lewis rats (Charles River Laboratories, Wilmington, Mass., USA), 175–200 g, were used in this study. The Lewis strain of rat was chosen because of its resistance to autotomy, or self-mutilation, following sciatic nerve transection (Carr, Best et al. 1992). The animals implanted per group were as follows Device A (n=4), Device B (n=4), Device C (n=5), Device D (n=4), Device E (n=3). All surgical procedures were performed in an aseptic environment, following a technique that had been previously described (Chamberlain, Yannas et al. 1998); Harley, Spilker et al, 2004). A 50 mg/kg dosage of sodium pentobarbital (50 mg/ml Nembutal sodium solution; Parke-Davis, Detroit, Mich., USA) was injected intraperitoneally to anesthetize each animal. The surgical area was shaved with animal clippers and cleansed with a providone-iodine sponge once the animal was fully anesthetized. The animal was placed in the prone position on a surgical board, with hind limbs held in 30° abduction. A 4 cm skin incision was made in the left leg parallel to and just posterior of the femur, exposing the muscle. The muscle and the fascia surrounding the sciatic nerve were dissected away so that the nerve was completely exposed and free from constraint between the sciatic notch and the distal bifurcation of the sciatic nerve. The exposed sciatic nerve was further anesthetized topically using a few drops of 1% lidocaine placed directly on the nerve at the transection site.

The left sciatic nerve was transected at the midpoint of the femur, midway between the sciatic notch and the distal bifurcation, using a fresh No. 11 scalpel blade. The collagen tube was placed in the gap, and the proximal and distal nerve stumps were inserted 3 mm into each end of the tube, leaving a 15 mm gap in the center between the stumps. The nerve stumps were secured inside the tube using two 10-0 nylon sutures (Ethicon, Somerville, N.J., USA) at each end. The lumen of each tube was filled with excess sterile saline and the muscle and skin were closed using 4-0 Vicryl sutures (Ethicon) and skin staples (Roboz Surgical Instrument, Rockville, Md., USA).

The animals were returned to their cages and monitored until fully alert. Postoperatively, the animals were treated with subcutaneous injections Lactated Ringer's solution to combat fluid loss, Ketofen as an analgesic, and Cefazolin as an

antibiotic. Ketofen and Cefazolin were continued once a day for the first 2 days following surgery and then as needed for the duration of the experiment. The animals were housed on wood chip bedding in a controlled environment with 12-hour on-off light cycles in separate cages for the duration of the experiment. Food and water were available ad libitum. The animals were monitored daily for signs of any abnormal behavior such as insufficient grooming, lack of appetite, aggressive behavior, or the appearance of autotomy. Detailed description of the animal surgery may be found in **Appendix B.4**.

All animals were sacrificed at 9 weeks postoperatively by carbon dioxide inhalation. The operated site was reopened, and all sciatic nerve tissue between the sciatic notch and the distal bifurcation was removed along with any tissue bridging the gap between the transected nerve stumps and any remaining tube; the entire tissue block was then prepared for histomorphometric analysis.

2.2.4 Histomorphometry

Nine weeks after injury, each newly formed nerve trunk was segmented into contractile capsule, C, and regenerate, R and assayed as described in **Fig. 2.1**.

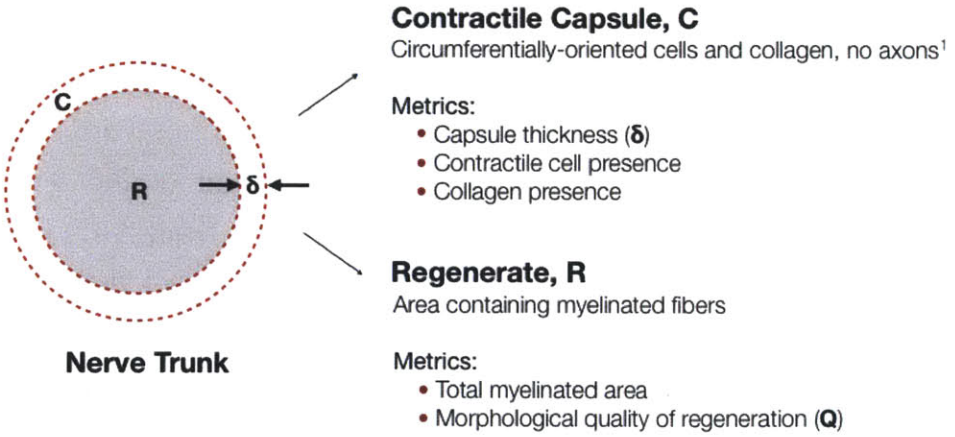

FIG. 2.1 OVERVIEW OF METRICS USED TO EVALUATE CONTRACTION AND QUALITY OF REGENERATION. Newly formed nerve trunks are segmented into contractile capsule, C, and regenerate, R.

Excised tissue was rinsed briefly in sterile saline and placed immediately in 4% paraformaldehyde (in 0.1 M sodium phosphate buffer) on ice. Regenerates were

photographed, and then the excised tissue was cut in half at the midpoint using a fresh # 11 scalpel.

The proximal portion was kept in 4% paraformaldehyde (in 0.1 M sodium phosphate buffer) for 8 hours at 4 deg. C and then transferred to a 30% sucrose solution (in 0.1 M sodium phosphate buffer) overnight with mild shaking. Regenerates were immersed in Optimal Cutting Temperature (OCT) embedding polymer-filled molds, flash frozen in liquid nitrogen, and stored at -20 deg C until sectioning. For immunofluorescence and immunohistochemistry, frozen blocks were sectioned at 10 um thickness on a mictrotome and collected on Superfrost® Plus Gold Slides.

Capsules were defined as structures containing collagen, circumferentially oriented contractile cells, and no axons. Capsules were analyzed using routine Gomori Trichrome-Aniline Blue staining of frozen sections was used to visualize collagen fibers. An immunofluorescence technique was used to permit visualization of myelinated fibers, contractile cells, and their nuclei on the same section. Briefly, frozen sections were allowed to air dry for 20 minutes, rinsed in Tris-buffered saline (TBS), and stained for 15 minutes with a cocktail of FluoroMyelin™ (Invitrogen), rhodamine-phalloidin (Invitrogen), and DAPI (Invitrogen). Sections were rinsed again in TBS and mounted with FluoroGel (Vector Labs). Differentiated myofibroblasts were labeled using routine immunohistochemistry and a primary antibody directed against the α-smooth muscle actin isoform (1:400, clone 1A4 IgG2a istoype). Images were captured on a Nikon E800 upright microscope using either Openlab acquisition software and a Hammamatsu C4742-95 camera (immunofluorescence) or Qimaging Color Micropublisher 3.3 CCD camera and software (immunohistochemistry). Detailed protocols for these procedures are included in **Appendix B.6**.

The regenerate is the area of the nerve trunk containing myelinated fibers. The quality of regeneration was assessed using the distal portion of the nerve trunk which was fixed in Yanoff's fixative (0.01 M monobasic sodium phosphate, 0.06 M dibasic sodium phosphate, 2% formaldehyde, and 0.5% glutaraldehyde) for 24 h, transferred into a 10% formalin solution for 24 h, and then stored in 70% ethanol at 4°C. The tissue was post-fixed in 1% osmium tetroxide (Sigma Aldrich Chemical Co.), and embedded in plastic resin (Poly/Bed® 812, Polysciences, Warrington, PA). The tissue sections for histomorphological analysis were prepared by sectioning the Epon-embedded samples

on an ultra microtome (Leica, Bensheim, Germany) at a 1 μm thickness; the sections were then mounted on standard slides. The sections were stained with toluidine blue (Fisher Scientific) to enhance the osmium tetroxide stain and cover-slipped with Permount (Fisher Scientific).

Low magnification-digitized images (Optronics Engineering) taken using the 10X objective were used in order to determine the area and perimeter of the regenerated nerves. High magnification images (100X objective) were used for the morphological characterization of the regenerated axons. A series of high magnification images were captured at locations across the tissue cross-section; the points for imaging were selected using a distribution map that provided equal representation from each of the quadrants of the tissue cross section. The total area of images captured and analyzed represented at least 20% of the total cross-sectional area of the nerve trunk. Previous analysis has shown that the randomly sampled collective image area need not be larger than 10% of the total nerve trunk cross-sectional area in order to obtain statistically representative results (Chamberlain, Yannas et al., 1998).

The digitized cross-sectional images were analyzed using the public domain NIH software ImageJ to determine the total area and perimeter of the regenerated nerve trunk as well as the number and morphological characteristics of regenerated nerve fibers (Chamberlain, Yannas et al., 1998; Harley, Spilker et al., 2004). Quantitative measurements of capsule thickness, δ, were made in 5 locations around the nerve trunk perimeter for each animal and averaged. Myelinated axons were counted and measured in each high magnification image to determine the density of axons. The total number of axons in a regenerated nerve trunk was calculated by multiplying the density of axons by the total nerve trunk area. For each myelinated nerve fiber (axon core and surrounding myelin sheath) ImageJ provides data describing the cross-sectional area and perimeter; nerve fiber diameter was calculated using the relation $Df = 4Af/Lf$ (Df = fiber diameter, Af = fiber cross-sectional area, Lf = fiber perimeter). This calculation allows for improved accuracy in calculating the average diameter for nerve fibers that are not perfectly circular or may have changed in shape as a result of histological processing. In addition, the total myelinated fiber area was determined by summing the areas of all myelinated axons in the analyzed sections; this value was used to calculate the N-Ratio of each regenerated nerve trunk. The N-Ratio is the ratio of the

total myelinated fiber area (the sum of the total axonal area of the nerve trunk) to the total nerve trunk area and is used as a measurement of the maturity of a regenerating nerve trunk (Vleggeert-Lankamp 2007); Chamberlain, Yannas et al., 1998; Harley, Spilker et al., 2004). Detailed protocol for histomorphometry techniques are included in **Appendix B.6**.

2.2.5 Statistics

Statistical significance was determined using Stata Data Analysis and Statistics Software (StataCorp, College Station, TX). One-way analysis of variance (ANOVA) was used to determine the effect of device identity (cross-linking treatment of collagen tubes) on capsule thickness, δ, and quality of regeneration, Q (regenerate area, total number of myelinated axons, average axon diameter, total number of large diameter axons, and N-ratio). Multiple comparisons were made with a Bonferroni post-hoc test, which controls conservatively for the family-wise error rate. Pairwise correlation analysis between δ and Q metrics was conducted using a Pearson product-moment correlation coefficient. In all cases, significance was accepted when $p < 0.05$.

2.3 Results

2.3.1 General Observations

The animals showed no signs of severe discomfort following the surgical procedures. No autotomy was observed, supporting previous conclusions (Carr, Best et al., 1992) and observations (Chamberlain, Yannas et al., 1998; Harley, Spilker et al, 2004) concerning the absence of self-mutilation following nerve transection in Lewis rats. There were no clinical signs of infection at the wound site for any of the animals. Eighteen of twenty animals formed a tissue cable reconnecting the transected nerve stumps. Two of the non-cross-linked tubes (Device A) did not form a reconnection (**Table 2.2**). Variable amounts of the collagen tubes remained across the homologous series at 9 weeks. Device A was completely degraded and in the instances when a tissue cable formed it was very thin and difficult to dissect from the surrounding fascia. Devices B and C seemed to be completely degraded and were the easiest to dissect from the surrounding fascia of all the tubes in the series. Device D was modestly degraded

near the stumps and the mass seemed to increase towards the center of the gap. Device E appeared to be non-degraded across the entire gap and seemed to be covered by a thick layer of fibrous tissue.

2.3.2. Pore Size Characterization of Collagen Tubes

During freeze-drying ice crystals nucleate in the collagen slurry and are subsequently removed by sublimation leaving void space (pores). Scanning electron micrographs (SEM, **Fig. 2.2**) show that the 5% tubes have porous walls and non-porous inner and outer layers. SEM images taken of cross sections of the tube wall along the radius of the tube (**Fig. 2.2**) and the long axis of the tube wall (not shown) and both reveal a homogenous, interconnected porous structure consisting of sheet-like struts with pores that are approximately 80 μm in diameter, in agreement with previous published reports (Harley, Spilker et al., 2004). The pore size did not appear to be

Group	Reconnection	Neuroma	Total	Scaffold presence at 9 weeks:
A	2	2	4	Degraded
B	4	0	4	Degraded
C	5	0	5	Degraded
D	4	0	4	Moderately degraded
E	3	0	3	Not degraded

Increased cross-link density,
Decreased degradation rate

Table 2.2 Macroscopic Outcomes of Regeneration for the Homologous Series of Collagen Devices. Observations made 9 weeks after implantation.

different along either axis of the tube. The pore size did not vary across the homologous series and the cross-linking treatments employed were not found to alter the pore structure of the tubes (Harley, Spilker et al., 2004). The inner lumen of the tube (**Fig. 2.2**) consisted of a solid, non-porous surface or film layer that was several microns thick. The outer shell of the tube had a similar appearance to the lumen and appeared to be a non-porous layer.

2.3.3. *In Vitro Degradation Rate of Collagen Tubes*

The cross-linking treatments utilized in this study yielded a homologous series with *in vitro* degradation rate measurements ranging from 13.38 to 1.412 μmol of peptides liberated, in the case of device A (non-cross-linked) and device E (EDAC-cross-linked), respectively (**Table 2.3, Fig. 2.3**). Device C measured an intermediate value of 11.51 μmol peptides liberated. Higher values indicate a larger concentration of peptides released during the collagenase digestion, and indicate a lower number of collagen cross-links present in the device and a faster degradation rate. Only devices A, C, and E of the homologous series were characterized in this assay.

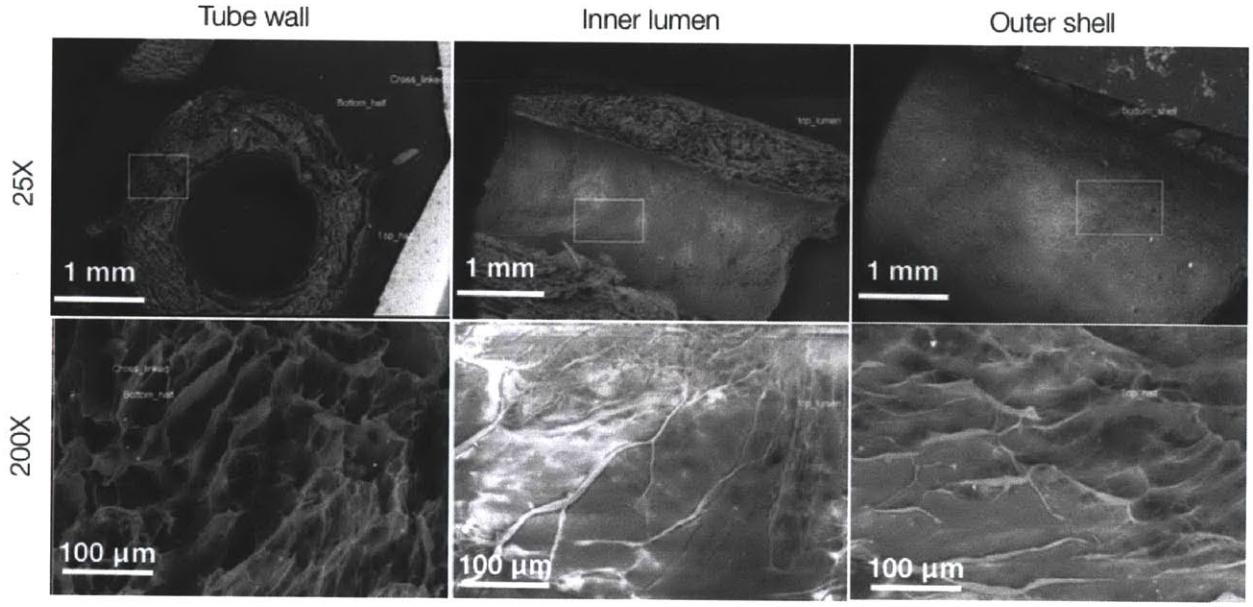

FIG. 2.2 STRUCTURE OF TYPE I COLLAGEN TUBES. SEM micrographs of 5% solids content collagen tubes show porous walls on the order of 80 μm with non-porous inner and outer surfaces.

A One-way between subjects Analysis of Variance (One-way ANOVA) was conducted to compare the effect of cross-linking treatment on μmol of peptides liberated. There was a significant effect of device identity on μmol of peptides at the $p < 0.05$ level for the three conditions [$F(2, 12) = 706.69$, $p = 0.0000$]. Post hoc comparisons using the Bonferroni test indicated mean μmol of peptides liberated was significantly different for devices A, C, and E ($p<0.000$). In vitro measurements of collagen device degradation rate using this method have been shown previously to correlate well with *in vivo* degradation behavior (Yannas et al., 1975).

2.3.4. *Contractile Capsule*

2.3.4.1. Mean Capsule Thickness, δ

Contractile capsules, defined as cohesive structures of circumferentially oriented cells and collagen and containing no axons, were readily visible around nerve

Device	μmol peptides liberated			n
A	13.38	±	0.30	5
C	11.51	±	0.29	5
E	1.41	±	0.01	5

Table 2.3. In Vitro Measurements of Degradation Rate of Homologous Series of Collagen Devices (mean ± SEM) in Response to Bacterial Collagenase. Mean ± SEM.

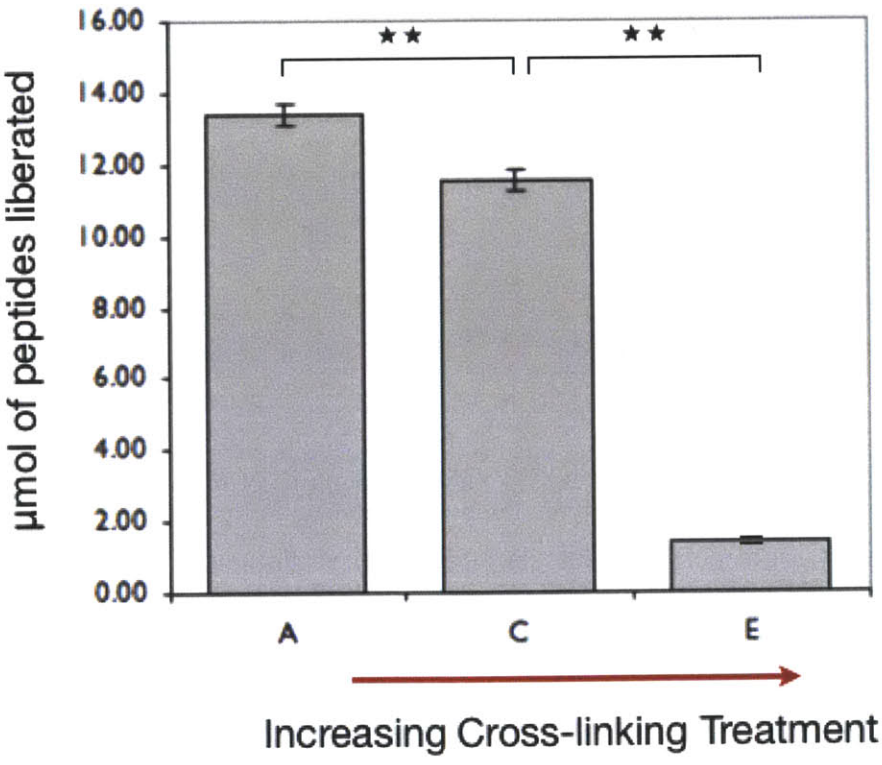

Fig. 2.3: In Vitro Measurements of Degradation Rate of Homologous Series of Collagen Devices in Response to Bacterial Collagenase. Mean ± SEM. Symbols: ns, $p > 0.05$; ★, $p<0.05$; ★★, $p<0.01$.

regenerates at the midpoint of the nerve gap at 9 weeks (**Fig. 2.4**) and varied greatly in thickness between the tubes in the homologous series. Collagen tubes minimized mean capsule thickness, δ, with intermediate cross-linking treatment (Device C) to 22 $\pm$ 2 μm, measured at the midpoint of nerve gap 9 weeks post-implantation. Non-cross-linked tubes (Device A) and highly cross-linked tubes (Device E) led to thicker capsules of 98 $\pm$ 9 μm and 73 $\pm$ 18 μm, respectively (**Table 2.4, Fig. 2.4**).

A one-way between subjects ANOVA was conducted to compare the effect of device identity (A-E) on capsule thickness, δ. There was a significant effect of device identity on δ at the $p<0.05$ level for the five conditions [$F(4, 13) = 8.73$, $p = 0.0012$]. Post hoc comparisons using the Bonferroni test indicated mean δ for device A was significantly different from mean δ for devices B, C, and D ($0.000 < p < 0.002$) and that mean δ for device E was significantly different from mean δ for devices B, C, and D ($0.005 < p < 0.033$). Mean δ did not significantly differ between devices A and E ($p < 0.898$) or between devices B, C, and D ($p < 1.000$).

2.3.4.2. Contractile Capsule Histology

The capsule of a normal sciatic nerve is a continuous, single layer of perineurial cells surrounding the myelinated fibers of the endoneurium, which are visible in **Fig. 2.4.f** and **Fig. 2.5**. A normal capsule has nominal collagen content and cells of the thin perineurium have prominent cytoskeletal features that stain positively for the contractile filament α-SMA. In the current study, thinner capsules formed around nerves regenerated with intermediately cross-linked tubes (Device C) with diminished perineurial collagen staining and fewer circumferentially oriented, F-actin-+ contractile capsular cells. Highly cross-linked tubes (Device E) result in significantly thicker capsules with prominent collagen staining (blue), and many circumferentially oriented, F-actin (+) and α-SMA (+) capsular cells. Thick capsules contained layers of collagen and circumferentially oriented cells that were positive for both contractile filaments F-actin and α-SMA (**Fig. 2.6**). Both F-actin and α-SMA staining was more prominent in cells located at the outermost portion of the capsules that formed in the presence of highly cross-linked tubes (Device E).

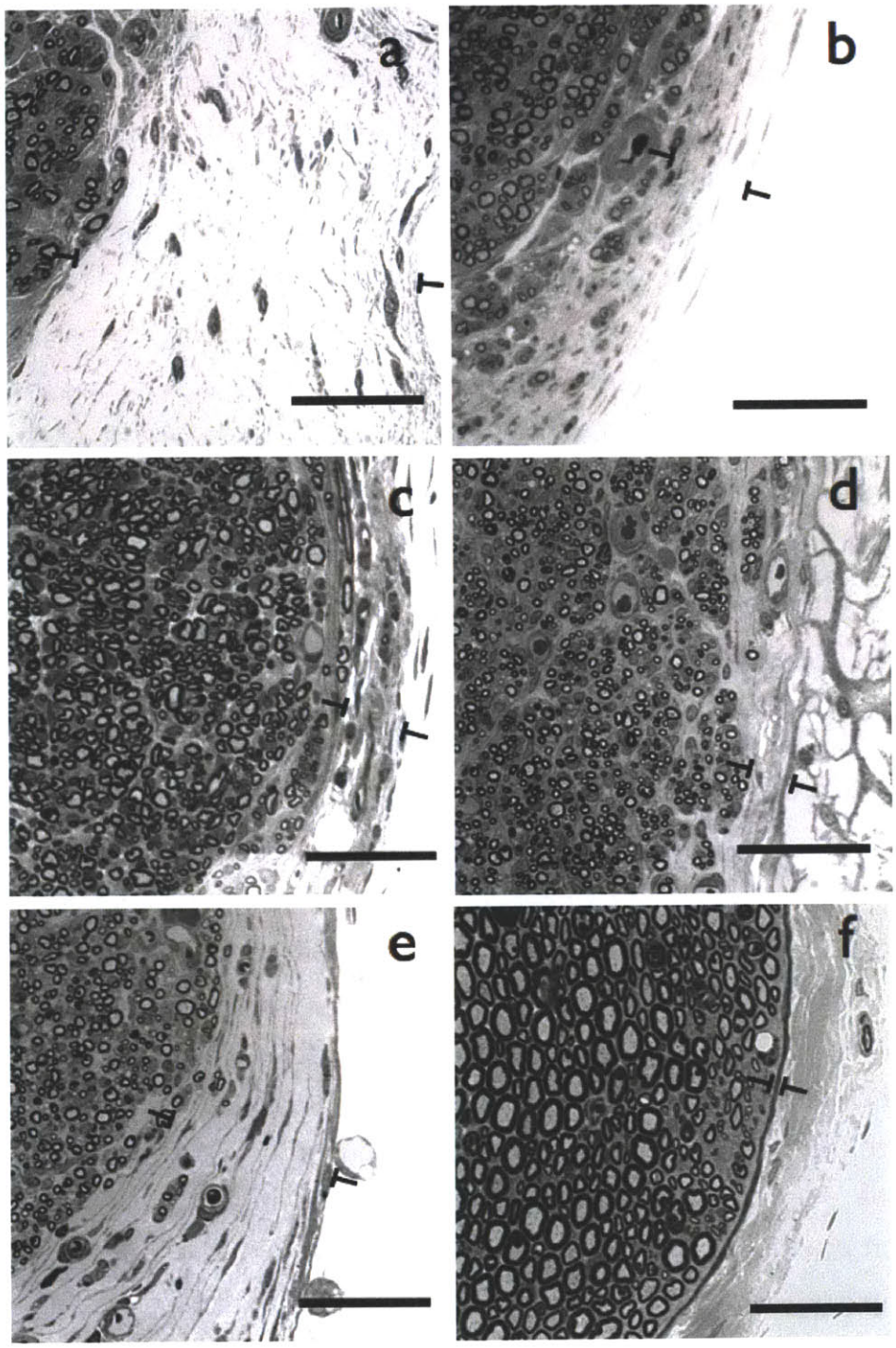

FIG. 2.4. COLLAGEN SCAFFOLDS WITH INTERMEDIATE CROSS-LINKING TREATMENT MINIMIZE CAPSULE THICKNESS. The capsule (bars) of a normal sciatic nerve **(f)** is a continuous, single layer of perineurial cells surrounding the myelinated fibers of the endoneurium, which are visible in, *black*, toluidine blue-stained, osmium-tetroxide-fixed semi-thin sections. Nine weeks post-transection, nerves regenerated with collagen tubes of intermediate cross-linking treatments (**b, c, d** Devices B, C, and D) yielded larger area regenerates with significantly more myelinated axons and a higher number of large diameter axons (A-fibers) than nerves regenerated with collagen tubes of no (**a**, Device A) or high (**e**, Device E) cross-linking treatment, measured at the midpoint of a 15 mm gap. Scale bars: 50 μm.

Device	δ, μm			n
A	98	±	9	2
B	36	±	6	4
C	22	±	2	5
D	31	±	5	4
E	73	±	18	3

Table 2.4. Morphological Measurements (mean ± SEM) of Contractile Capsule Thickness, δ, at 9 weeks post-implantation, midpoint of gap.

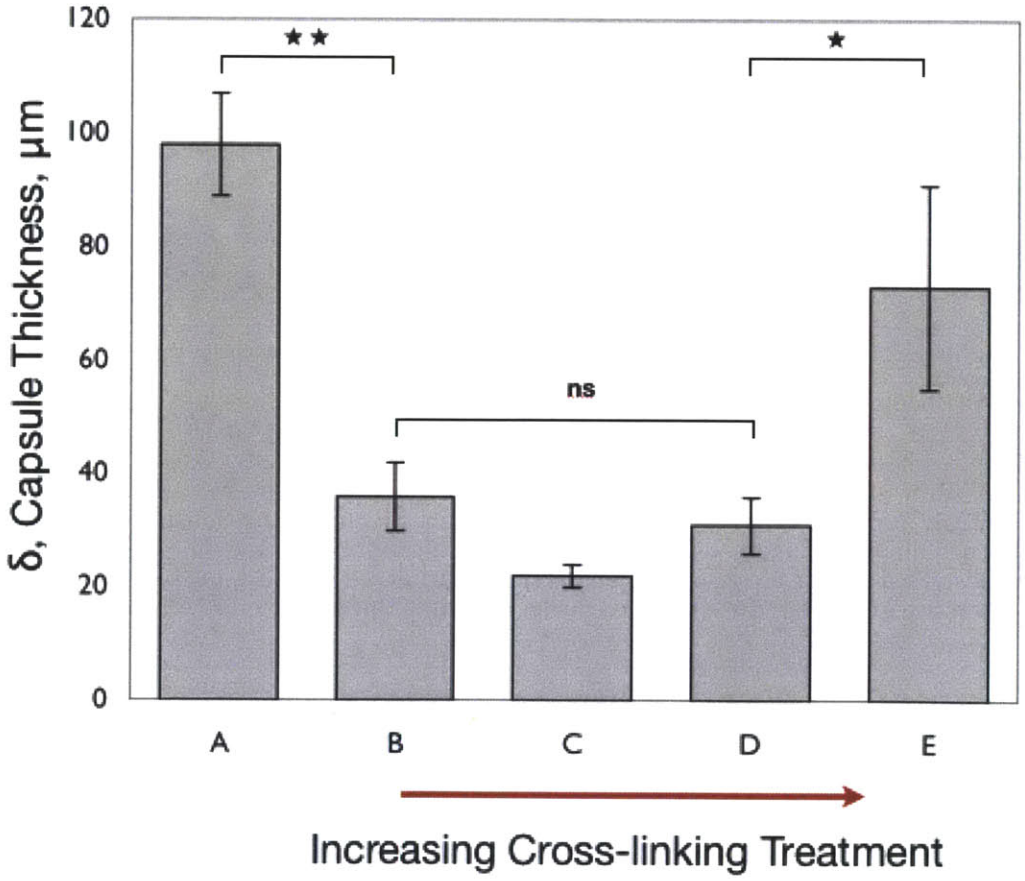

FIG. 2.5. COLLAGEN TUBES OF INTERMEDIATE DEGRADATION RATE MINIMIZE CAPSULE THICKNESS. Morphological measurements of contractile capsule thickness, δ, at 9 weeks post-implantation, midpoint of gap. Mean ± SEM. Symbols: ns, $p > 0.05$; ★, $p<0.05$; ★★, $p<0.01$.

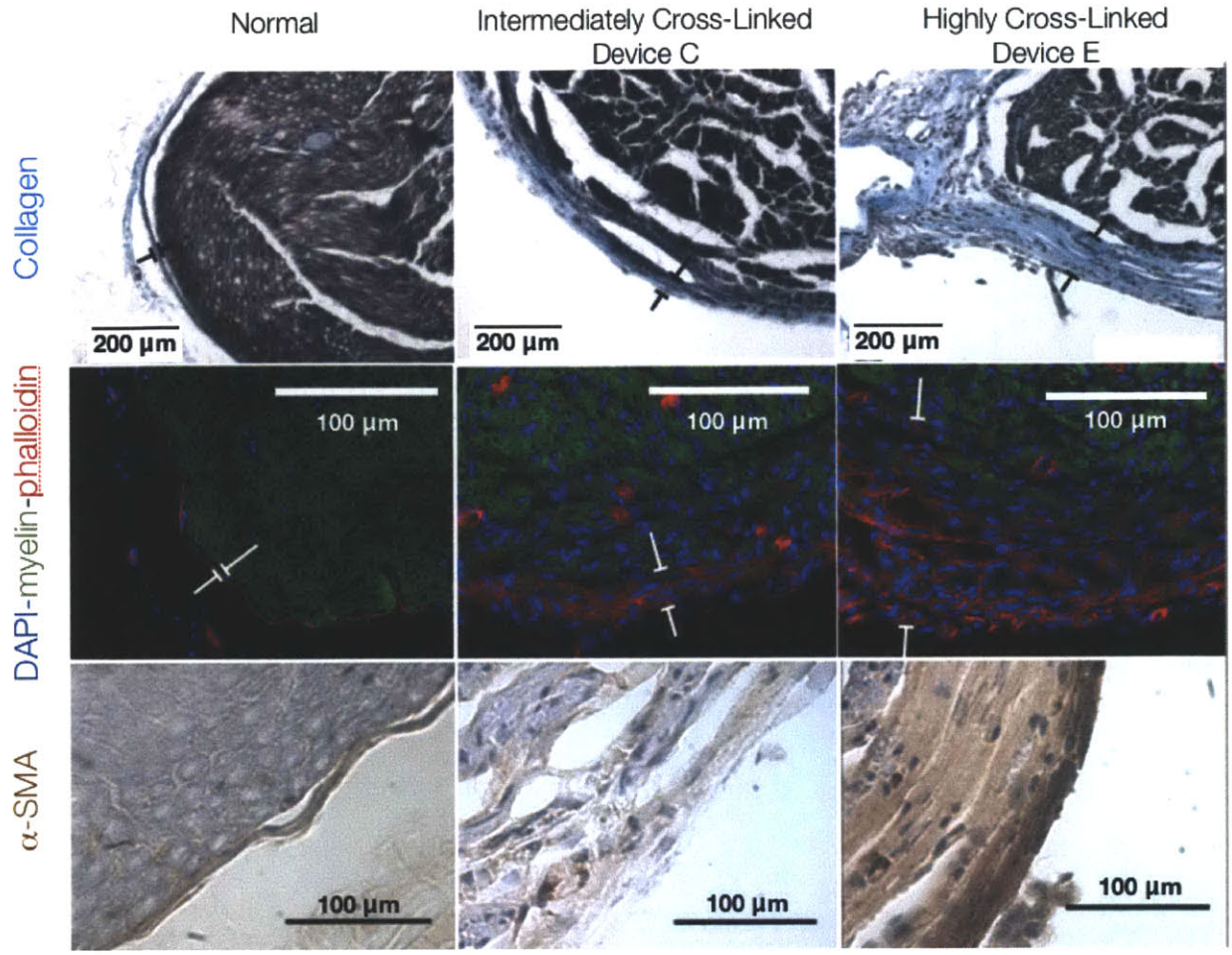

FIG. 2.6. INTERMEDIATELY CROSS-LINKED COLLAGEN DEVICES YIELD THINNER CAPSULES WITH BOTH DIMINISHED COLLAGEN CONTENT AND FEWER CONTRACTILE CELLS. Thinner capsules (bars) form around nerves regenerated with intermediately cross-linked tubes (Device C) at 9 weeks post-neurotmesis with less perineurial collagen staining and fewer circumferentially-oriented, F-actin-+ (red) and α-SMA (+) (brown) contractile capsular cells. Highly cross-linked tubes (Device E) result in significantly thicker capsules with prominent collagen staining and many circumferentially oriented, F-actin-+ and α-SMA (+) capsular cells. First row of images: collagen is bright blue, nerve fibers are purple/black. Second row: myelinated fibers are green, F-actin is red, and nuclei are blue. Third row: α-SMA is brown.

2.3.5. Quality of Axonal Regeneration, Q

The quality of axonal regeneration, Q, is a composite of several important parameters, including the regenerate area, the number and density of myelinated nerve fibers, the average myelinated nerve fiber diameter, and the number and percentage of A-fibers (large-diameter myelinated fibers with diameter greater than 6 μm), and the N-ratio (ratio of myelinated axonal area to nerve trunk area).

A previous kinetic study of the number and density of regenerated, myelinated axons indicated that a plateau region is not reached until 20-30 weeks after transection (Chamberlain, Yannas et al. 1998). This study evaluates axonal regeneration at 9 weeks. A previous study showed that this was a suitable time point to detect statistically significant differences in quality of regeneration metrics between degradable collagen devices (Harley, Spilker et al, 2004). The number of myelinated axons is a useful histomorphometric due to its positive correlation with a functional measurement, the signal amplitude of the regenerated nerve (Mackinnon and Dellon 1988). Among these metrics, average fiber diameter and the number of A-fibers are also particularly important because they correlate well with electrophysiological measurements of regenerated nerve function. A-fibers, or fibers larger than 6 μm, are considered relatively permanent and have likely reached the distal target (Sanders and Young 1944; Sanders and Young 1946; Aitken, Sharman et al. 1947; Aitken 1949). In addition, fibers in the "A" fiber range contribute most significantly to the total compound action potential of the electrophysiological measurement (Arbuthnott, Boyd et al. 1980). A-fibers have faster conduction velocities and improved functional performance over smaller myelinated fibers.

2.3.5.1. Total Myelinated Area

There was a significant effect of cross-linking treatment on the total myelinated area (the area of the nerve trunk containing myelinated fibers) at the midpoint of the gap, 9 weeks post-neurotmesis. Total myelinated area ranged from 0.07 ± 0.03 mm^2 for Device A to 0.28 ± 0.03 mm^2 for Device C (**Table 2.5**).

A one-way between subjects ANOVA was conducted to compare the effect of device identity (A-E) on total myelinated area. There was a significant effect of device

Device	Total Myelinated Area, mm^2
A	0.07 ± 0.02
B	0.23 ± 0.02
C	0.28 ± 0.03
D	0.14 ± 0.02
E	0.10 ± 0.02

Table 2.5. Morphological Measurements (Mean ± SEM) of Total Area of Nerve Trunk Occupied by Myelinated Fibers (not including capsule) at 9 weeks post-implantation. Normal nerve value is approximately 0.8 mm^2.

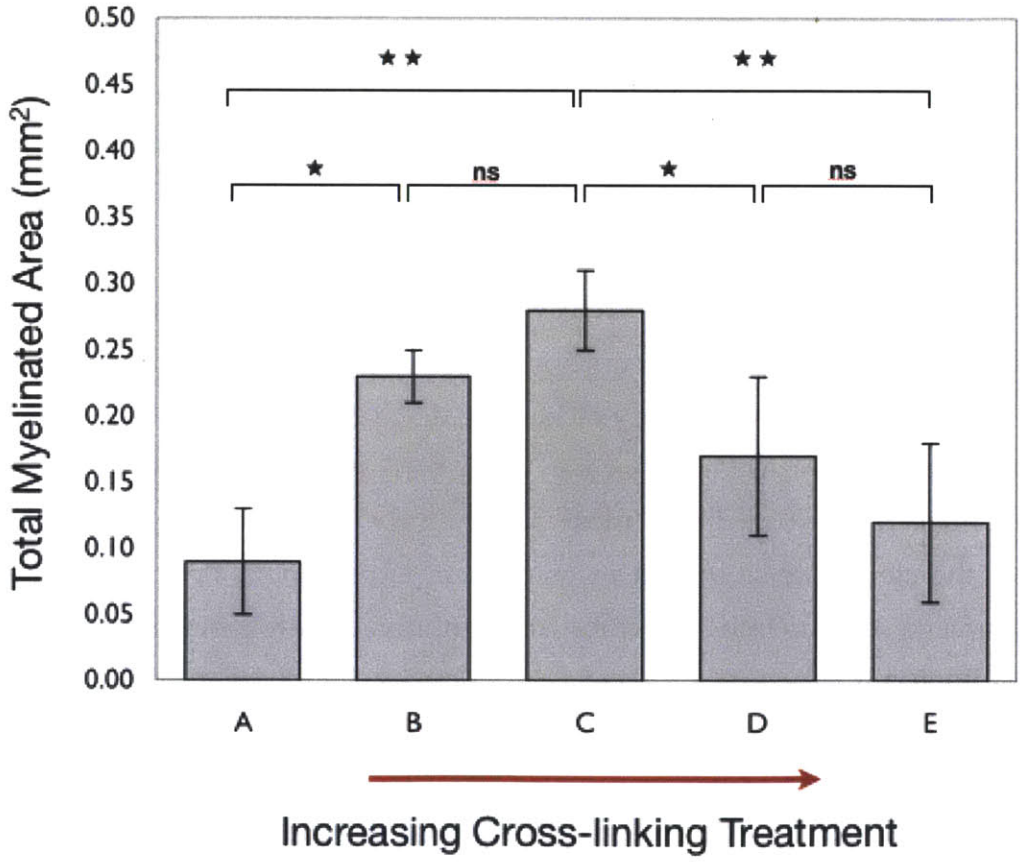

FIG. 2.7. COLLAGEN TUBES OF INTERMEDIATE DEGRADATION RATE MAXIMIZE TOTAL MYELINATED AREA. Graphical representation of morphological measurements of total area of nerve trunk occupied by myelinated fibers (not including capsule) at 9 weeks post-implantation. Normal nerve value is approximately 0.8 mm^2. Mean ± SEM. Symbols: ns, $p > 0.05$; ★, $p<0.05$; ★★, $p<0.01$.

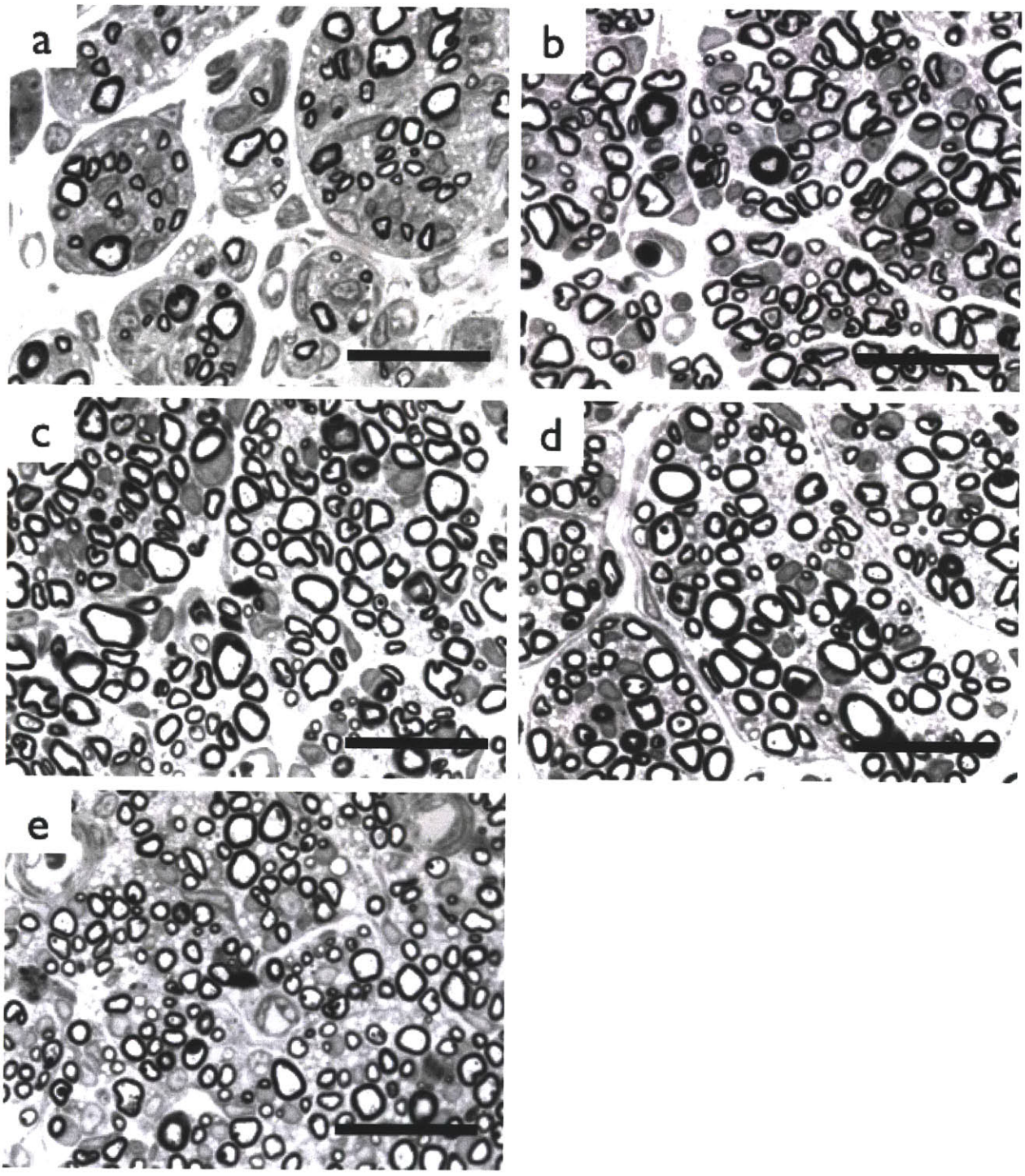

FIG. 2.8. MORPHOLOGY OF NERVE FIBERS REGENERATED USING THE HOMOLOGOUS SERIES OF COLLAGEN TUBES. Representative histology at midpoint of gap for Devices A-E (a-e). Number of myelinated fibers, % of A-fibers and # of A-fibers were maximized by tubes with intermediate levels of cross-linking (b, c). Scale bars: 25 μm

identity on δ at the $p<0.05$ level for the five conditions [$F(4, 13) = 10.40$, $p = 0.0005$]. Post hoc comparisons using the Bonferroni test indicated total myelinated area for device A was significantly different from total myelinated area for devices B and C ($0.004 < p < 0.029$) and that total myelinated area for device E was significantly different from total myelinated area for devices B and C, and D ($0.002 < p < 0.027$). In addition, there was a significant difference between total myelinated area for device C and device D ($p < 0.030$). No significant differences existed in total myelinated area between Devices A, D, and E ($0.950 < p < 1.000$) or between Devices B and C ($p < 1.000$) (**Fig. 2.7**).

2.3.5.1. Density and Number of Myelinated Nerve Fibers

The density of myelinated nerve fibers ranged from 0.016 ± 0.004 to 0.035 ± 0.003 fibers/μm^2 in nerves regenerated at 9 weeks post-neurotmesis using the homologous series of collagen devices (**Table 2.6, Fig. 2.9**). A one-way between subjects ANOVA was conducted to compare the effect of device identity (A-E) on density of myelinated fibers. There was a significant effect of device on fiber density at the $p < 0.05$ level for the five conditions [$F(4, 13) = 10.28$, $p = 0.0006$]. Post hoc comparisons using the Bonferroni test indicated mean fiber density for Device E was significantly different from fiber density for all other devices ($0.008 < p < 0.03$). One-way ANOVA suggested a difference in fiber density between Device A and Device C ($p < 0.106$), but this was not significant at the 0.05 level. No significant differences existed in fiber density between Devices A and B ($p < 0.561$), between Device D and Device E ($p<0.695$) or between Devices B, C, and D ($p < 1.000$).

The mean total number of myelinated nerve fibers regenerated per nerve trunk was calculated using measurements of the average density of myelinated fibers and the total cross-sectional area of the nerve trunk containing myelinated fibers. The mean total number of myelinated axons per nerve trunk varied between 935 ± 55 to 7060 ± 967 fibers. (**Table 2.7, Fig. 2.10**). These values compare favorably to the known average number of myelinated nerve fibers per trunk for normal adult Lewis rats (reported previously to be 6500, Chamberlain, Yannas et al, 1998).

A one-way between subjects ANOVA was conducted to compare the effect of device identity (A-E) on total number of myelinated fibers regenerated using the collagen devices. There was a significant effect of device identity on myelinated fiber

Device	Myelinated Fiber Density fibers/μm^2	n
A	0.016 ± 0.004	2
B	0.023 ± 0.002	4
C	0.025 ± 0.001	5
D	0.020 ± 0.003	4
E	0.035 ± 0.0003	3

Table 2.6. Density of Myelinated Fibers (Mean ± SEM) for regenerated nerves using the homologous series of collagen tubes at 9 weeks post-implantation, evaluated at the midpoint of a 15 mm gap. Normal nerve values are based on (Chamberlain, Yannas et al. 1998).

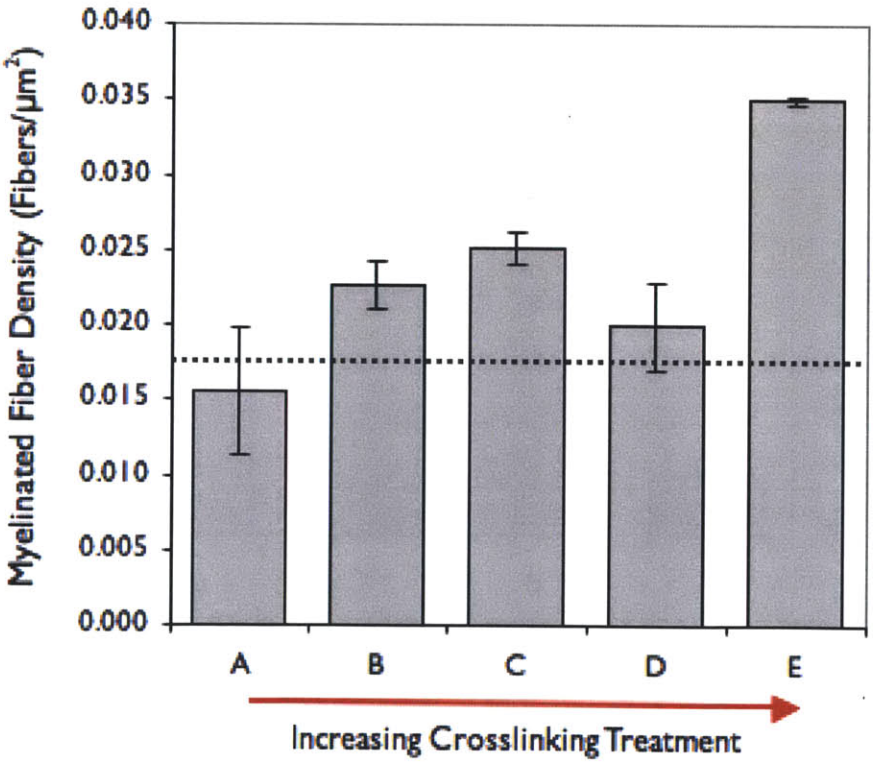

FIG. 2.9. DENSITY OF MYELINATED FIBERS FOR HOMOLOGOUS SERIES OF COLLAGEN TUBES (Mean ± SEM) at 9 weeks post-implantation. Density of the normal rat sciatic nerve is marked with a dashed line and was measured in Harley, Spilker, et al, 2004; Chamberlain, Yannas et al, 1998.

Device	Number of Myelinated Fibers		n
Normal	6500		
A	935	± 55	2
B	5380	± 935	4
C	7060	± 967	5
D	2930	± 499	4
E	2969	± 651	3

Table 2.7. Total Number of Myelinated Nerve Fibers (mean ± SEM) for regenerated nerves using the homologous series of collagen tubes at 9 weeks post-implantation, evaluated at the midpoint of a 15 mm gap. Normal nerve values are based on (Chamberlain, Yannas et al. 1998).

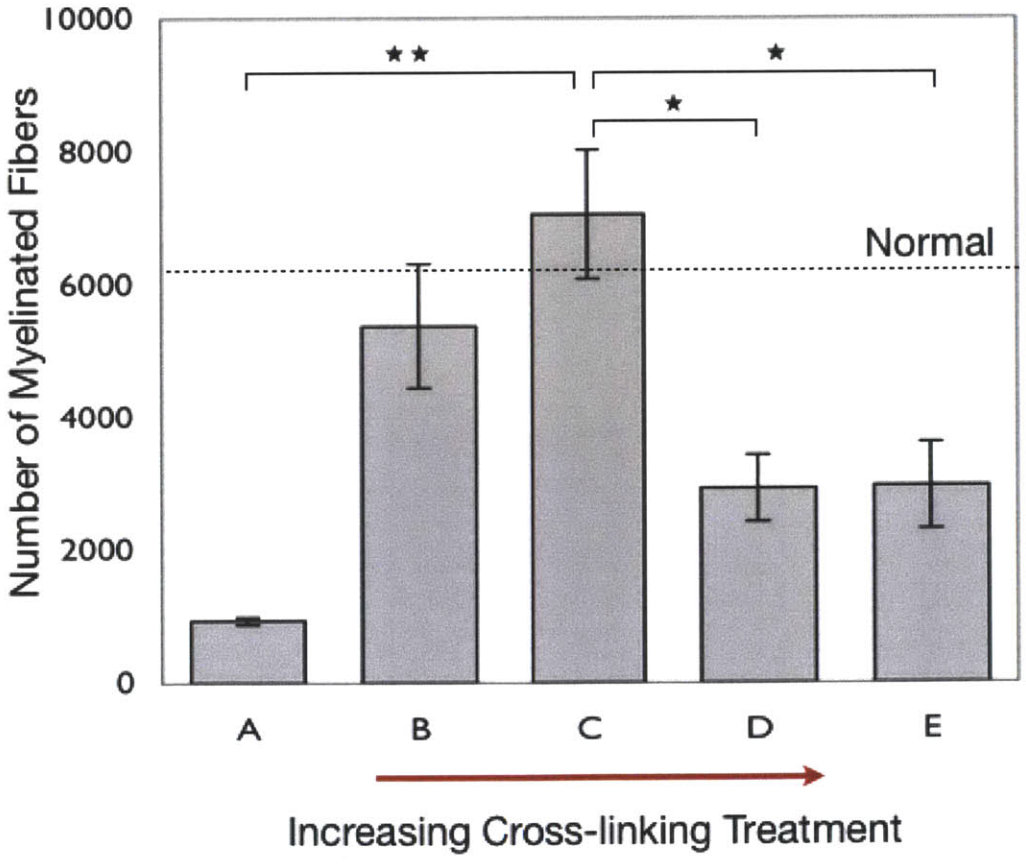

FIG. 2.10. TOTAL NUMBER OF MYELINATED NERVE FIBERS FOR HOMOLOGOUS SERIES OF COLLAGEN TUBES (Mean ± SEM) at 9 weeks post-implantation. Value for normal rat sciatic nerve from Harley, Spilker, et al, 2004; Chamberlain, Yannas et al, 1998) is indicated by a dashed line. Mean ± SEM. Symbols: ns, $p > 0.05$; ★, $p<0.05$; ★★, $p<0.01$.

number at the $p < 0.05$ level for the five conditions [$F(4, 13) = 7.29$, $p = 0.0026$]. Post hoc comparisons using the Bonferroni test indicated total number of myelinated fibers regenerated with device C was significantly different from number of fibers regenerated with devices A, D and E ($0.006 < p < 0.045$). The data suggested a difference between devices A and B but this was not statistically significant ($p < 0.078$). No significant differences existed between Devices B and D ($p < 0.539$), Devices B and E ($p < 0.753$) and Devices A, D, and E ($p < 1.00$) or between Devices B and C ($p < 1.00$).

2.3.5.2. Mean Myelinated Fiber Diameter

The mean diameter of myelinated fibers regenerated using the homologous series of collagen devices ranged from 2.78 ± 0.02 μm to 3.20 ± 0.09 μm, evaluated at the midpoint of a 15 mm nerve gap, 9 weeks post-neurotmesis (**Table 2.8, Fig 2.11**). The mean fiber diameter compared favorably to previous reports of regenerated mean fiber diameter using collagen devices (Harley, Spilker et al, 2004) evaluated at this time point in this injury model. The mean diameter of myelinated fibers in the normal adult Lewis rat sciatic nerve is 8.5 μm Chamberlain, Yannas et al 1998).

A one-way between subjects ANOVA was conducted to compare the effect of device identity (A-E) on mean myelinated fiber diameter regenerated using the collagen devices. There was a significant effect of cross-linking treatment on mean myelinated fiber diameter for the five conditions [$F(4, 13) = 3.93$, $p = 0.0265$]. However, post hoc comparisons using the Bonferroni test did not indicate a significant effect of the device identity on the mean myelinated fiber diameter. The data suggested a difference between Device B and D ($p < 0.099$). No significant differences were found between Device A and Devices B, C ($0.146 < p < 0.300$), and Device C and Device D ($p < 0.226$). No significant differences were detected between Devices B and E ($p < 0.661$), Devices A and D, E ($p < 1.00$) and Devices E and C, D ($p < 1.00$).

2.3.5.3. Number and Percentage of A-fibers

The percentage of large diameter A-fibers ranged from 4.50 ± 1.30 % to 10.10 ± 2.60 % of all myelinated fibers regenerated using the homologous series of collagen devices, evaluated at the midpoint of the gap, 9 weeks post-neurotmesis (**Table 2.9, Fig. 2.12**). The normal A-fiber % in the rat sciatic nerve is 68.4 % (Chamberlain, Yannas et al, 1998).

Device	Mean Myelinated Fiber Diameter	n
A	2.78 ± 0.02	2
B	3.28 ± 0.13	4
C	3.20 ± 0.09	5
D	2.84 ± 0.10	4
E	2.97 ± 0.09	3

Table 2.8. Mean Myelinated Fiber Diameter (mean ± SEM) for regenerated nerves using the homologous series of collagen tubes at 9 weeks post-implantation, evaluated at the midpoint of a 15 mm gap. Normal nerve value is based on (Chamberlain, Yannas et al. 1998).

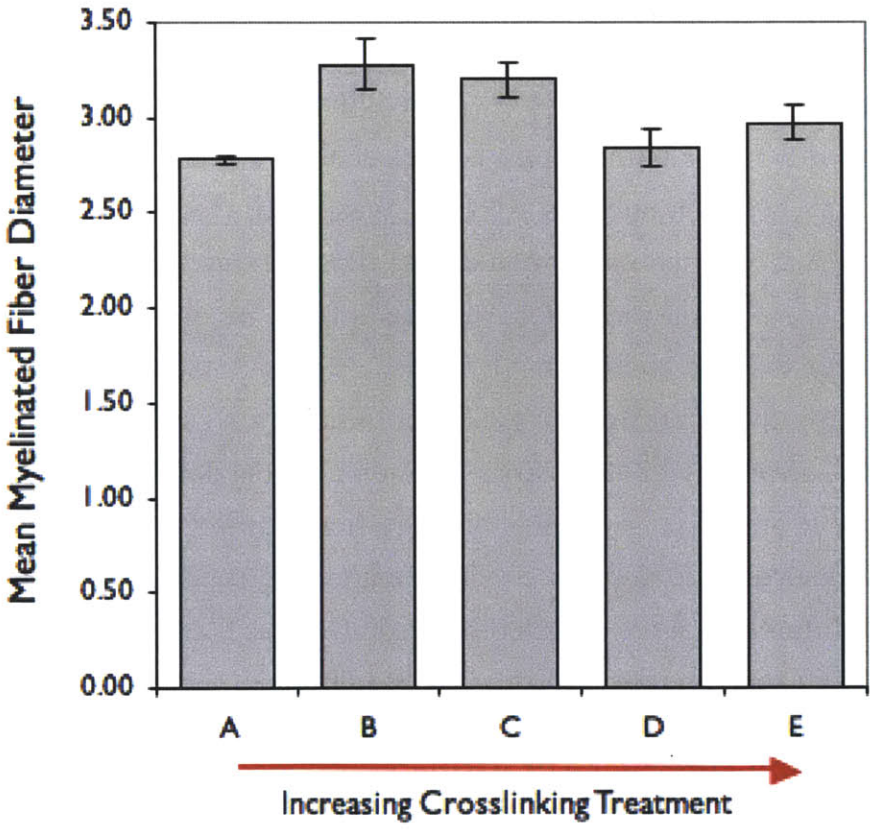

FIG. 2.11. MEAN MYELINATED FIBER DIAMETER FOR HOMOLOGOUS SERIES OF COLLAGEN TUBES (Mean ± SEM) at 9 weeks post-implantation, evaluated at midpoint of 15 mm gap. Normal value for adult female Lewis rat is 8.5 μm.

The total number of A-fibers (myelinated fibers whose diameter is greater than 6 μm) regenerated was calculated from the total area of the regenerate containing myelinated axons, the density of myelinated axons, and the percentage of A-fibers. The mean total number of A-fibers ranged from 50 ± 8 to 654 ± 106 in nerves regenerated using the homologous series of collagen devices **Table 2.10, Fig. 2.13**. While much lower than the number of A-fibers in the normal rat sciatic nerve (4500), the number of regenerated A-fibers is known to increase steadily over time after neurotmesis in the nerve chamber model (Chamberlain, Yannas et al, 1998). The values reported here compare favorably to previously reported A-fibers regenerated using collagen devices evaluated at 9 weeks-post neurotmesis in this injury model (Harley, Spilker et al, 2004).

A one-way between subjects ANOVA was conducted to compare the effect of device identity (A-E) on total number of A-fibers regenerated using the collagen devices. There was a significant effect of device identity on A-fiber number at the $p < 0.05$ level for the five conditions [$F(4, 13) = 8.73$, $p = 0.0012$]. Post hoc comparisons using the Bonferroni test indicated total number of A-fibers regenerated with Device C was significantly higher than A-fibers regenerated with devices A, D and E ($0.006 < p < 0.021$). The data suggested a difference between Devices A and B ($p < 0.083$), and Devices B and D, E ($.074 < p < .212$) but this was not statistically significant. No significant differences existed between Devices A, D and E ($p < 1.000$) or between Devices B and C ($p < 1.000$).

2.3.5.4 N-ratio

The N-ratio was calculated using measurements of the total myelinated fiber area divided by measurements of the total area of the nerve trunk that contains myelinated fibers (referred to previously as the regenerate area). It is a useful measure of the maturity of the nerve trunk. The N-ratio of regenerated nerve trunks varied between 0.11 ± 0.01 and 0.34 ± 0.02. (**Table 2.9, Fig. 2.12**). While lower than the known N-ratio of mature rat sciatic nerves (0.76, Chamberlain, Yannas et al, 1998), the N-ratio has been observed to increase continuously in the period after neurotmesis in the nerve chamber model.

A one-way between subjects ANOVA was conducted to compare the effect of cross-linking treatment on N-ratio of nerves regenerated using collagen devices. There was a significant effect of device identity on myelinated fiber number at the $p < 0.05$

Device	Percentage of A-fibers	n
A	5.30 ± 0.50	2
B	10.10 ± 2.60	4
C	9.30 ± 0.70	5
D	4.50 ± 1.30	4
E	5.40 ± 1.00	3

Table 2.9. Percentage of A-fibers (mean ± SEM) for regenerated nerves using the homologous series of collagen tubes at 9 weeks post-implantation, evaluated at the midpoint of a 15 mm gap. Normal rat sciatic nerve contains 68.4% A-fibers (Chamberlain, Yannas et al, 1998).

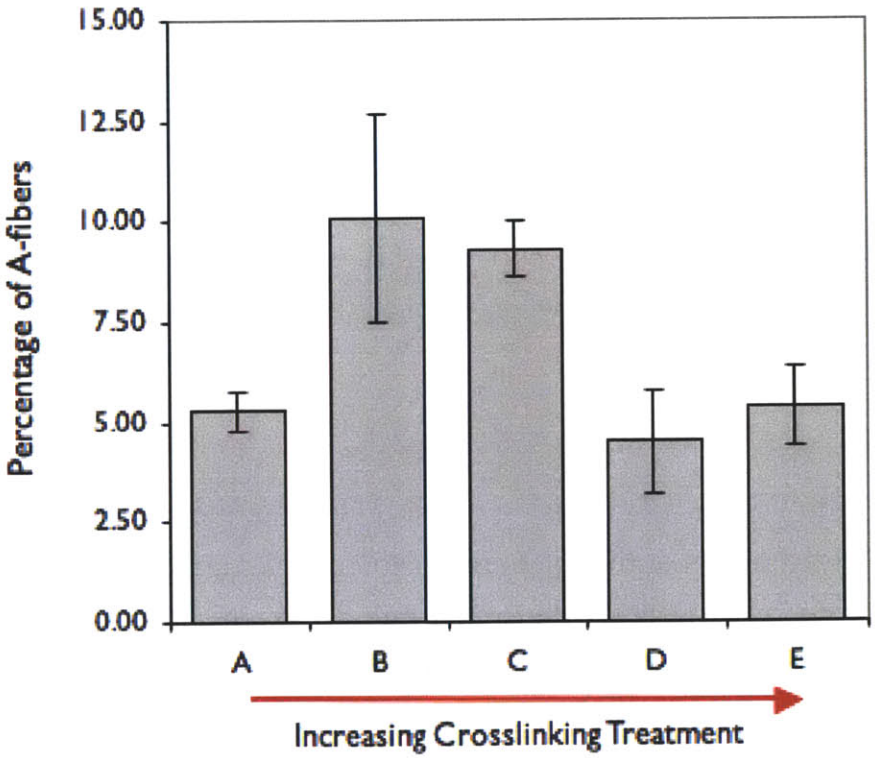

FIG. 2.12. PERCENTAGE OF A-FIBERS FOR HOMOLOGOUS SERIES OF COLLAGEN TUBES (Mean ± SEM) at 9 weeks post-implantation.

Device	Number of A-fibers	n
Normal	4500	
A	50 ± 8	2
B	516 ± 104	4
C	654 ± 106	5
D	128 ± 37	4
E	170 ± 59	3

Table 2.10. Total Number of A-fibers (mean ± SEM) for regenerated nerves using the homologous series of collagen tubes at 9 weeks post-implantation, evaluated at the midpoint of a 15 mm gap. Normal nerve value is based on (Chamberlain, Yannas et al. 1998).

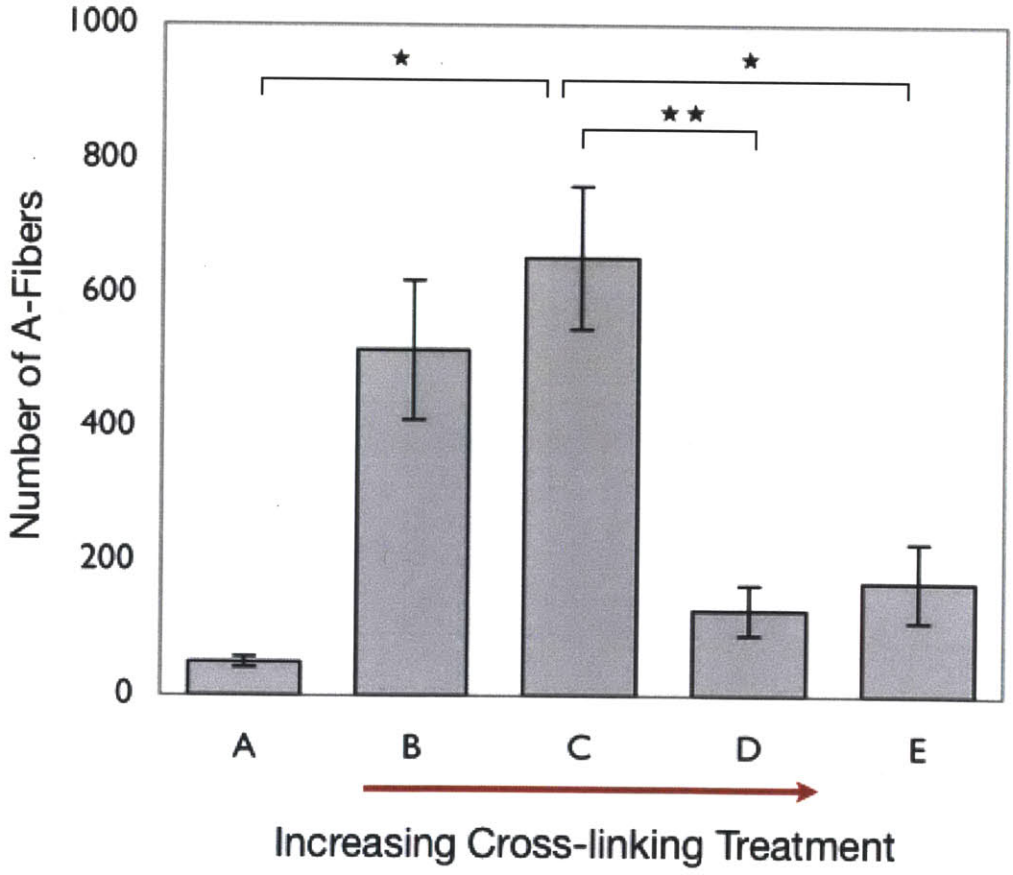

FIG. 2.13. TOTAL NUMBER OF A-FIBERS FOR HOMOLOGOUS SERIES OF COLLAGEN TUBES (Mean ± SEM) at 9 weeks post-implantation. Value for normal rat sciatic nerve is 4500 A-fibers from (Harley, Spilker, et al, 2004; Chamberlain, Yannas et al, 1998).

Device	N-Ratio	n
Normal	0.76	
A	0.11 ± 0.01	2
B	0.29 ± 0.03	4
C	0.34 ± 0.01	5
D	0.20 ± 0.02	4
E	0.34 ± 0.02	3

Table 2.11. Histomorphometry: N-ratio (mean ± SEM) for regenerated nerves using the homologous series of collagen tubes at 9 weeks post-implantation, evaluated at the midpoint of a 15 mm gap. Normal nerve value is based on (Chamberlain, Yannas et al. 1998).

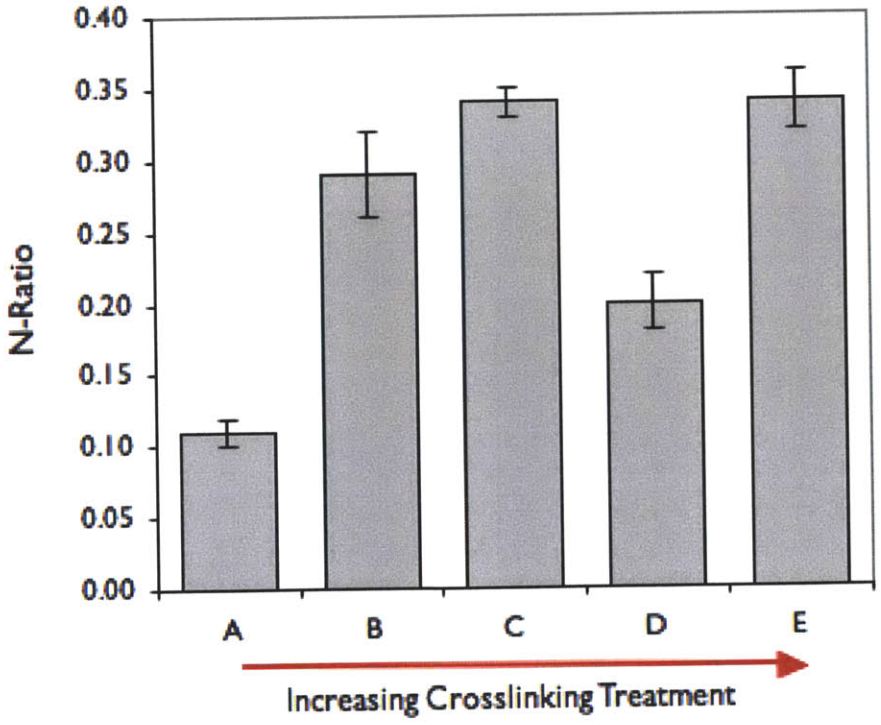

FIG. 2.14. N-RATIO FOR HOMOLOGOUS SERIES OF COLLAGEN TUBES (Mean ± SEM) at 9 weeks post-implantation.

level for the five conditions [F (4, 13) = 15.91, p = 0.0001]. Post hoc comparisons using the Bonferroni test indicated the N-ratio of nerves regenerated with device C was significantly different from the N-ratio of nerves regenerated with devices A and D ($0.000 < p < 0.007$). Significantly different N-ratios existed between Devices A and B ($p < 0.002$) and D and E ($p < 0.007$). The data suggested a difference between devices B and D but this was not statistically significant ($p < 0.064$). No significant differences existed between Devices B, C, and E ($p < 1.000$).

2.3.6 Relationship between Capsule Thickness, δ, and Quality of Regeneration, Q

The relationship between δ and various Q metrics was investigated with a pairwise Pearson correlation test. The test assesses the degree of linear dependence between two variables (e.g. X and Y) and yields a correlation coefficient between -1 and +1. For example, in the case of a positive value this implies a positive association (large values of X tend to be associated with large values of Y).

It is important to note that correlation coefficients cannot be used alone to imply or establish causal relationships between two variables. However, they are a useful starting point for interrogating the relationship between two variables of interest in the absence of a predictive model.

2.3.6.1 Correlation between δ and Total Myelinated Area

A Pearson product-moment correlation coefficient was computed to assess the relationship between the capsule thickness, δ, and the total myelinated area (the area of the regenerated nerve trunk containing myelinated axons. There was a negative correlation between the two variables ($r = -0.6686$, $n = 18$, $p = 0.0024$). A scatter plot summarizes the results (**Fig. 2.15**). Overall, there was a large, negative correlation between capsule thickness, δ, and total myelinated area. Higher values of capsule thickness tended to be associated with smaller values of regenerate area for the 18 animals investigated using the homologous series of collagen tubes at 9 weeks post-neurotmesis, evaluated at the midpoint of the 15 mm gap.

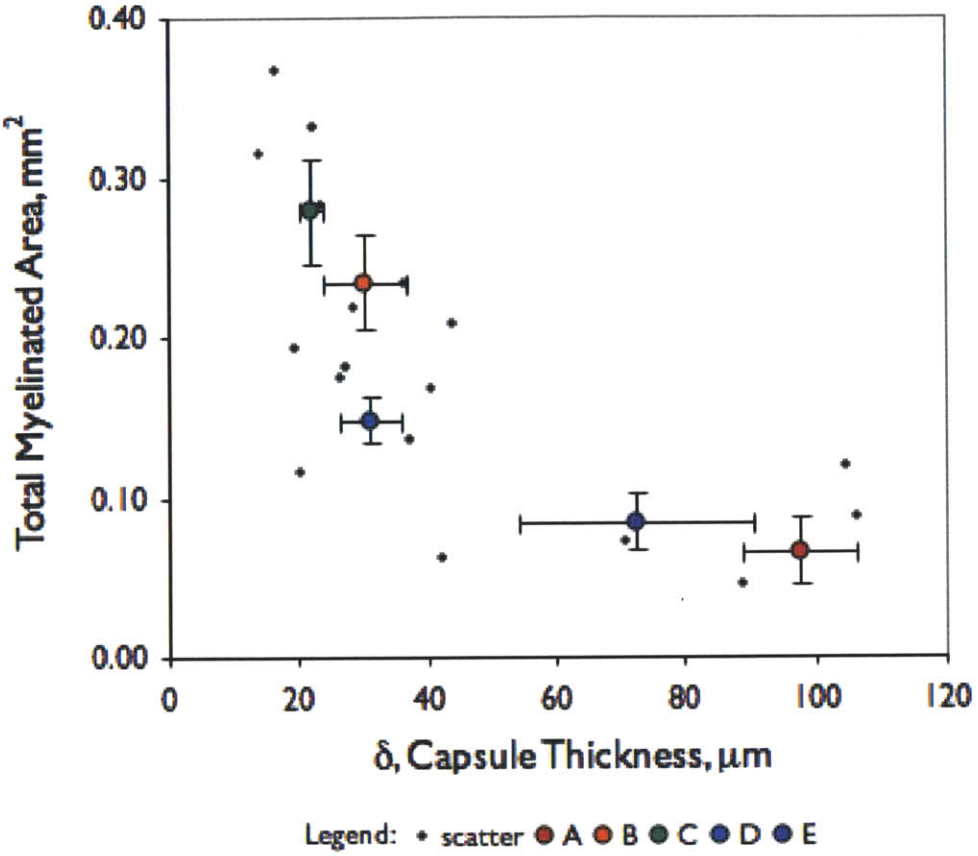

FIG. 2.15. SCATTER PLOT OF TOTAL MYELINATED AREA OF REGENERATE AS A FUNCTION OF CAPSULE THICKNESS, δ, for the homologous series of collagen tubes at 9 weeks post-implantation. Mean values ± SEM for each device type are shown in color.

2.3.6.2 Correlation between δ and Total Number of Myelinated Fibers

A Pearson product-moment correlation coefficient was computed to assess the relationship between the capsule thickness, δ, and the total number of myelinated fibers that were regenerated using the collagen devices. There was a negative correlation between the two variables ($r = -0.6009$, $n = 18$, $p = 0.0084$). A scatter plot summarizes the results (**Fig. 2.16**). Overall, there was a strong, negative correlation between capsule thickness, δ, and the total number of myelinated fibers. Higher values of capsule thickness tended to be associated with smaller values of myelinated fibers for the 18

animals investigated using the homologous series of collagen tubes at 9 weeks post-neurotmesis, evaluated at the midpoint of the 15 mm gap.

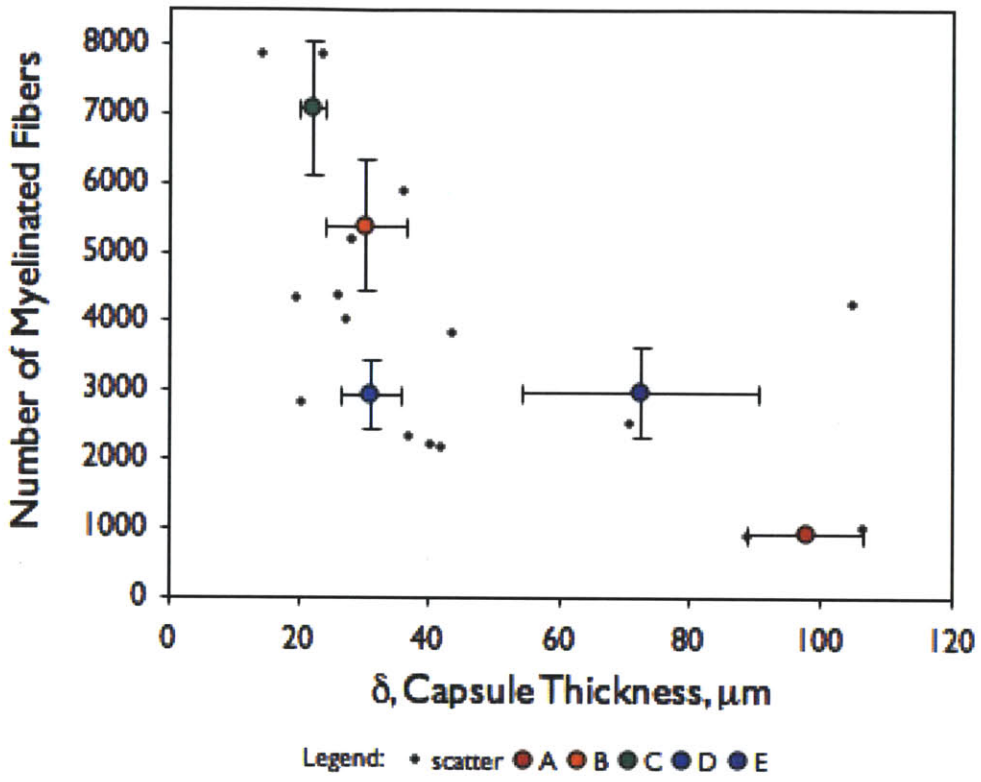

FIG. 2.16. SCATTER PLOT OF TOTAL NUMBER OF MYELINATED FIBERS AS A FUNCTION OF CAPSULE THICKNESS, δ, for the homologous series of collagen tubes at 9 weeks post-implantation. Mean values ± SEM for each device type are shown in color.

2.3.6.2 Correlation between δ and Total Number of A-fibers

A Pearson product-moment correlation coefficient was computed to assess the relationship between the capsule thickness, δ, and the total number of myelinated A-fibers that were regenerated using the collagen devices. There was a negative correlation between the two variables ($r = -0.5512$, $n = 18$, $p = 0.0177$). A scatter plot summarizes the results (**Fig. 2.17**). Overall, there was a moderate negative correlation between capsule thickness, δ, and the total number of A-fibers. Higher values of capsule thickness tended to be associated with smaller values of myelinated A-fibers for the 18 animals investigated using the homologous series of collagen tubes at 9 weeks post-neurotmesis, evaluated at the midpoint of the 15 mm gap.

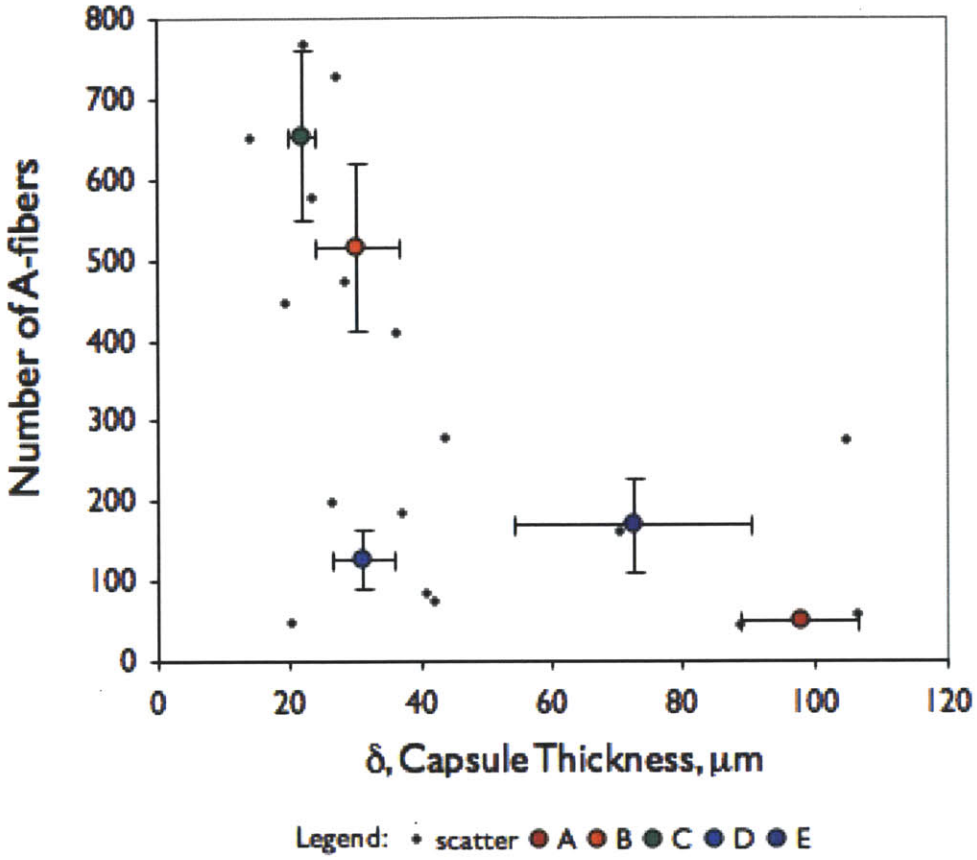

FIG. 2.17. SCATTER PLOT OF A-FIBERS AS A FUNCTION OF CAPSULE THICKNESS, δ, for the homologous series of collagen tubes at 9 weeks post-implantation. Mean values ± SEM for each device type are shown in color.

2.3.6.3 Correlation between δ and Other Q metrics

Pearson product-moment correlation coefficients were computed to assess the relationship between the capsule thickness, δ and other Q metrics. These were not statistically significant but are listed here: mean fiber diameter ($r = -0.3664$, $n = 18$, $p = 0.1348$), N ratio, ($r = -0.3891$, $n = 18$, $p = 0.1105$).

2.3.6.4 Summary of Correlation between δ and Q metrics

Capsules thickness, δ, had a large, negative, and statistically significant association with three Q metrics (total myelinated area, number of myelinated fibers,

and number of A-fibers). Correlation coefficients between δ and other Q metrics (mean fiber diameter, N-ratio) were not significant.

Correlation	Coefficient (r)	p value
δ and Total Myelinated Area	- 0.669	0.002
δ and Number of Myelinated Fibers	- 0.601	0.008
δ and Number of A-fibers	- 0.551	0.018
δ and Mean Fiber Diameter	- 0.367	0.135
δ and N-ratio	-0.389	0.111

Table 2.12 Summary of Pearson Product moment Correlation Coefficients for δ and Q metrics

2.3.7 Capsule Thickness, δ and Regenerate Area as a Function of Distance

At 9 weeks post-neurotmesis, the capsule thickness, δ, and regenerate area were measured in three places along the length of the regenerate from the original site of transection to the midpoint of the gap (**Table 2.13, Table 2.14**). For Device C, both regenerate area and capsule thickness decreased with distance from the site of transection (and measured towards the midpoint of the regenerate) (**Fig.2.18**). For Device E, capsule thickness remained constant with distance from the site of transection and regenerate area decreased (**Fig. 2.19**).

Device	Capsule Thickness, δ, μm									n
	0 mm			*4.5 mm*			*7.5 mm*			
C	57	±	6	37	±	4	19	±	4	3
E	128	±	16	115	±	9	115	±	37	3

Table 2.13 Capsule Thickness, δ, as a Function of Distance from the Site of Transection
Distance measured in mm for devices C and E, 9 weeks post-neurotmesis from the site of transection towards the midpoint of the regenerate.

Device	Total Myelinated Area, mm^2									n
	0 mm			*4.5 mm*			*7.5 mm*			
C	0.56	±	0.06	0.54	±	0.16	0.12	±	0.02	3
E	0.64	±	0.11	0.14	±	0.07	.096	±	0.05	3

Table 2.14 Total Myelinated Area (Area Containing Myelinated Fibers) as a Function of Distance from the Site of Transection for Devices C and E, 9 weeks post-neurotmesis. Distance measured in mm for devices C and E, 9 weeks post-neurotmesis from the site of transection towards the midpoint of the regenerate.

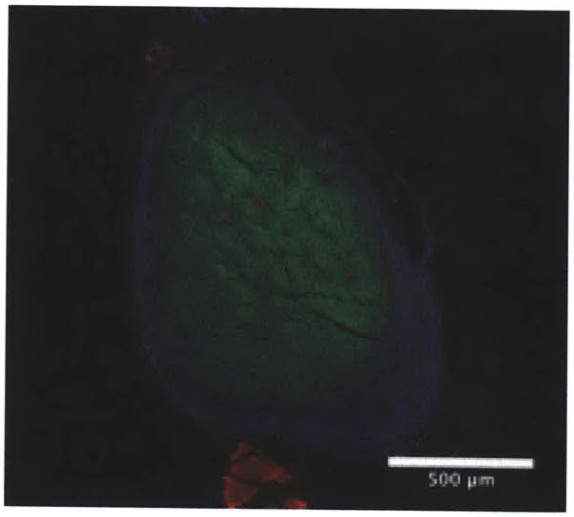

Site of Transection,
0 mm

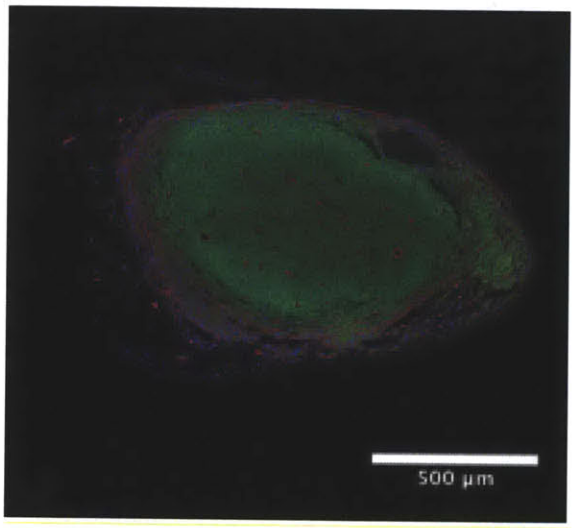

4.5 mm

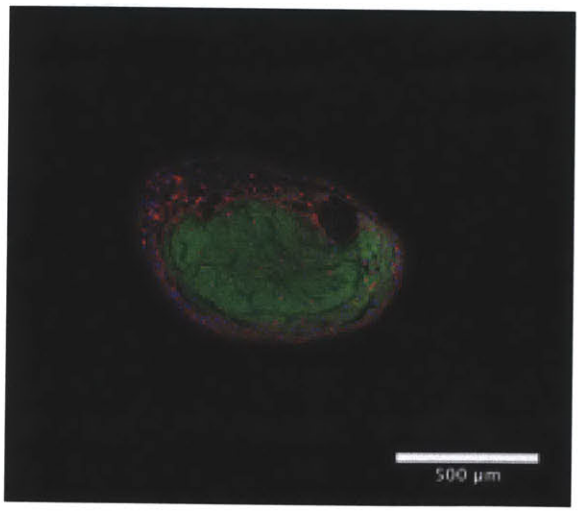

Midpoint of Gap,
7.5 mm

FIG. 2.18 INTERMEDIATELY CROSS-LINKED COLLAGEN DEVICES (DEVICE C) DECREASE IN REGENERATE AREA AND CAPSULE THICKNESS measured from the site of transection, 0 mm (*TOP*) to the midpoint of the regenerate, 7.5 mm into the gap (*BOTTOM*). measured at 9 weeks after injury. Contractile cells in capsule are red (F-actin), myelinated fibers are green, nuclei are blue (DAPI). Scale bars: 500 µm.

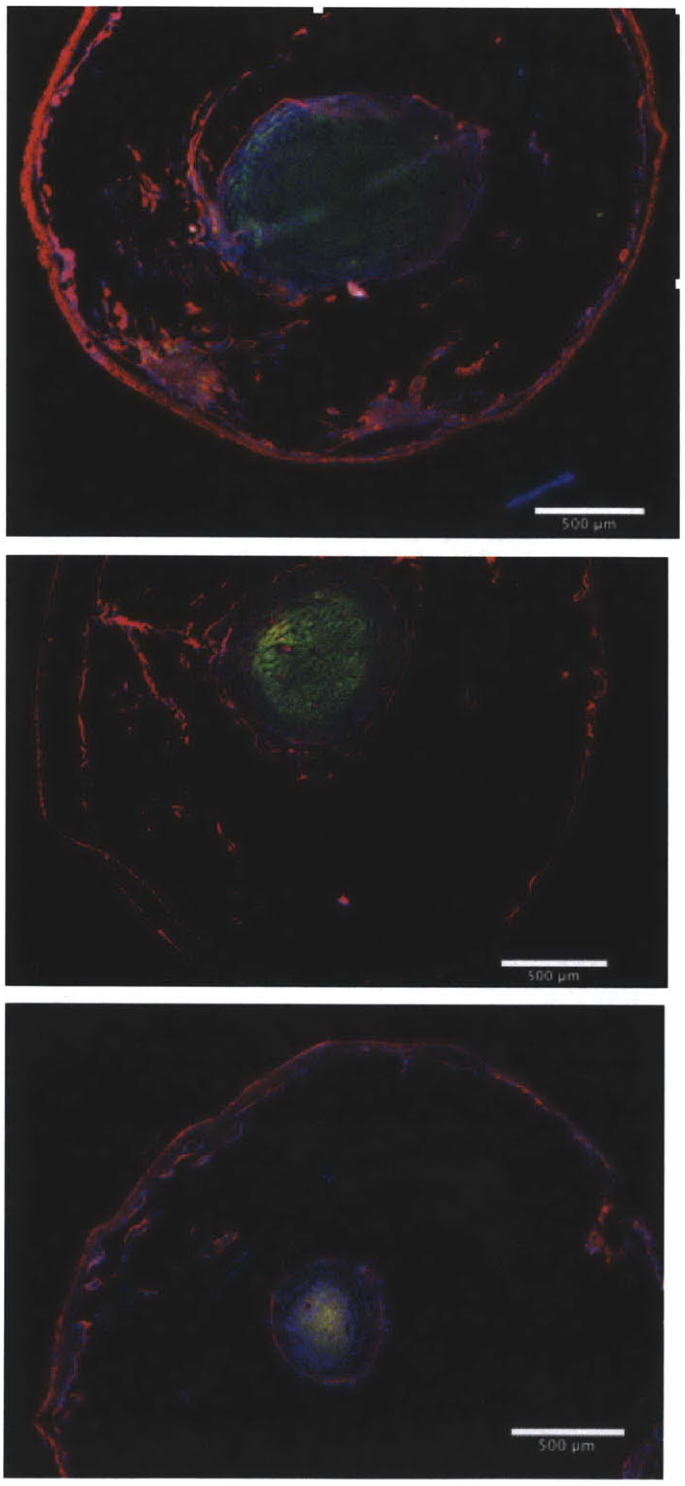

Site of Transection,
0 mm

4.5 mm

Midpoint of Gap,
7.5 mm

FIG. 2.19 HIGHLY-CROSSLINKED COLLAGEN DEVICES (DEVICE E) DECREASE DRAMATICALLY IN REGENERATE DIAMETER BUT MAINTAIN RELATIVELY CONSTANT CAPSULE THICKNESS FROM THE SITE OF TRANSECTION (a) to the midpoint of the regenerate (c). Red: F-actin, green: myelin, blue: DAPI. Scale bars: 500 µm.

2.3.8 Cell-Scaffold Interactions Appear to Coincide with Decreased δ

Highly cross-linked scaffolds (device E) had negligible degradation at 9 weeks post-neurotmesis and the initially cell-impermeable inner lumens of Device E appeared to be intact. Inner linings were not intact in Device D, which as moderately degraded at 9 weeks after neurotmesis. Immunofluorescence study of these collagen devices revealed that few if any contractile cells had infiltrated the tube walls of these devices (**Fig. 2.20.a**). Trichrome staining, which permits visualization of the collagen scaffold, showed similar results (**Fig. 2.21**). In contrast, intermediately-cross-linked devices (device D) appeared to have lost mass at 9 weeks, initially-cell impermeable lumens had been degraded and tube walls that were filled with randomly-oriented F-actin (+) and α-SMA (+) cells (**Fig. 2.22**). These cell-scaffold interactions appeared to coincide with decreased thickness of the contractile capsule (**Fig. 2.20**). Less cross-linked devices in the homologous series (A-C) were degraded by 9 weeks time point, precluding direct observation of cells in intact tube walls for these devices.

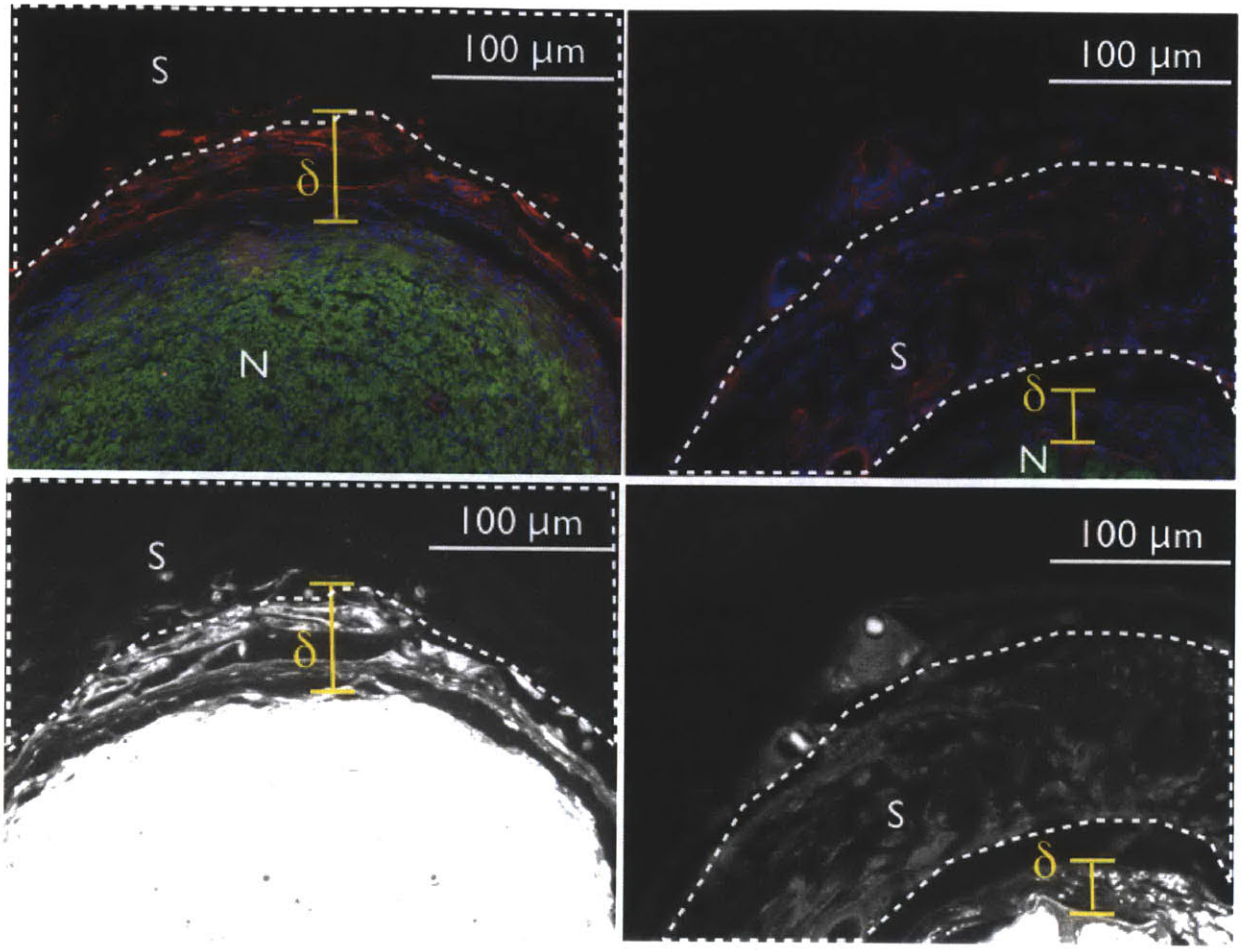

FIG. 2.20. COLLAGEN TUBES OF INTERMEDIATE DEGRADATION RATE DISRUPT CAPSULE FORMATION. *(TOP LEFT)*: Cells (blue nuclei) stain brightly for filamentous actin (red) and are circumferentially oriented in a thick capsule (d) around a regenerating nerve (N, myelin, green) in a non-degrading collagen tubular scaffold (Device E). The collagen scaffold (S) contains virtually no cells. *(TOP RIGHT):* A collagen tubular scaffold of intermediate degradation rate (Device D) minimizes capsule thickness (d) while capsular cells stain less intensely for filamentous actin (red). Numerous cells appear to be randomly oriented in the pores of the collagen scaffold (S) of intermediate degradation rate. *(BOTTOM LEFT, BOTTOM RIGHT)* Over-exposed green channel allows pores of scaffold (S) to be visualized (grey) for reference for Device E and Device D, respectively. Nerves imaged near the site of proximal transection, 9 weeks after injury. Scale bars: 100 µm.

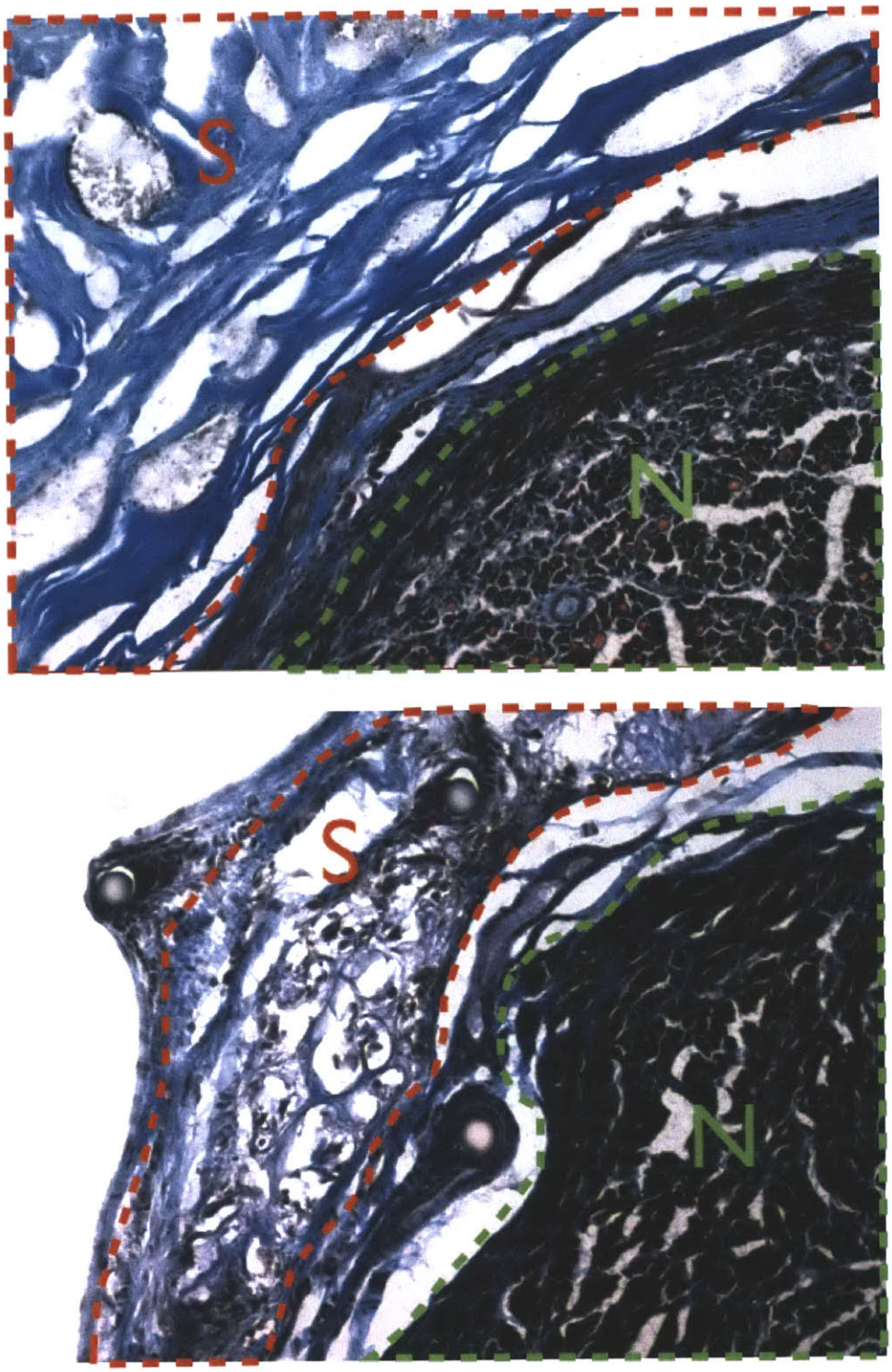

FIG. 2.21 COLLAGEN TUBES OF INTERMEDIATE DEGRADATION RATE DISRUPT CAPSULE FORMATION. *Top*: Highly cross-linked collagen devices (Device E) develop thick, cohesive capsules and cells do not infiltrate the scaffold (S, blue) during the 9 week experiment. *Bottom:* Intermediately cross-linked collagen devices (Device D) have thinner capsules and scaffolds are in the process of being degraded by numerous cells (black nuclei) that have infiltrated the tube walls. Nerves (N) imaged near the site of proximal transection 9 weeks after injury. Scale bars: 100 μm.

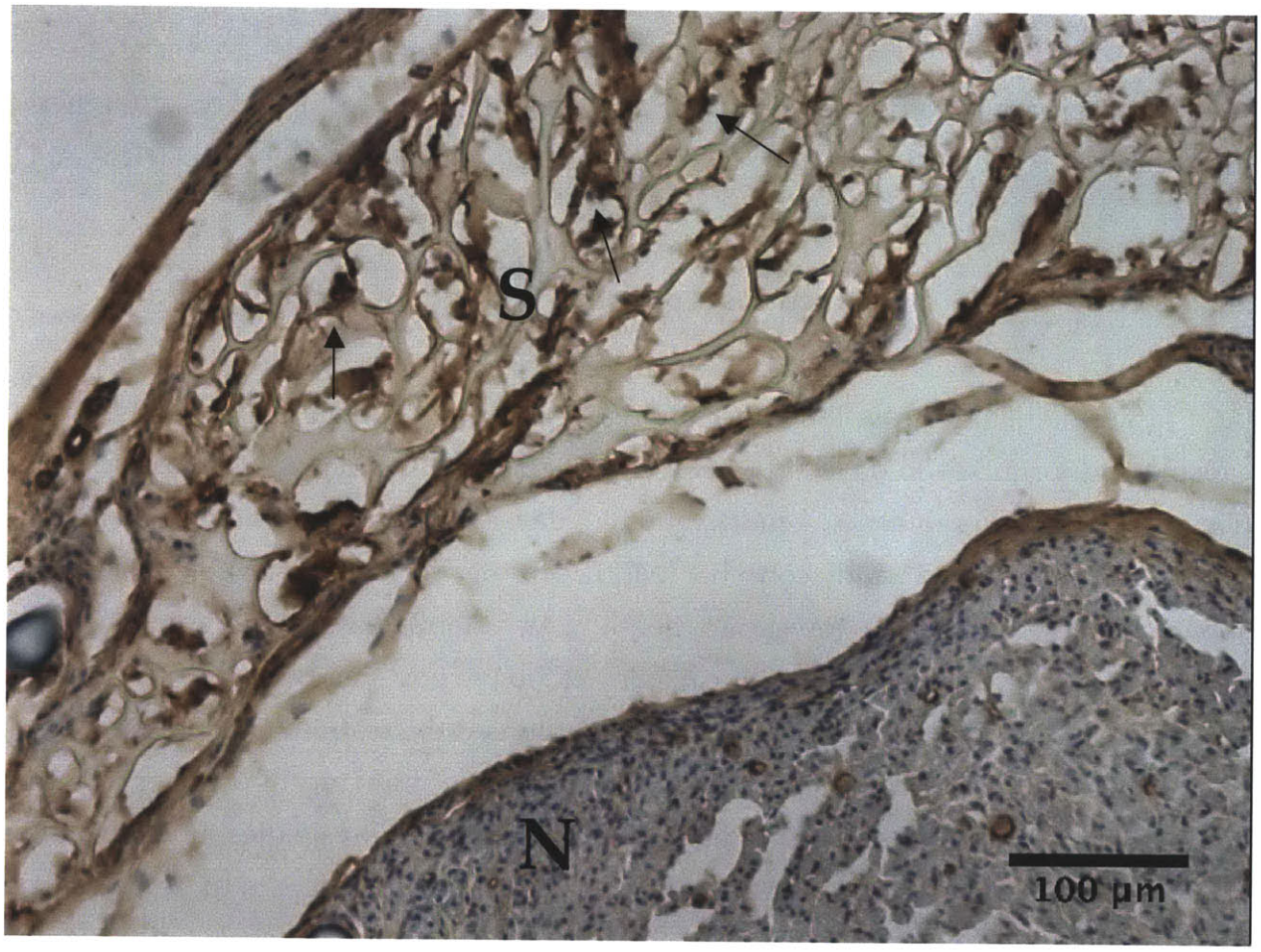

FIG. 2.22 COLLAGEN TUBES OF INTERMEDIATE DEGRADATION (DEVICE D) APPEAR TO HAVE EXTENSIVE MYOFIBROBLAST – SCAFFOLD INTERACTIONS at 9 weeks-post-neurotmesis. Myofibroblasts (arrows, brown) stain positively for α-smooth muscle actin (α-SMA). The separation of scaffold (S) and nerve regenerate (N) is an artifact of the sectioning procedure. Nerves imaged near the site of proximal transection. Scale bar: 100 µm.

2.3.8. Preliminary Results from 7 Days After Injury

A preliminary study investigated the capsule presence at 7 days after nerve transection in response to selected scaffolds from the homologous series (Devices A, D, E).

2.3.8.1. MFB-Scaffold Interactions Appear to Coincide with Reduced d

Intermediately cross-linked scaffolds disrupt the spontaneous myofibroblast capsule that forms seven days after neurotmesis **(Fig. 2.23).** Non-cross-linked scaffolds (Device A) degrade rapidly (< 1 week) and at 7 days have done very little to thwart the thick, highly oriented and cohesive MFB capsule (brown, α-SMA) that forms spontaneously around the transected nerve. An intermediately degrading scaffold (Device D) seems to dissociate MFB capsules at 7 days post-neurotmesis, reducing the thickness of the capsule. MFBs (brown) have infiltrated the scaffold (S) pores and seem to be randomly oriented. The capsule (C) seems to be dramatically thinner. Highly cross-linked scaffolds (Device E) lead to thick, cohesive MFB capsules at 7 days after injury. The cell-impermeable inner lumen of the scaffold (S) appears to be intact and there is little to no cell infiltration and no evidence of capsule dissociation. Speculatively, the preliminary data suggests that MFB-scaffold interactions coincide with reduced contraction at early time points.

2.3.8.2. Thick MFB Capsules Appear to Compress Transected Nerve Stumps

Regeneratively "inactive" scaffolds (Device A) are mostly degraded within 7 days after neurotmesis (**Fig. 2.24**). At this time the thick MFB capsule has formed around the transected nerve stump with many MFBs highly-oriented with the circumference of the nerve stump. Previous studies indicate that at 7 days there has not been significant axon elongation (Williams et al., 1983) into the gap. Observations of the thick MFB capsule coincide with a dramatic increase in the circularity of the transected stump in the presence of capsule (**Fig. 2.24**). The nerve stump appears to be deformed in the presence of a thick MFB capsule seven days after injury.

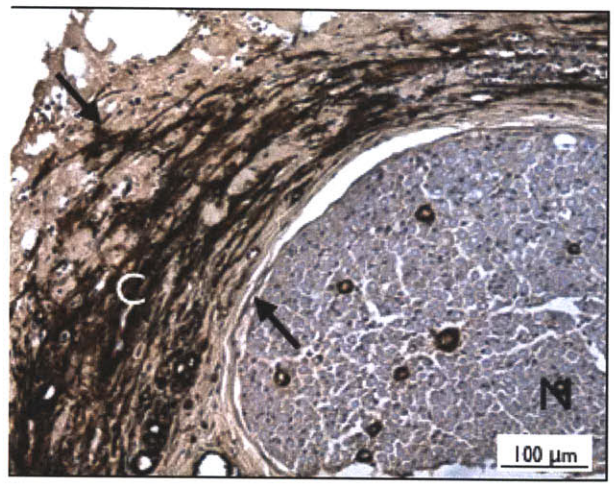

Rapidly-degrading
Device A
Thick capsule

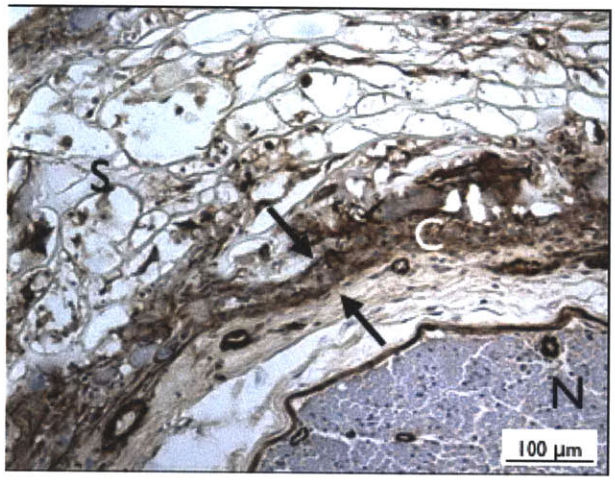

Intermediately-degrading
Device D
Thin capsule

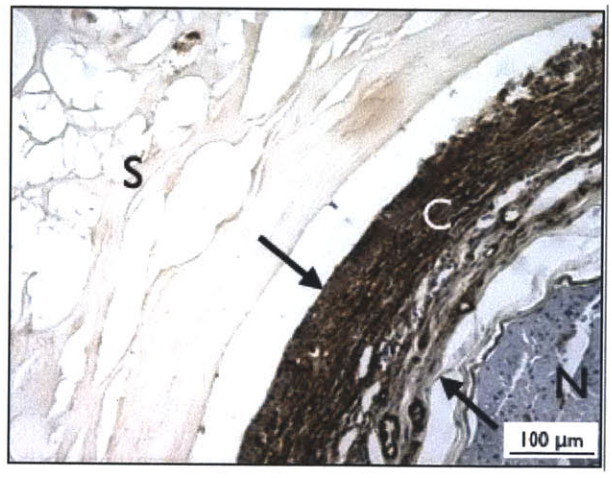

Non-degrading
Device E
Thick capsule

FIG. 2.23. SPECULATIVELY, MYOFIBROBLAST-SCAFFOLD INTERACTIONS COINCIDE WITH DECREASED δ 7 DAYS AFTER INJURY. S: Scaffold, C: Capsule, N: Nerve, Myofibroblast (MFB, α-SMA brown). TOP: A thick capsule of circumferentially oriented MFBs surrounds a nerve stump inserted into Device A (non-cross-linked tube) that has degraded by 7 days. MIDDLE: An intermediately degrading device (Device D) leads to a reduced MFB capsule. MFBs are disorganized and found in the scaffold walls (S). BOTTOM: A thick, cohesive MFB capsule in a Device E-treated animal. The scaffold (S) has virtually no cellular content. All images were taken close to the site of nerve transection, proximal stump.

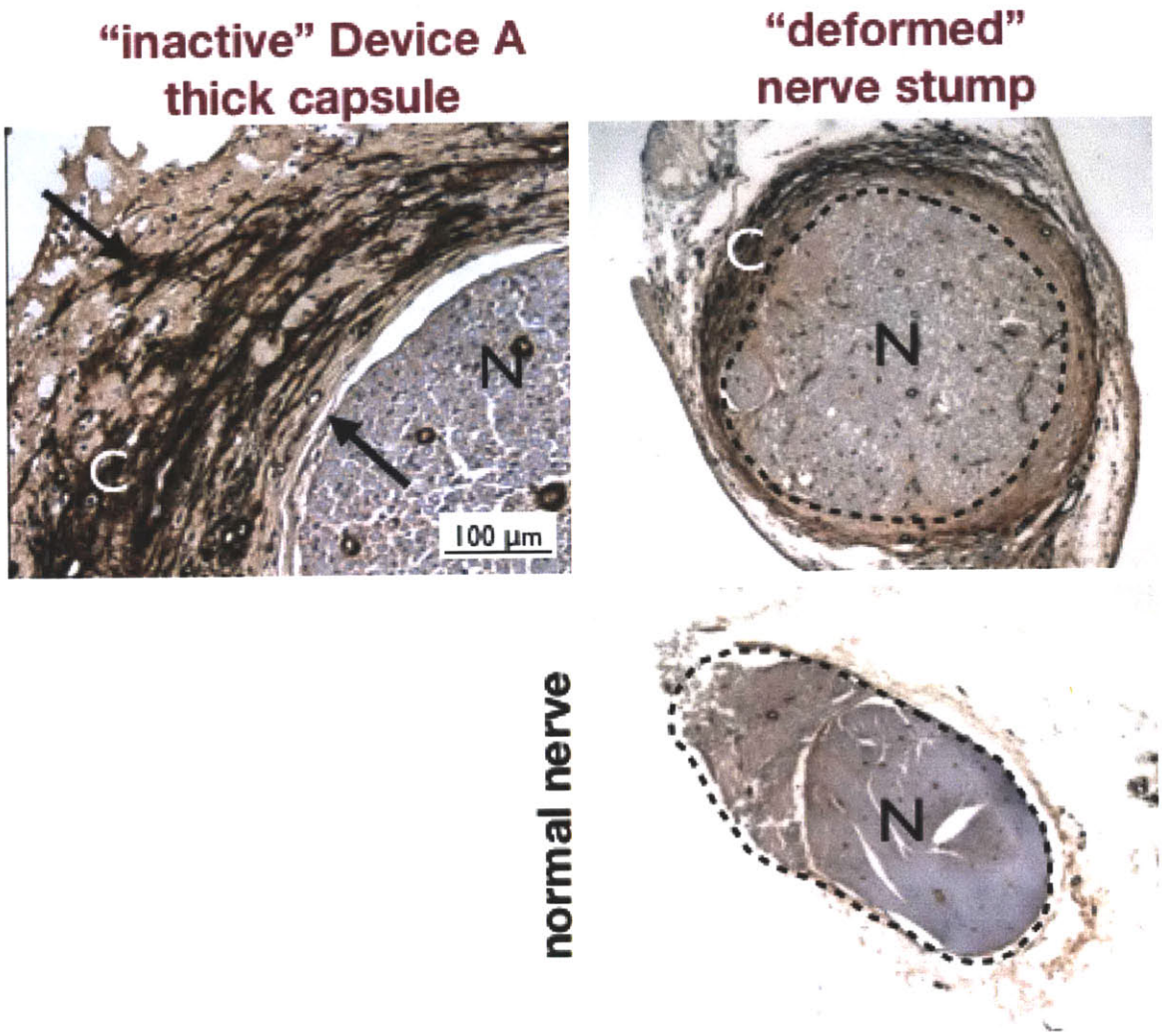

FIG. 2.24 THICK CONTRACTILE CAPSULES APPEAR TO COMPRESS NERVE STUMPS SEVEN DAYS AFTER INJURY. *Top Left:* A thick capsule (C) with large δ and numerous MFBs (brown, alpha-SMA) aligned with the Θ axis has formed seven days after transection around the proximal nerve stump in a Device A (non-cross-linked) – treated animal. Device A is almost completely degraded. *Bottom Left:* Transverse section of a normal nerve (dashed lines) has a circularity of 0.80 and an aspect ratio of 2.1. *Top Right:* Seven days after neurotmesis, the axonal area of a transected nerve stump (dashed lines) that has been grafted with a rapidly degrading scaffold (Device A) has undergone a dramatic shape change (circularity 0.97, aspect ratio 1.0). The once oblong nerve resembles a perfect circle and is surrounded by a thick MFB capsule. The shape change is consistent with that predicted by the "pressure cuff" theory in which the mechanical effect of a cohesive, circumferential MFB capsule is modeled as a uniform hoop stress on the nerve stump, compressing it along the radius. Circularity = 4π*Area/Perimeter^2. A value of 1.0 indicates a perfect circle. As the value approaches 0.0, it indicates an increasingly elongated shape. Aspect ratio = major axis / minor axis.

2.4 Discussion & Conclusions

2.4.1. Contractile Capsule Thickness, δ, Has a Large Negative Association with the Quality of Induced Regeneration, Q.

Taken together, the major findings of this chapter constitute the first quantitative link between contraction and induced regeneration of the injured peripheral nerve. The data indicates that the contractile capsule thickness, δ, has a strong negative and statistically significant association with quality of regeneration, Q. Large values of δ tended to be associated with small values of Q metrics (regenerate area containing myelinated fibers, number of myelinated fibers, and number of large-diameter A-fibers. Correlations between δ and N-ratio and mean myelinated fiber diameter were not statistically significant.

Several improvements could be made to the study to reduce the error and improve the significance of the data. For small samples sizes, statistical power can be limited. In this work statistically significant differences between groups were identified using a One-way ANOVA, which requires a normal distribution of the data. Where applicable (for $n \geq 4$), the Lillefors test was used to test the available data against any possible normal distributions. All data for devices B, C, and D were normal, with $p > 0.05$. Due to the small sample size of Devices A and E, the statistically-significant effect of cross-linking treatment on δ and Q metrics (found using One-way ANOVA) was confirmed using a non-parametric ANOVA (Kruskal-Wallis), which does not assume normality. Increasing the number of animals would improve the statistical power of the study. Better sampling of the cross-linking treatment within the homologous series (by more carefully controlling the DHT cross-linking) could be used in the future. In the current study the intermediately degrading devices (B, C, and D) did not have statistically significant differences in δ at 9 weeks.

2.4.2 Collagen Tubes of Intermediate Cross-linking Minimize Contractile Capsule Thickness, δ, and Reduce Capsule "Contractility"

In the current study, the contraction-blocking nature of biodegradable, type I collagen devices after sciatic neurotmesis was elucidated in a quantitative manner. Intermediately cross-linked type I devices reduced contractile capsule thickness, δ, from 73 ± 18 μm in the case of a highly cross-linked type I collagen tube to 22 ± 2 μm for intermediately cross-linked type I collagen tube at the midpoint of a regenerate spanning a 15 mm gap of the adult rat at 9 weeks post-neurotmesis. The percentage reduction in δ between the two devices was 70%, which was comparable to the 90% reduction in capsule thickness that a type I collagen nerve guide demonstrated over a biodurable silicone nerve guide in a previous study (Chamberlain, Yannas et al, 1998). In that study the use of a biodegradable type I collagen tube (Neuragen™, Integra Life Sciences) reduced the contractile capsule thickness around regenerated nerves from ~50 μm in the case of a biodurable silicone elastomer tube to ~5 μm for the collagen tube, evaluated at 30 weeks post-sciatic neurotmesis in a 10 mm gap of the adult rat.

In addition to the demonstrated reduction in δ, intermediately cross-linked tubes in the current study seemed to dramatically reduce the number of capsular cells staining positively for the contractile filament, α-smooth muscle actin (α-SMA). Thick capsules that formed around regenerates in the presence of Device E at 9 weeks post-neurotmesis appeared to be more cohesive: they contained multiple layers of dense collagen fibers and numerous cells that stained positively for contractile filaments F-actin and α-smooth muscle actin (α-SMA). The data suggest that capsules that formed around regenerates at the midpoint in the current study differed in "contractility." Cells expressing the α-SMA phenotype are classified as myofibroblasts and are capable of generating significantly higher forces on their substrates than fibroblastic cells that do not express the protein (Tomasek et al., 2002). Thicker capsules appear to contain more cells that are capable of generating higher amounts of force. The reduction in number of α-SMA (+) cells was also demonstrated in the Chamberlain study.

Of note is the spatial heterogeneity of thick capsules in the current study. At 9 weeks post-neurotmesis, the innermost layers of Device E capsules (the first ~50 μm

measured along the radial axis outward from the myelinated fibers) consist of mostly thick collagen fibers with a modest number of circumferentially oriented contractile cells between adjacent collagen layers. These capsular cells have long aspect ratios and stain positively for F-actin, but do not appear to express the α-SMA phenotype. In contrast, the outermost portions of thick capsules in Device E-treated nerves tended to consist of ~5 cohesive layers of contractile cells which stained prominently for both F-actin and α-SMA (**Fig. 2.25.d**). Thinner capsules (Device C) appeared less cohesive and were harder to distinguish from the regenerate without the aid of staining techniques for myelinated fibers. Nerve trunks with thinner capsules exhibited a smoother transition from regenerate to capsule. Thinner capsules contained less collagen content, contained only a few layers of capsular cells, likely proto-myofibroblasts, that stained positively for F-actin and did not stain appreciably for the α-SMA isoform (**Fig. 2.25.c**). These cells are capable of generating less force than differentiated MFBs (Tomasek et al., 2002).

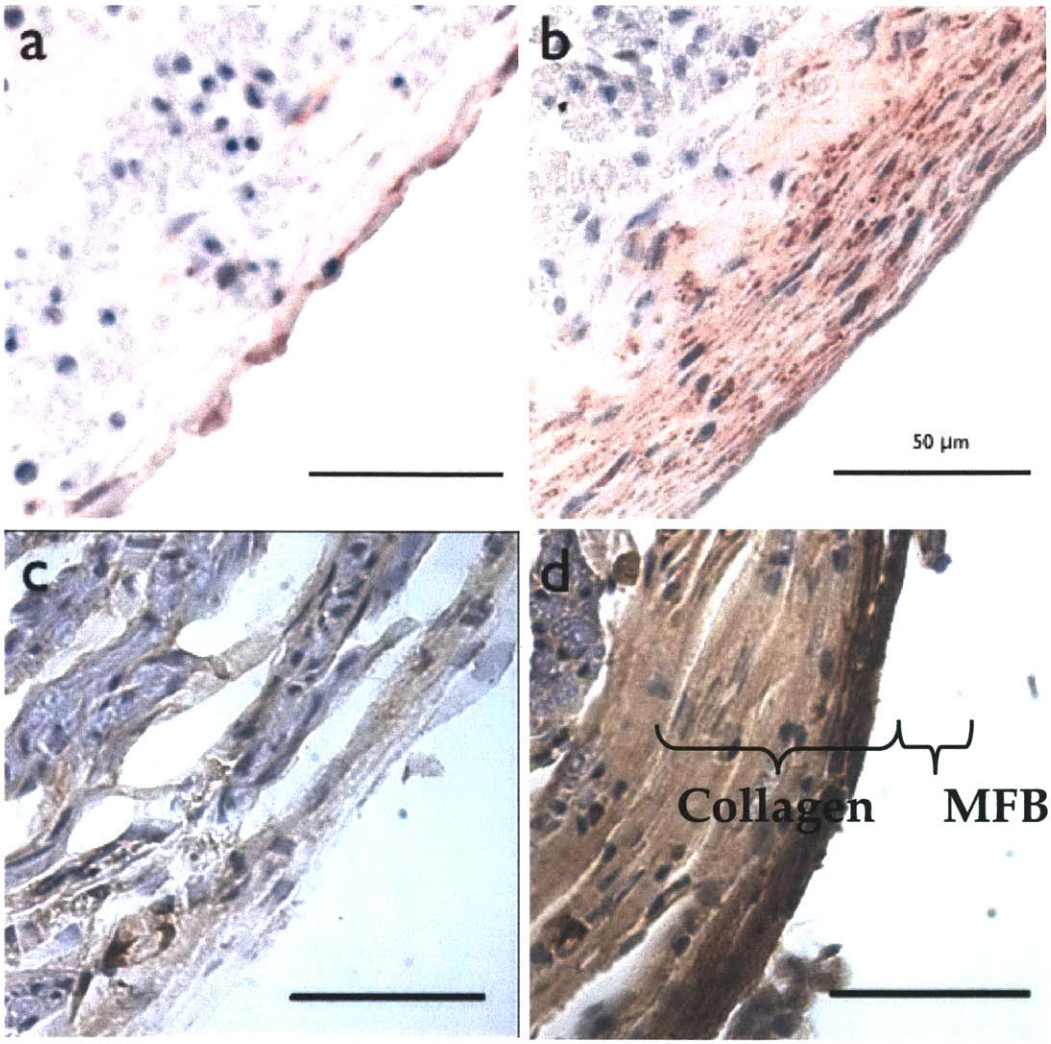

FIG. 2.25. OBSERVATIONS OF CONTRACTILE CAPSULE REDUCTION BY DEGRADABLE COLLAGEN DEVICES. Contractile capsules containing myofibroblasts (MFBs) staining positively for α-SMA are visible in red at 30 weeks surrounding nerves regenerated across a 10 mm gap with (a) Neuragen™, a collagen nerve guide widely used in the clinic and (b) a biodurable silicone nerve guide (Chamberlain, Yannas et al, 1998) and in brown at 9 weeks surrounding nerves regenerated with (c) intermediately-degrading collagen tubes (Device C current study) and (d) highly-cross-linked collagen tubes (Device E current study). Scale bars: 50 µm.

A speculative model for capsule growth that could explain these observations is based on the behavior of myofibroblasts in granulation tissue in skin wounds (Tomasek et al., 2002):

1. Growth of the contractile capsule begins with the proliferation and differentiation of α-SMA (+) cells at the periphery of the severed nerve trunk. The exact origin of the MFBs is unknown but candidate sources include

endoneurial fibroblasts (FBs), perineurial cells, and/or fibrocytes from the exudate, which is known to collect inside the tube in the space initially separating the two nerve stumps.

2. As contractile cells migrate into the provisional fibrin matrix that fills the nerve gap in the 1-2 weeks following injury, the capsule also grows radially outward from the transected nerve stumps. Preliminary data indicates that at 1 week post-injury in Device A the capsule thickness has grown to more than 200 μm with continuous layers of α-SMA (+) cells near the severed proximal stump.

3. Differentiated MFBs in the capsule begin to lay down collagen matrix and other ECM molecules, as they do in full-thickness skin wounds (Tomasek et al., 2002). Based on observations of MFBs in skin wounds, collagen matrix deposition may establish stress-shielded zones in the inner portions of the capsule. Stress-shielded MFBs, in the absence of their tensional stimuli, may disassemble their cytoskeletons and apoptose, leaving behind thick, scar-like collagen layers in the innermost portions of thick capsules.

4. The persistence of multiple cohesive layers of MFBs at the periphery of thick capsules suggest that connective tissue-contracture and/or compression of the regenerate is still taking place at 9 weeks post-injury. In Chamberlain et al., layer of MFBs persisted even at 60 weeks surrounding regenerates in silicone tubes.

The current surgical model was a more demanding test of induced axonal regeneration in a nerve chamber than the Chamberlain study (15 mm in the current study and 10 mm gap in the earlier study) but the specific effect of the increase in gap length on contractile capsule formation in the presence of a nerve guide is not known. Several key differences exist between the devices used in the Chamberlain study and devices used in the current study, all of which could conceivably influence the degree of capsule formation, namely the chemical composition (type I collagen vs. silicone) and the biodegradability. Silicone elastomers are known to elicit a heightened foreign body reaction compared to collagen devices (Yannas, 2001) and the silicone surface is not populated with ligands specific to integrins of contractile cells as is the case with type I collagen nerve guides. This, combined with the biodurable nature of the silicone

elastomer seem to favor the development of a contractile myofibroblast phenotype in cells at the periphery of the defect, and increase the likelihood of MFB-MFB interactions on the inner and outer surfaces of the nerve guide (Chamberlain, Yannas et al, 1998), ultimately leading to a thicker connective tissue capsule that persists at 30 weeks post-neurotmesis (**Fig.2.25.b**).

The current work advances the study of contractile capsule formation after severe nerve injury by making use of a homologous series of collagen devices with identical chemical composition and structural properties though differing in cross-link density which controls the degradation rate (Harley, Spilker et al, 2004). While the initial cell permeability of the collagen devices used in this study was not measured, the cell permeability of highly porous collagen biomaterials has been shown to rely intimately on the pore structure (O'Brien, Harley et al. 2005; O'Brien, Harley et al. 2007). The homologous series has identical pore size and structure and likely has similar values of initial permeability to small molecules, although this was not measured in this study. The film layer that forms the lumen of the collagen devices suggests that the homologous series is initially impermeable to cell traffic.

The independent variable of the homologous series in this study is the cross-linking treatment. Higher levels of cross-linking across the series lead to a higher density of collagen molecular cross-links in the device and a reduced *in vivo* degradation rate in the presence of wound-healing fibroblasts following neurotmesis (current study, Harley et al, 2004). Over time, collagenases act to reduce the mass of collagen biomaterials and to increase their porosity *in vivo* (current study; Harley, Spilker et al, 2004).

In the current study, experimental observations of the homologous series suggest that the cross-linking treatment mediates the cell permeability of the type I collagen devices at 1 and 9 weeks after neurotmesis. Observations of contractile cells distributed throughout the walls of the degrading device (Device D) coincided with a reduction in contractile capsule thickness, δ at 9 weeks post-neurotmesis (**Fig. 2.20, Fig 2.21, Fig. 2.22**). The most heavily cross-linked device in the homologous series (Device E) did not degrade appreciably by 9 weeks and appeared to have the initially cell-impermeable lumen still intact. The absence of contractile cells in the walls of Device E coincided with thicker contractile capsules with more myofibroblasts present in the capsule.

Further strength comes from preliminary observations at 1 week after injury (**Fig. 2.23**) in which a thick MFB capsule had already developed between the interface of Device E and the nerve stump. No myofibroblasts were detected in the walls of Device E and the lumen of the scaffold was intact. Conversely, a dramatically thinner capsule formed at the interface between Device D and the nerve stump. The capsule appeared less cohesive in this case and numerous myofibroblasts were detected interacting within the walls of the Device D tube. Speculatively, the preliminary data suggests that MFB-scaffold interactions in optimally degrading tubes coincide with blocking contraction at early time points.

2.4.3. Collagen Tubes of Intermediate Cross-linking Maximize Histomorphometric Quality of Regeneration, Q

The regenerative activity of biodegradable type I collagen devices was elucidated in a quantitative manner with a challenging model of induced axonal regeneration. The intermediately-cross-linked type I collagen devices of the homologous series led to higher values of histomorphometric quality of axonal regeneration for biodegradable type I collagen devices across a 15 mm gap at 9 weeks post-neurotmesis (total myelinated area of 0.28 $\pm$ 0.03 mm^2, 7060 $\pm$ 967 myelinated fibers and 654 $\pm$ 106 large diameter A-fibers) than a previous study using collagen tubes of very similar structural determinants and evaluated at the same time point (Harley et al., 2004). In particular, the number of myelinated fibers and the number of A-fibers are known to correlate well with functional measurements of regenerated nerves. Taken together, these results highlight the clinical relevance of induced axonal regeneration using optimally degrading type I collagen devices. These Q metrics were significantly higher than previously reported values of axonal regeneration in this injury model at 9 weeks using type I collagen devices with identical cross-linking treatments and the Integra Neuragen™ device, the most widely used degradable nerve guide in the clinic today (Harley, Spilker et al, 2004).

Despite very similar methodologies between this study and the Harley study, slightly different optimal degradation parameters for induced regeneration were identified. Devices B and C exhibited maximal Q in the current study whereas Devices

C and D maximized Q in the Harley study. Notable differences in the methodology include the age and lot of microfibrillar collagen used, the model and age of freeze dryer, and the age of the molds and vacuum pump (used for dehydrothermal cross-linking treatment). A likely explanation for the shift in regenerative activity of the homologous series may be that the scaffolds used in the current study were generally easier to degrade than the Harley scaffolds. Harley also reported that the homologous series of tubes in that study had an average pore size of 80 μm at the inner lumen. Scanning electron micrographs of the homologous series in the current study reveal an ~80 μm pore size in the tube wall but a several micron thick cell-impermeable film layer in the inner lumen and the outer shell of the collagen tubes. No film layer was reported in the Harley study. Due to the thin nature of this layer (visualized in the current study with scanning electron microscopy), if it did exist in the Harley tubes it is unlikely to have been detected with the embedding and sectioning technique that was used in that study.

2.4.4. The Pressure Cuff Theory and the Homologous Series

The pressure cuff theory posits that contractile MFB capsules with large δ generate a large circumferential compressive stress on transected nerve stumps that impedes the formation of new nerve tissue. This prediction is supported by direct quantitative measurements in the current study at 9 weeks post-neurotmesis and the identification of large, negative and statistically significant correlations between δ and total myelinated area, number of myelinated fibers, and number of A-fibers. Further support for the pressure cuff theory comes from preliminary data at 7 days after neurotmesis, which suggests that spontaneous MFB capsules with high δ appear to coincide with deformation of the transected nerve stump in a manner that is consistent with a circumferential hoop stress.

Speculatively, the data support cell-permeability as a plausible explanation for why regeneratively active scaffolds (intermediately cross-linked devices B, C, and D) appear to down regulate capsule formation and regeneratively inactive scaffolds (non-cross-linked device A and highly cross-linked device E) do not. In this study device A only bridged a 15 mm gap with 50% success. This fast-degrading device may have poor

regenerative activity because it fails to remain intact long enough to disrupt the contractile capsule that forms in the first 1-2 weeks after injury. On the other end of the homologous series of type I collagen devices, the highly cross-linked device E does not appear to be cell-permeable during this time scale. Contractile myofibroblasts build up at the interface of the nerve and the cell-impermeable scaffold 7 days after injury. The gain in regenerative activity between Device E and Devices B and C coincides with a reduction in capsule thickness and may be explained by the fact that reduced cross-linking treatment of these scaffolds to cell permeability of these nerve guides.

2.4.5. Future Work

The speculative role that cell permeability plays in the regenerative activity of the collagen scaffolds motivates future studies of how scaffold properties mediate capsule formation. Future work should focus on the design of biomaterials that enhance contractile cell – scaffold interactions at early time points (before significant capsule formation or nerve stump constriction occurs). Such a study might quantify cell-cell interactions (via cadherin expression, for example) and cell-scaffold interactions (via focal adhesion expression) in response to carefully controlled scaffold properties that affect MFB-scaffold interactions.

A useful research tool is a homologous series with identical chemical composition and solids content but different average pore size in the same injury model. More numerous, smaller pores in the collagen device could lead to more myofibroblast-scaffold interactions by increasing the specific density of ligands and may lead to the discovery of an improved device that reduces capsule formation to unprecedented levels and maximizes axonal regeneration by increasing cell traffic in the scaffold. Recently, a homologous series of type I collagen tubes with the desired characteristics for this study were synthesized by modulating the freezing temperature between -20 °C and -196 °C. The fabrication and characterization of these tubes is described in **Appendix A.1**.

Future work should also investigate the influence of capsule thickness on the unit cell processes of axonal regeneration (e.g. Schwann cell migration, neovascularization). Identifying a quantitative link between the capsule and these molecular events could further support the pressure cuff theory.

2.5 Literature Cited

Aitken, J. T. (1949). "The effect of peripheral connexions on the maturation of regenerating nerve fibres." J Anat **83**(Pt. 1): 32-43.

Aitken, J. T., M. Sharman, et al. (1947). "Maturation of regenerating nerve fibres with various peripheral connexions." J Anat **81**(1): 1-22.

Arbuthnott, E. R., I. A. Boyd, et al. (1980). "Ultrastructural dimensions of myelinated peripheral nerve fibres in the cat and their relation to conduction velocity." J Physiol **308**: 125-157.

Carr, M. M., T. J. Best, et al. (1992). "Strain differences in autotomy in rats undergoing sciatic nerve transection or repair." Ann Plast Surg **28**(6): 538-544.

Chamberlain, L. J., I. V. Yannas, et al. (1998). "Early peripheral nerve healing in collagen and silicone tube implants: myofibroblasts and the cellular response." Biomaterials **19**(15): 1393-1403.

Chamberlain, L. J., I. V. Yannas, et al. (2000). "Connective tissue response to tubular implants for peripheral nerve regeneration: the role of myofibroblasts." J Comp Neurol **417**(4): 415-430.

Chamberlain, L. J., I. V. Yannas, et al. (1998). "Collagen-GAG substrate enhances the quality of nerve regeneration through collagen tubes up to level of autograft." Exp Neurol **154**(2): 315-329.

Chen, Z. L., W. M. Yu, et al. (2007). "Peripheral regeneration." Annu Rev Neurosci **30**: 209-233.

Deumens, R., A. Bozkurt, et al. (2010). "Repairing injured peripheral nerves: Bridging the gap." Prog Neurobiol **92**(3): 245-276.

Foltan, R., K. Klima, et al. (2008). "Mechanism of traumatic neuroma development." Med Hypotheses **71**(4): 572-576.

Hinz, B. (2007). "Formation and function of the myofibroblast during tissue repair." J Invest Dermatol **127**(3): 526-537.

Jiang, X., S. H. Lim, et al. (2010). "Current applications and future perspectives of artificial nerve conduits." Exp Neurol **223**(1): 86-101.

Lundborg, G., F. M. Longo, et al. (1982). "Nerve regeneration model and trophic factors in vivo." Brain Res **232**(1): 157-161.

Mackinnon, S. E. and A. L. Dellon (1988). Surgery of the peripheral nerve. New York, Thieme Medical Publishers.

Mandl, I., J. D. Maclennan, et al. (1953). "Isolation and characterization of proteinase and collagenase from Cl. histolyticum." J Clin Invest **32**(12): 1323-1329.

O'Brien, F. J., B. A. Harley, et al. (2007). "The effect of pore size on permeability and cell attachment in collagen scaffolds for tissue engineering." Technol Health Care **15**(1): 3-17.

O'Brien, F. J., B. A. Harley, et al. (2005). "The effect of pore size on cell adhesion in collagen-GAG scaffolds." Biomaterials **26**(4): 433-441.

Sanders, F. K. and J. Z. Young (1944). "The role of the peripheral stump in the control of fibre diameter in regenerating nerves." J Physiol **103**(1): 119-136 112.

Sanders, F. K. and J. Z. Young (1946). "The influence of peripheral connexion on the diameter of regenerating nerve fibres." Journal of Experimental Biology **22**: 203-212.

Sigma-Aldrich. (1996). "Enzymatic Assay of Collagenase." from http://www.sigmaaldrich.com/etc/medialib/docs/Sigma/Enzyme_Assay/collagenaseddig.Par.0001.File.tmp/collagenaseddig.pdf.

Tomasek, J. J., G. Gabbiani, et al. (2002). "Myofibroblasts and mechano-regulation of connective tissue remodelling." Nat Rev Mol Cell Biol **3**(5): 349-363.

Vleggeert-Lankamp, C. L. (2007). "The role of evaluation methods in the assessment of peripheral nerve regeneration through synthetic conduits: a systematic review. Laboratory investigation." J Neurosurg **107**(6): 1168-1189.

Williams, L. R., F. M. Longo, et al. (1983). "Spatial-temporal progress of peripheral nerve regeneration within a silicone chamber: parameters for a bioassay." J Comp Neurol **218**(4): 460-470.

Yannas, I. V. (2001). Tissue and organ regeneration in adults. New York, Springer.

Yannas, I. V., J. F. Burke, et al. (1975). "Correlation of in vivo collagen degradation rate with in vitro measurements." J Biomed Mater Res **9**(6): 623-628.

Yannas, I. V., E. Lee, et al. (1989). "Synthesis and characterization of a model extracellular matrix that induces partial regeneration of adult mammalian skin." Proc Natl Acad Sci U S A **86**(3): 933-937.

Yannas, I. V., M. Zhang, et al. (2007). "Standardized criterion to analyze and directly compare various materials and models for peripheral nerve regeneration." J Biomater Sci Polym Ed **18**(8): 943-966.

Zhang, M. and I. V. Yannas (2005). "Peripheral nerve regeneration." Adv Biochem Eng Biotechnol **94**: 67-89.

This page intentionally left blank.

3

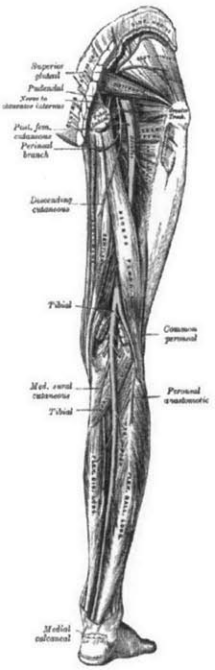

Nerves of the Right Lower Extremity, Posterior view

Gray's Anatomy

This page intentionally left blank.

3

A Pilot Study of Y-27632, a Soluble Inhibitor of Actin-Myosin Contractility, and its Effect on the Early Response to Sciatic Neurotmesis

3.1 Introduction

Induced regeneration studies from three organs in the adult mammal (skin, peripheral nerves, and the conjunctiva) suggest an antagonistic relationship between myofibroblast-mediated contraction of wounds and induced regeneration (Yannas, 2001). In each instance of induced regeneration, contraction blocking was accomplished using regeneration templates, or scaffolds of highly specific structural and chemical properties that mainly control the environment or the density of contractile cells (myofibroblasts).

In addition to scaffolds, diffusible factors could be used to inhibit specific components of the intracellular pathway in an effort to further evaluate the relationship between cell-mediated contraction and induced peripheral nerve regeneration. The crucial role that Rho-associated coiled-coil forming protein serine/threonine kinase (ROCK) seems to play in cell-mediated contraction and cytoskeletal remodeling behavior of fibroblasts make it an attractive target for pharmacological inhibition.

3.1.1 Intracellular Pathways Leading to Contraction

The scaffolds described above seem to impart contraction-blocking activity primarily by controlling the local microenvironment of contractile cells. Increasingly, the complex inflammatory response of the adult mammal to injury is elucidated by on-going research at the cellular and molecular level. This work has shed meaningful light on the intracellular pathways that lead to expression of the contractile phenotype and force generation in connective tissue cells. Pharmacological inhibitors of various components of these pathways have been developed with varying degrees of specificity. In addition to serving as important diagnostic tools for further probing

these complex processes, these inhibitors have potential clinical benefit as contraction-blocking agents in studies of induced regeneration.

Cellular behavior results from a complex interaction of both mechanical and biochemical factors. The Rho GTPases have been identified as important molecular switches that play a major role in the modulation of many cellular processes including cell migration, actomyosin contractility, and cell differentiation in response to mechanical forces and other agonists, including TGF-β1 (Chrzanowska-Wodnicka and Burridge 1992; Chrzanowska-Wodnicka and Burridge 1996).

3.1.2. Rho GTPases

The Rho GTPases are signaling proteins that are essential to a number of cellular processes, notably the regulation of actin cytoskeleton dynamics and actomyosin contractility (Riento and Ridley 2003). Three main classes of Rho GTPases are thought to be involved in the regulation of these cellular activities: Rho, Rac, and Cdc42.

Both the extending and contracting forces of a migrating cell are regulated by Rho-family GTPases (Riento and Ridley 2003). These forces are necessary for cell locomotion and other cell processes, including the remodeling of the extracellular matrix (ECM) that occurs in tissue differentiation and wound healing. The G proteins Rac and Rho have been identified as key regulators of cellular morphology in three-dimensional matrices. Rac stimulates cell protrusion while Rho inhibits protrusion and stimulates contraction.

The leading edge extension of the cellular surface is driven by the Rho-family GTPases Rac1 and Cdc42 through actin polymerization. Rho kinase (ROK/RhoK/ROCK, called ROCK in this paper) has two isoforms (ROCKI and ROCKII). In non-muscle cells ROCK regulates several functions, notably actin-cytoskeleton assembly and cell contractility. Specifically, ROCK isoforms play roles in mediating the formation of RhoA induced stress fibers and focal adhesions through effects on phosphorylation of MLC and actomyosin contractility.

3.1.3 Contraction Overview

Many processes in the body depend on actomyosin contractility, including cell migration and stress fiber formation (Chrzanowska-Wodnicka and Burridge 1996). Myosin II is a major cytoskeletal protein in muscle and non-muscle cells that is

responsible for converting the chemical energy of ATP into the mechanical energy of contraction. Originally, myosin-mediated contraction was thought to be regulated by a cytostolic increase in Ca2+ according to the traditional smooth muscle model of Ca^{2+} coupled contraction. Within the last 10 years, several Ca2+-independent myosin II motor pathways were elucidated.

The current consensus is that smooth muscle contraction arises from the combination of two major pathways: an initial Ca^{2+}-calmodulin interaction to stimulate an initial rapid contraction via phosphorylation of the myosin light chain (MLC) and a sustained level of phosphorylated MLC due to inhibition of the action of myosin phosphatase (dephosphorylation of the MLC) by the RhoA / Rho kinase (ROCK) pathway, leading to maintained force generation (Webb 2003).

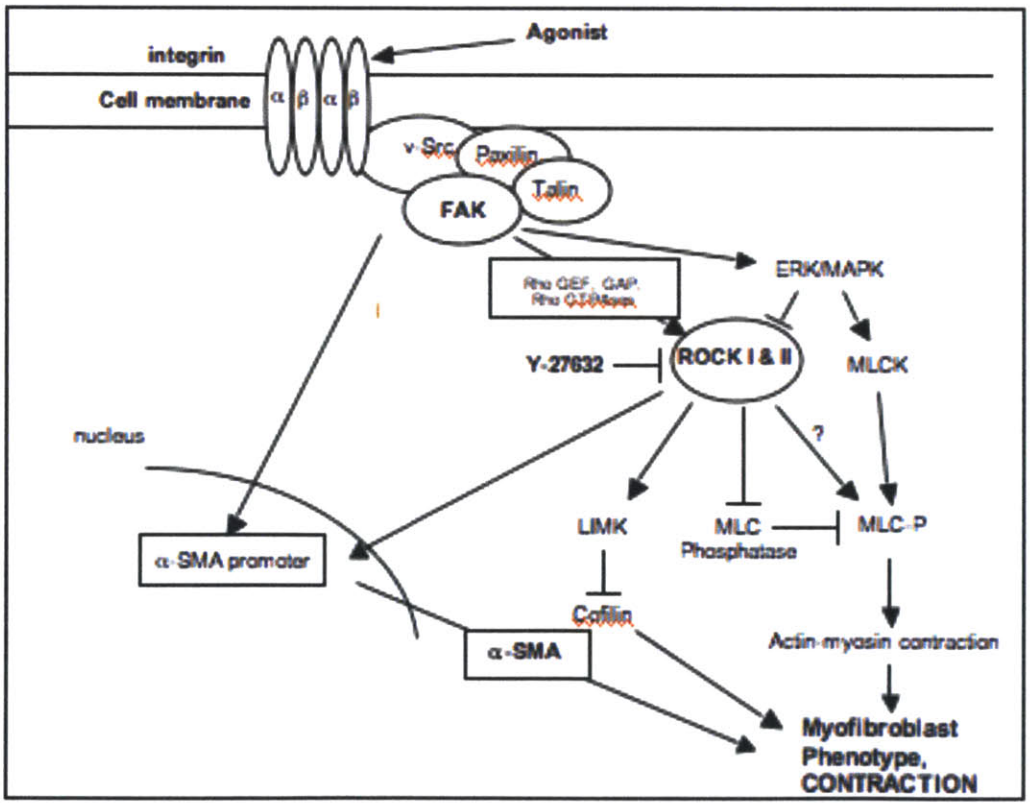

FIGURE 3.1: INTRACELLULAR PATHWAYS LEADING TO SYNTHESIS OF α-SMOOTH MUSCLE ACTIN (α-SMA). Two agonists (top) are widely recognized: mechanical tension and TGF-β1 (Tomasek, Gabbiani et al. 2002). The pathway is a modification of pathways described in (Burridge and Chrzanowska-Wodnicka 1996) and (Carragher and Frame 2004).

Numerous non-muscle cell types (such as fibroblasts in wound beds) exhibit the ability to generate and sustain contractile forces for an extended period of time. Recent work suggests that this force is generated by stress fibers composed of bundles of actin microfilaments, non-muscle myosin and, in the case of the differentiated myofibroblast, both E-DA fibronectin and α-SM actin and that this isometric tension is regulated by inhibition of myosin phosphatase by ROCK. (Hinz and Gabbiani, 2003). Briefly, ROCK II mediates stress fiber formation by phosphorylating the MBA binding site of MLC phosphatase, inhibiting its activity and leading to increased MLC phosphorylation (Riento and Ridley 2003). The result is increased binding of actin as well as actin-induced ATPase activity of myosin II, ultimately leading to contraction. Because myosin is effective at cross-linking F-actin, enhanced myosin-actin binding leads to formation of F-actin into stress fibers and focal adhesions (FAs) (Chrzanowska-Wodnicka and Burridge 1996).

The phosphorylation of the motor protein myosin II at the MLC_{20} (regulatory chain) has been elucidated as a key role in regulating actomyosin contractility in non-muscle cells (Komatsu, Yano et al. 2000).

3.1.4 Inhibition of ROCK and Contraction

In response to external tension, fibroblasts exert sustained isometric force on their surrounding environment via a Rho/Rho-kinase (ROCK)-mediated, actomyosin contractile apparatus. (Kimura, Ito et al. 1996; Amano, Chihara et al. 1997; Hall 1998; Katoh, Kano et al. 2001; Katoh, Kano et al. 2001). This three-dimensional, transcellular structure consists of stress fiber bundles made up of actin microfilaments, non-muscle myosin and, in the case of the differentiated myofibroblast, both E-DA fibronectin and α-SM actin (Serini, Bochaton-Piallat et al. 1998; Dugina, Fontao et al. 2001). Through the inhibitory phosphorylation of myosin phosphatase (Kawano, Fukata et al. 1999), ROCK promotes myosin light-chain (MLC) phosphorylation by MLC kinase (MLCK). The resultant increase in myosin filament assembly and actin-activated myosin ATPase activity lead to sustained contraction (Burridge and Chrzanowska-Wodnicka 1996), (**Fig 3.1**). In addition to MLC, Rho-ROCK activation of other substrates including LIM kinase (LIMK), cofilin, mDia and PIP4-5 kinase contributes to actin polymerization and stress fiber formation (Van Aelst and D'Souza-Schorey 1997; Arber, Barbayannis et al. 1998; Kaibuchi, Kuroda et al. 1999; Maekawa, Ishizaki et al. 1999).

The crucial role of the downstream effector Rho kinase (ROCK) in cell-mediated contraction in response to various agonists makes it an attractive target for pharmacological inhibition. Treatment of fibroblasts and other non-muscle cells cultured in 3-D collagen lattices with Y-27632, (R)-(+)-*trans*-4-(1-aminoethyl)-N-(4-pyridyl) cyclohexanecarboxamide dihydrochloride, a specific inhibitor of the Rho-associated coiled-coil forming protein serine/threonine kinase (ROCK) family of protein kinases (Narumiya, Ishizaki et al. 2000) leads to relaxation of matrix stress and prevention of myofibroblast morphology and focal adhesion maturation. Specifically, in a reversible and dose-dependent manner, Y-27632 treatment abrogates stress fibers (Masamune, Kikuta et al. 2003; Patel, Harding et al. 2003; Vishwanath, Ma et al. 2003), significantly reduces ⟨-SMA expression (Masamune, Kikuta et al. 2003; Patel, Harding et al. 2003; Zheng, Bando et al. 2004), and inhibits contractile force generation measured using a stress-relaxed collagen lattice model (Parizi, Howard et al. 2000; Zheng, Bando et al. 2004), an isometric culture force monitor (Yee, Melton et al. 2001; Tangkijvanich, Melton et al. 2003) and finite element modeling analysis (Vishwanath, Ma et al. 2003). In addition, several studies suggest the absence of toxicity or short-term side effects from Y-27632 use in animal models for the treatment of hypertension and liver fibrosis (Uehata, Ishizaki et al. 1997; Itoh, Yoshioka et al. 1999; Tada, Iwamoto et al. 2001; Murata, Arii et al. 2003).

A preliminary *in vitro* study (Soller 2005) led to evaluation of the effect of Y-27632, a specific pharmacological inhibitor of ROCK, on the contraction of highly porous, three-dimensional type I collagen-glycosaminoglycan (CG) matrices over time by attached NR6WT fibroblasts treated with TGF-β1, a known upregulator of both fibroblast contraction and expression of the contractile filament α-smooth muscle actin (⟨-SMA). The latter is a hallmark of the myofibroblast phenotype. The demonstrated ability of Y-27632 to inhibit *in vitro* TGF-β1-stimulated force generation of a collagen-GAG scaffold by fibroblasts (Soller 2005) support its use in an *in vivo* study that evaluates the relationship between contraction blocking using pharmacological inhibitors and induced regeneration in a peripheral nerve wound model.

3.1.2. Project Goal & Major Findings:

The goal of this study was to evaluate the dose-dependent effects of a diffusible, small-molecule inhibitor of actomyosin contractility on the MFB capsule thickness, δ. A range of dosages of the inhibitor was used in a demanding model of peripheral nerve regeneration (rat sciatic neurotmesis, 15 mm gap) and the effects were evaluated at an early time point (2 weeks post-neurotmesis).

The diffusible, small-molecule agent Y-27632 permits controlled pharmacological disruption of actomyosin contractility (via continuous, small-molecule inhibition of Rho kinase, ROCK) in non-muscle cells. Along this direction, a new drug delivery system was designed which consists of an implanted osmotic minipump to continuously deliver a range of dosages of the inhibitor to a transected peripheral nerve, entubulated in a silicone nerve chamber (Lundborg model) with an inter-stump gap length of 15 mm. Previous studies suggested that an appropriate way to achieve local control of the MFB phenotype *in vivo* is to insert the two nerve stumps into a biodegradable tubular scaffold of highly specific structural and chemical properties [Harley et al, 2004; Chamberlain et al, 2000]. Use of such scaffolds has led to significant thinning, and in some cases almost complete extinction, of the MFB capsule and to unprecedented levels of quality of nerve regeneration. In addition to scaffolds, diffusible factors could be used to inhibit specific components of the intracellular pathway in an effort to evaluate the relationship between contraction and induced regeneration.

3.2. Materials and Methods

3.2.1. Design and Fabrication of a Biodurable Nerve Guide, Continuous Drug Delivery System

The novelty of the drug delivery system utilized in this study is the incorporation of an osmotic minipump in lieu of an injection port, which allows continuous drug delivery to a "T tube" nerve chamber. This modification reduces labor time and likely reduces experimental error relating to the delivery of the injection by the operator. Specifically, the timing of injection and the velocity of injection are both

sources of error that could affect the microenvironment of the immature regenerate at early time points.

Custom Silicone "T tubes" were designed and fabricated based on previous reports (McDonald and Zochodne 2003; Kemp, Walsh et al. 2007) that used similar devices in conjunction with mini-injection ports. The custom-built silicone "T tube" (# 1, **Fig. 3.2**) was fabricated from two sections of Dow Corning standard Silastic® tubing (I.D. 1.47 mm), which have been used previously in *in vivo* studies of regeneration in the presence of silicone nerve guides (Chamberlain, Yannas et al. 1998). The first section was cut to 21 mm long, and served as the nerve chamber component of the "T tube." A 15 gauge needle was threaded into the lumen of this 21 mm section and a 1 mm-diameter circular hole was made in one side of the tube wall of the nerve chamber at the midpoint (10.5 mm from the end of the tube) using a sterile skin biopsy punch (Miltex).

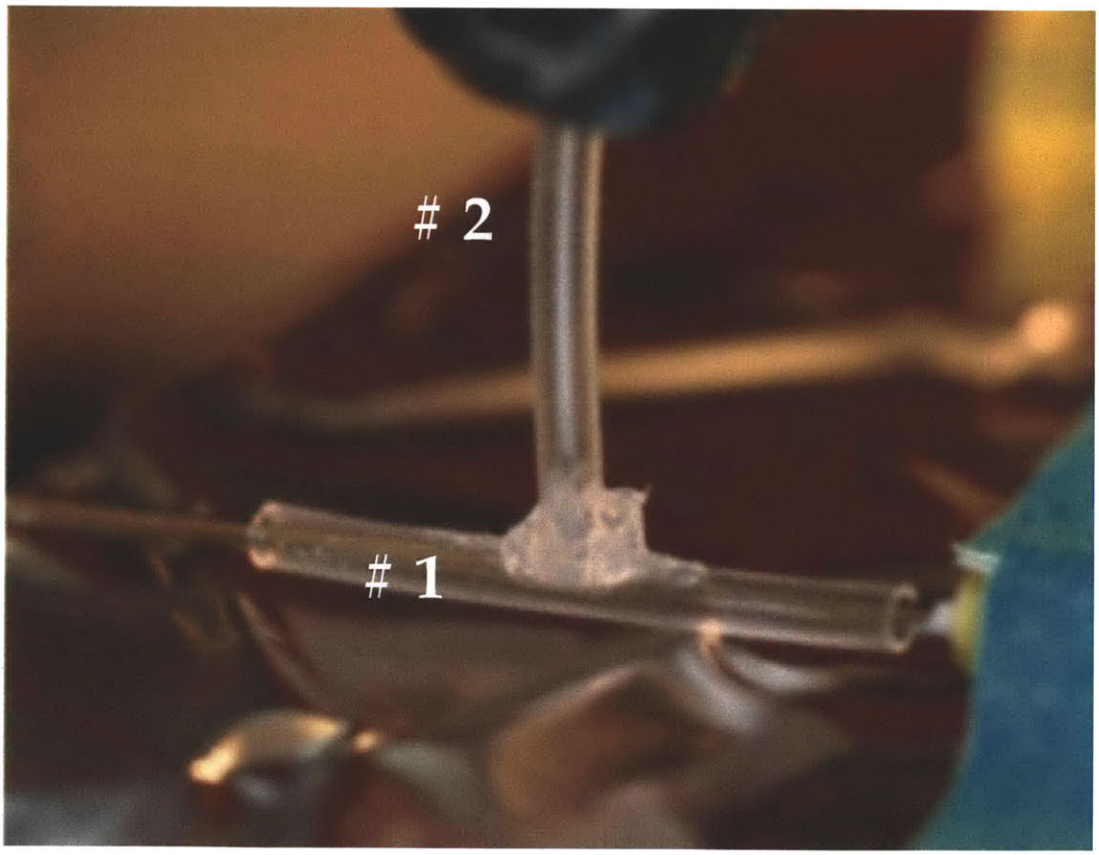

FIG. 3.2 A CUSTOM-BUILT SILICONE "T TUBE" is fabricated from two pieces of Dow Corning standard Silastic® tubing (I.D. 1.47 mm) and Type A Silastic® Medical adhesive silicone. # 1 serves at the nerve chamber and # 2 serves as the access tube to the catheter of the drug delivery system. All devices were sterilized via autoclave prior to implantation. Design is adapted from (McDonald and Zochodne, 2003).

A second section of silicone tube (**#2, Fig. 3.2**) of excess length was clamped perpendicular to the 1 mm hole and serves as the access tube from the catheter to the nerve chamber. Type A Silastic® Medical adhesive silicone (Dow Corning) was applied liberally to the joint between the two tubes using sterile probes. Once applied, the "T tube" was left to cure at room temperature in this position for a minimum of 48 hours.

3.2.2. "T Tube" Testing & Sterilization

Following curing of the adhesive, each "T tube" was tested for inner patency and the absence of leaks. "T tubes" were placed on wax paper and carefully held upright with forceps. The stem of each "T tube" was injected slowly with sterile, distilled, deionized H_2O using a small gauge needle. Nerve chambers that did not fill with H_2O or had noticeable liquid loss from the device at the joint were discarded. Each "T tube" was sterilized via autoclave for 30 minutes. Select "T tubes" from each batch of implants were tested after autoclave treatment for patency and leakage (as described above) and for adequate handling strength of the adhesive joint.

3.2.3. In Vivo *Testing of Drug Delivery System*

The *in vivo* performance of a novel system for continuous drug delivery was tested by loading osmotic minipumps with sterile 1% aqueous methylene blue dye and implanting these devices for 6 days (n=3 animals) and 14 days (n=3 animals) as described in the surgical protocol below. At the prescribed time points, the animals were sacrificed according to NIH guidelines described below and the "T tubes" were inspected for presence of the dye to verify delivery.

3.2.4. Surgical Procedure

A novel version of the Lundborg nerve chamber model (Lundborg et al., 1982), which allows for continuous delivery of soluble factors was used in the current study and is described in detail here. The modified components of the surgery include the implantation of the osmotic minipump on the dorsum, the tunneling of the catheter from the minipump to the T tube, and the connection of the catheter to the T tube. The left sciatic nerve of adult female Lewis rats (175-250 g) was transected as described in

Chapter 2 and the stumps are inserted 3 mm into a custom-built silicone "T tube" (**Fig. 3.2**) fabricated from Dow Corning standard Silastic® tubing (I.D. 1.47 mm) and Type A Silastic® Medical adhesive silicone. The stumps are be secured with 10-0 suture, and the inter-stump gap length is 15 mm (**Fig. 3.3**). At a 15 mm gap length in a silicone tube, the success rate of regeneration is expected to be 0 % (Spilker 2000).

NIH guidelines for the care and use of laboratory animals (NIH Publication No. 85-23 Rev. 1985) were observed. Adult female Lewis rats (Charles River Laboratories, Wilmington, Mass., USA), 175–200 g, were used in this study. The Lewis strain of rat was chosen because of its resistance to autotomy, or self-mutilation, following sciatic nerve transection (Carr, Best et al. 1992).

All surgical procedures were performed in an aseptic environment, following a technique that had been previously described (Chamberlain, Yannas et al. 1998; Chamberlain, Yannas et al. 1998; Chamberlain, Yannas et al. 2000; Chamberlain, Yannas et al. 2000; Harley, Spilker et al. 2004). A 50 mg/kg dosage of sodium pentobarbital (50 mg/ml Nembutal sodium solution; Parke-Davis, Detroit, Mich., USA) was injected intraperitoneally to anesthetize each animal. The surgical area was shaved with animal clippers and cleansed with a providone-iodine sponge once the animal was fully anesthetized. The animal was placed in the prone position on a surgical board, with hind limbs held in 30° abduction. Using a sterile skin marker, the desired path of the vinyl catheter was traced onto the skin from dorsum to left leg (**Fig. 3.3a**). A 4 cm skin incision was made in the left leg parallel to and just posterior of the femur, exposing the muscle. The muscle and the fascia surrounding the sciatic nerve were dissected away so that the nerve was completely exposed and free from constraint between the sciatic notch and the distal bifurcation of the sciatic nerve (**Fig. 3.3b**). A 3 cm skin incision was made on the dorsum, and the fascia was dissected away exposing the animal's acromiotrapeziusmuscles (**Fig.3.3c**). A blunt steel probe was used to tunnel subcutaneously along the desired path of the vinyl catheter from the dorsum down the back and penetrating the left biceps muscle (**Fig. 3.3d**). The exposed sciatic nerve was further anesthetized topically using a few drops of 1% lidocaine placed directly on the nerve at the transection site. The left sciatic nerve was transected at the midpoint of the

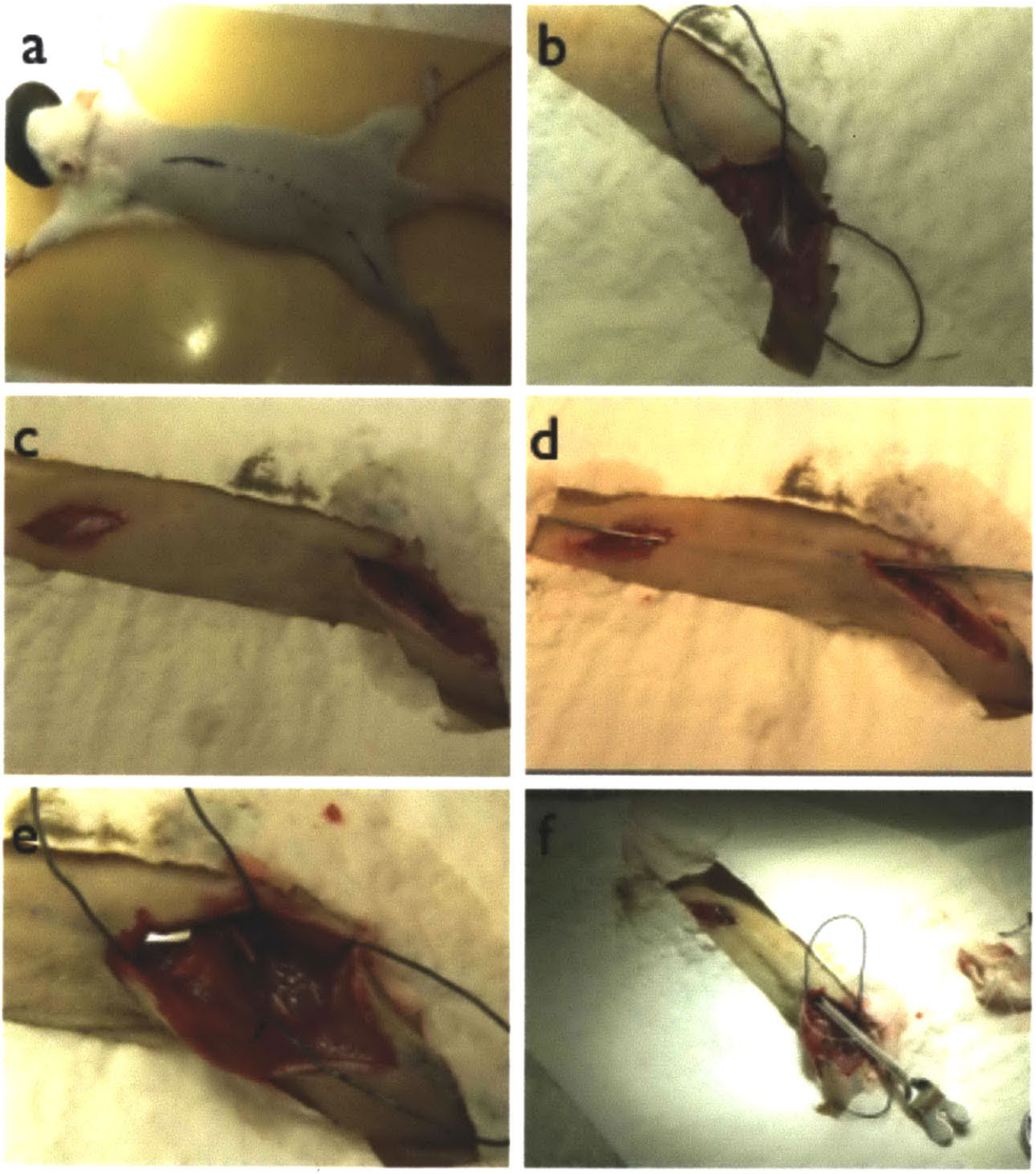

FIG. 3.3 A NOVEL SURGICAL PROCEDURE FOR CONTINUOUS DRUG DELIVERY TO A BIODURABLE NERVE GUIDE. Continuous drug delivery to the transected nerve stumps was accomplished through subcutaneous implantation of an osmotic minipump and catheter with the following major modifications to the traditional Lundborg model: the creation of an additional full-thickness skin wound in the dorsum (**c**), subcutaneous tunneling through the dorsum from posterior to anterior, and the threading of the catheter onto the stylet of a spinal biopsy needle (g) to pull it into position (**h**). The osmotic minipump was secured with metal sutures (**i**) and the dorsal skin wound was closed normally. The silicone "T tube" was implanted normally (**k**) leaving a 15 mm inter-stump gap and finally the vinyl catheter was inserted into the "T tube" and secured with several drops of cyanoacrylate (**l**).

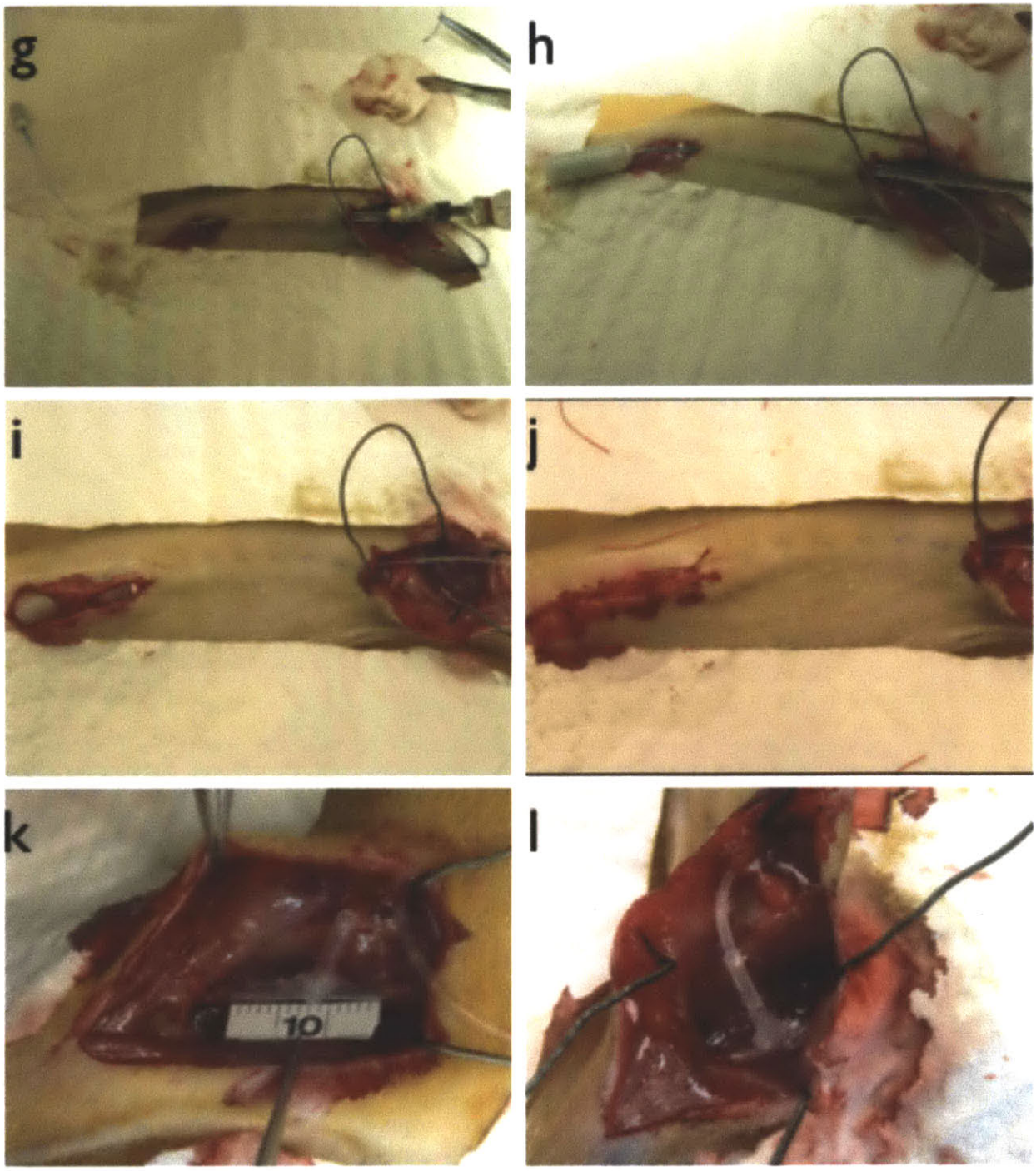
g
h
i
j
k
10
l

femur, midway between the sciatic notch and the distal bifurcation, using a fresh No. 11 scalpel blade (**Fig.3.3e**). A metal guide for the biopsy needle was inserted (Fig.3.3f) from posterior to anterior in the subcutaneous path. The stylet from a spinal needle was threaded through the subcutaneous path along the metal guide and inserted into open end of the vinyl catheter (attached to the minipump (**Fig.3.3g**). The style was retracted carefully, pulling the vinyl catheter through the subcutaneous space until the osmotic minipump rested in the 3 cm skin incision (**Fig.3.3h**). The osmotic minipump was secured in place with steel sutures (to prevent movement and the dorsal skin wound was closed normally with 4-0 vicryl sutures (j). The silicone "T tube" was placed in the gap, and the proximal and distal nerve stumps were inserted 3 mm into each end of the tube, leaving a 15 mm gap in the center between the stumps (**Fig.3.3k**). The nerve stumps were secured inside the tube using two 10-0 nylon sutures (Ethicon, Somerville, N.J., USA) at each end. The lumen of the tube was filled with sterile saline and the muscle and skin were closed using 4-0 Vicryl sutures (Ethicon) and skin staples (Roboz Surgical Instrument, Rockville, Md., USA).

The animals were returned to their cages and monitored until fully alert. Postoperatively, the animals were treated with subcutaneous injections Lactated Ringer's solution to combat fluid loss, Ketofen as an analgesic, and Cefazolin as an antibiotic. Ketofen and Cefazolin were continued once a day for the first 2 days following surgery and then as needed for the duration of the experiment. The animals were housed on wood chip bedding in a controlled environment with 12-hour on-off light cycles in separate cages for the duration of the experiment. Food and water were available ad libitum. The animals were monitored daily for signs of any abnormal behavior such as insufficient grooming, lack of appetite, aggressive behavior, or the appearance of autotomy.

All animals were sacrificed at 2 weeks postoperatively by carbon dioxide inhalation. The operated site was reopened, and the vinyl catheter connecting the minipump and the silicone "T tube" was severed. All sciatic nerve tissue between the sciatic notch and the distal bifurcation was removed along with any tissue bridging the gap between the transected nerve stump and the intact silicone T tube. The entire tissue block was then prepared for histomorphometric analysis.

Delivery of Y-27632

The reversible nature of Y-27632 required continuous local delivery of the molecule to the site of injury. Sterile-filtered Y-27632 in 0.9% saline was loaded into Alzet osmotic minipumps (model 2002 Durect Corp., 0 μg (n=3), 1 μg (n=3), 3 μg (n=3), 10 μg (n=3), and 100 μg (n=3); 200 μL and 0.5 μL/hr, **Table 3.1**), incubated overnight at 37 °C, and implanted subcutaneously on the back of each animal as described above. A vinyl catheter (attached to the pump after loading) was tunneled subcutaneously and attached to the access port of the silicone "T tube" with a few drops of cyanoacrylate (3M, St Paul, Minnesota).

Group	Soluble Factor	Dosage	N
C	Saline (control)	0	3
Y1	Y-27632 (saline)	1 μg	3
Y3	Y-27632 (saline)	3 μg	3
Y10	Y-27632 (saline)	10 μg	2
Y100	Y-27632 (saline)	100 μg	3

Table 3.1: Dosage Schedule for Y-27632.

3.2.5. Tissue Processing and Histomorphometric Procedures

Excised tissue was rinsed briefly in sterile saline and regenerates were photographed. The explants were fixed in Yanoff's fixative (0.01 M monobasic sodium phosphate, 0.06 M dibasic sodium phosphate, 2% formaldehyde, and 0.5% glutaraldehyde) for 24 h, transferred into a 10% formalin solution for 24 h, and then stored in 70% ethanol at 4°C. At this point, the silicone T tubes were carefully dissected from the immature regenerates and the tissue was sectioned as in **Fig.3.4**, and embedded in paraffin wax blocks. Tissue sections for histomorphological analysis were prepared by sectioning the paraffin-embedded samples on a microtome (Leica, Bensheim, Germany) at a 6 μm thickness; the sections were then mounted on Superfrost Plus slides.

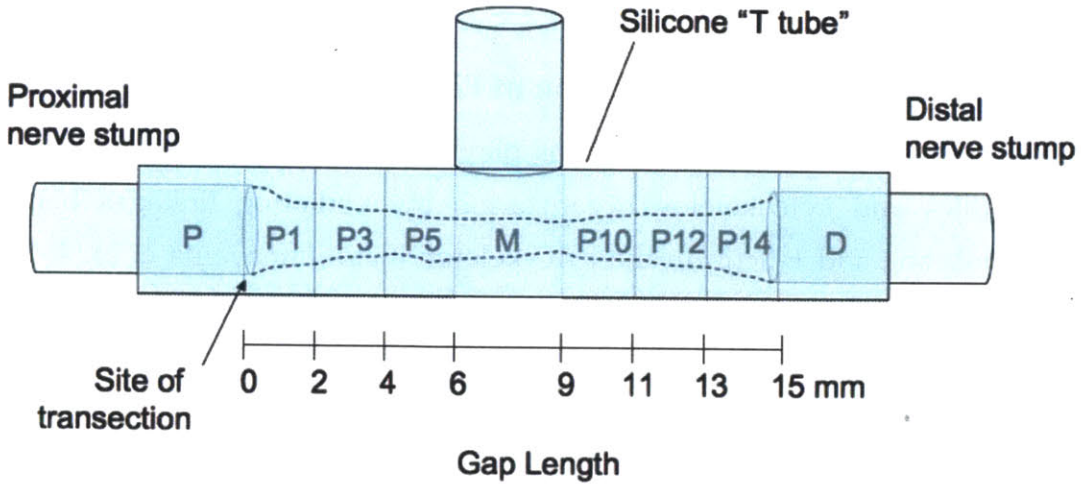

FIG. 3.4 SECTIONING OF EXPLANTS FOR HISTOLOGICAL ANALYSIS.

3.2.5.1. α-SMA Staining of Capsule

Two staining techniques were used to detect the presence of contractile cells (myofibroblasts) in the tissue formed at the 2-week time period of healing in the wound model. The first method was an immunohistochemical technique that used an antibody to the α-smooth muscle actin isoform, which is present only in myofibroblasts, smooth muscle cells and pericytes. Paraffin sections, cut to 6 μm thickness, were deparaffinized and treated with a 0.1% trypsin solution (Sigma Chemical Co., St. Louis, MO) for 60 min at room temperature to unmask antigen sites blocked by formalin fixation. The slides were treated with a 3% hydrogen peroxide solution for 10 minutes, followed by a protein solution (Dako, Carpinteria, CA) for 15 minutes, which served as the blocking agent. The primary antibody was a mouse monoclonal antibody against α-smooth muscle actin (Sigma Chemical Co., St. Louis, MO). The slides were soaked in the primary antibody (1 : 400 solution in Antibody Diluent, Dako) for 15 min at room temperature. The antibody was detected using the LSAB®2 System-HRP (Dako, Carpinteria, CA) which was specifically designed for use on Rat Specimens. The detection system consists of a biotinylated secondary antibody, which reacts with several peroxidase-conjugated streptavidin molecules. Following this, the AEC chromogen (Dako, Carpinteria, CA) was applied for 10 minutes, slides were lightly counterstained with Mayer's hematoxylin, and slides were mounted with aqueous-

based mounting medium.

3.2.5.2. Immunohistochemical Staining of Phosphorylation Targets of ROCK

Ezrin-radixin-moesin (ERM) proteins play an important role in the regulation of actin dynamics and cytoskeleton organization by mediating linkages between the plasma membrane and F-actin in the cytoskeleton (Sato, Funayama et al. 1992). Rho-kinases phosporylate various protein targets, including ERM proteins and this dephosphorylation is associated with inactivation of the enzyme. The net effect of Rho-kinase inhibition is consistent with decreased phosphorylation of ERM. A previous study testing in an animal model of atherosclerosis indicates the effect of Y-27632 on p-ERM staining can be detected histologically (Rekhter, Chandrasekhar et al. 2007).

In the current study, paraffin sections were subjected to heat-induced antigen retrieval in citrate buffer and stained for p-ERM (Phospho-Ezrin (Thr567)/Radixin (Thr564)/Moesin (Thr558) (41A3) Rabbit mAb, # 3149, 1:100 dilution, Cell Signaling Technology,) and ERM (Ezrin/Radixin/Moesin, # 3149, 1:200 dilution, Cell Signaling Technology) and detected with the LSAB®2 System-HRP for use on Rat Specimens (Dako, Carpinteria, CA).

3.3. Results

3.3.1. General Observations

The animals showed no signs of severe discomfort following the surgical procedures. No autotomy was observed, supporting previous conclusions (Carr et al, 1992) and observations (Chamberlain et al., 1998, Harley et al, 2004) concerning the absence of self-mutilation following nerve transection in Lewis rats. There were no clinical signs of infection at the wound site for any of the animals. The new drug delivery system appeared to be well tolerated by the animals.

In almost all cases a tissue cable formed between the two transected nerve stumps at 2 weeks post-neurotmesis. Macroscopically, there did not appear to be a dose-related effect of the inhibitor on the cohesiveness or size of the cable that had formed between the two stumps.

3.3.2. *Confirmation of Vehicle Delivery In Vivo*

At both post operative days 6 and 14, "T tubes" explanted from animals treated with 1% methylene blue dye (**Fig. 3.4**) contained uniform presence of blue dye in the lumen of the tube. This suggests that the new drug delivery system reliably delivers soluble factors to the nerve guide over 2 weeks *in vivo* in the adult rat.

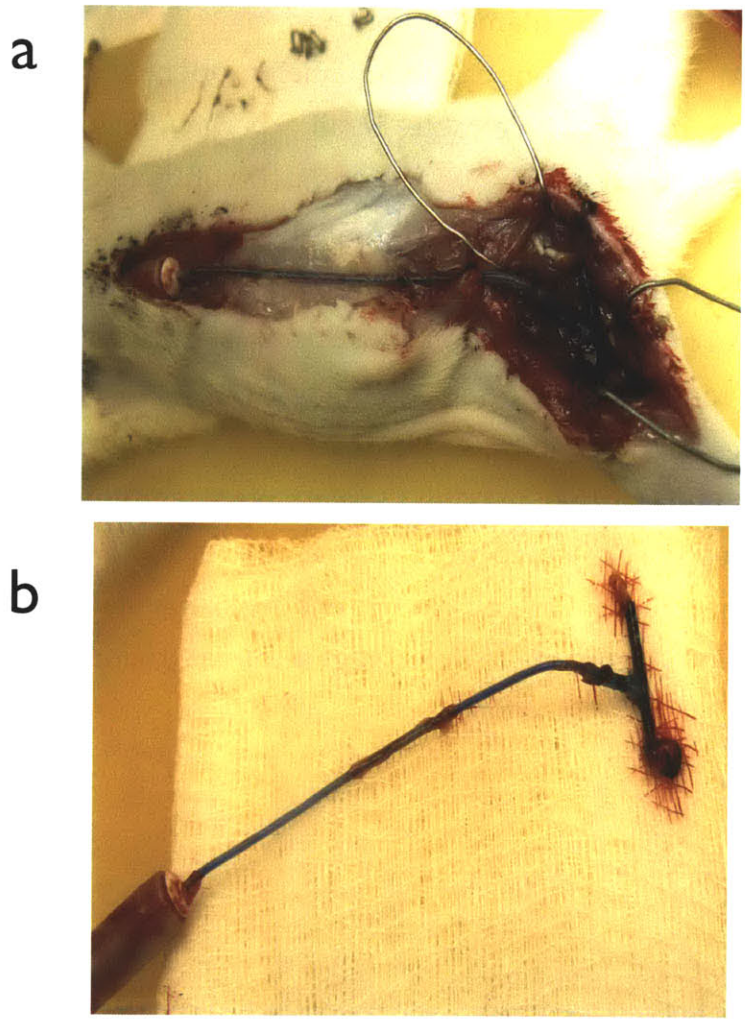

FIG. 3.4 *IN VIVO* VEHICLE DELIVERY OF MINIPUMP VERIFIED WITH 1% METHYLENE BLUE DYE. All animals (n=3) had nerve guides filled with the dye on post-operative day 14. (**a**) Drug delivery system in situ and explanted drug deliver system (**b**).

3.3.3. Effect of Y-27632 on Capsule Histology, Thickness

3.3.3.1 Capsule Histology

The capsule of a normal sciatic nerve is a continuous, single layer of perineurial cells surrounding the myelinated fibers of the endoneurium. A normal capsule consists of the cells of the thin perineurium which have prominent cytoskeletal features that stain positively for the contractile filament α-SMA.

In the current pilot study, circumferentially oriented cells formed at the periphery of the newly formed tissue cables in all experimental groups and these cells stained positively for the contractile α-SMA isoform. Myofibroblasts, identified by their positive expression of a-SMA (+), and fibroblastic appearance, were present in a capsular arrangement at the circumferential portion of the tissue in all dosage groups and the vehicle control group. In addition, blood vessels of the endoneurium as well as fibroblastic-like cells in the endoneurium exhibited (+) α-SMA staining. The thickness, δ, of the MFB capsules appeared to be on the order of 50 – 100 μm. Precise quantitation of capsule thickness at this early time point (2 weeks post-neurotmesis) proved difficult. Capsules were not clearly segmented from regenerative structures in the tissue cables, particularly due to the presence of cells in the endoneurium staining positively for α-SMA and the absence of a technique to detect regenerative structures.

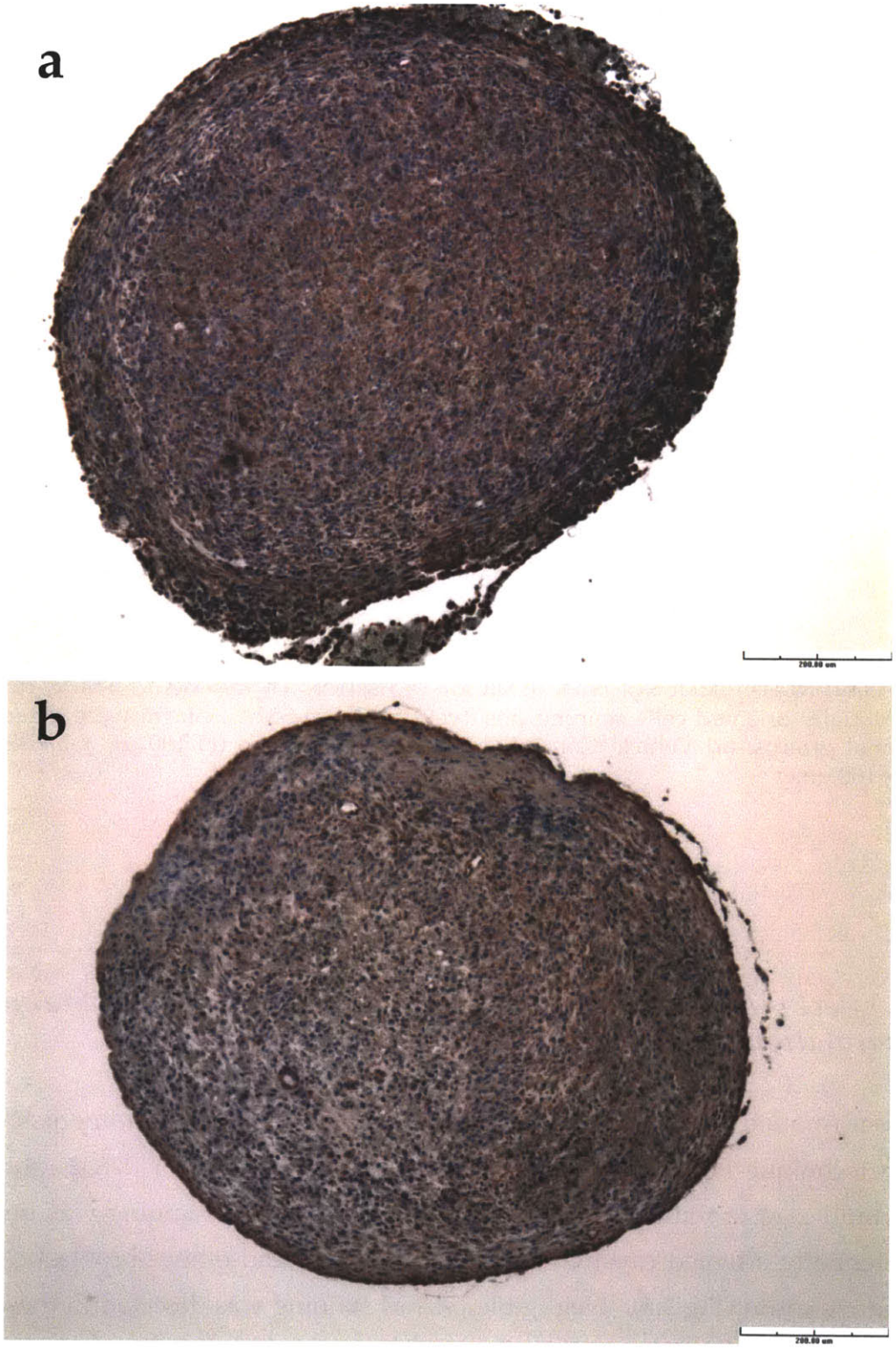

FIG. 3.5. IMMUNOHISTOCHEMICAL DETECTION OF α-SMA. Thick capsules of circumferentially oriented cells staining positively for the α-SMA isoform were detected in all experimental groups. (**a**) Vehicle Control, 0.9% saline (**b**) 10 μg/200 μL Y-27632 and (**c**) 100μg /200 μL Y-27632 animals. Scale bars 100 microns.

FIG. 3.5 CONTINUED. IMMUNOHISTOCHEMICAL DETECTION OF α-SMA. Thick capsules of circumferentially oriented cells staining positively for the α-SMA isoform were detected in all experimental groups. (**a**) Vehicle Control (**b**) 10 μg Y-27632 and (**c**) 100 μg Y-27632 animals. Scale bars 100 μm.

3.3.5. Effect of Y-27632 on Immunohistochemical Staining of Phosphorylation target of ROCK

Confirmation of Y-27632 action was attempted using an immunohistochemical detection technique for the phosphorylated ROCK target ERM. Y-27632 inhibition of ROCK would lead to reduced p-ERM staining. Robust ERM staining was detected in circumferentially oriented capsular cells, blood vessels, and other fibroblastic-like cells of the endoneurium (**Fig.3.6**). Negligible p-ERM staining was detected in these cells in control animals. In the absence of ROCK inhibition, robust p-ERM staining is expected in contractile cells.

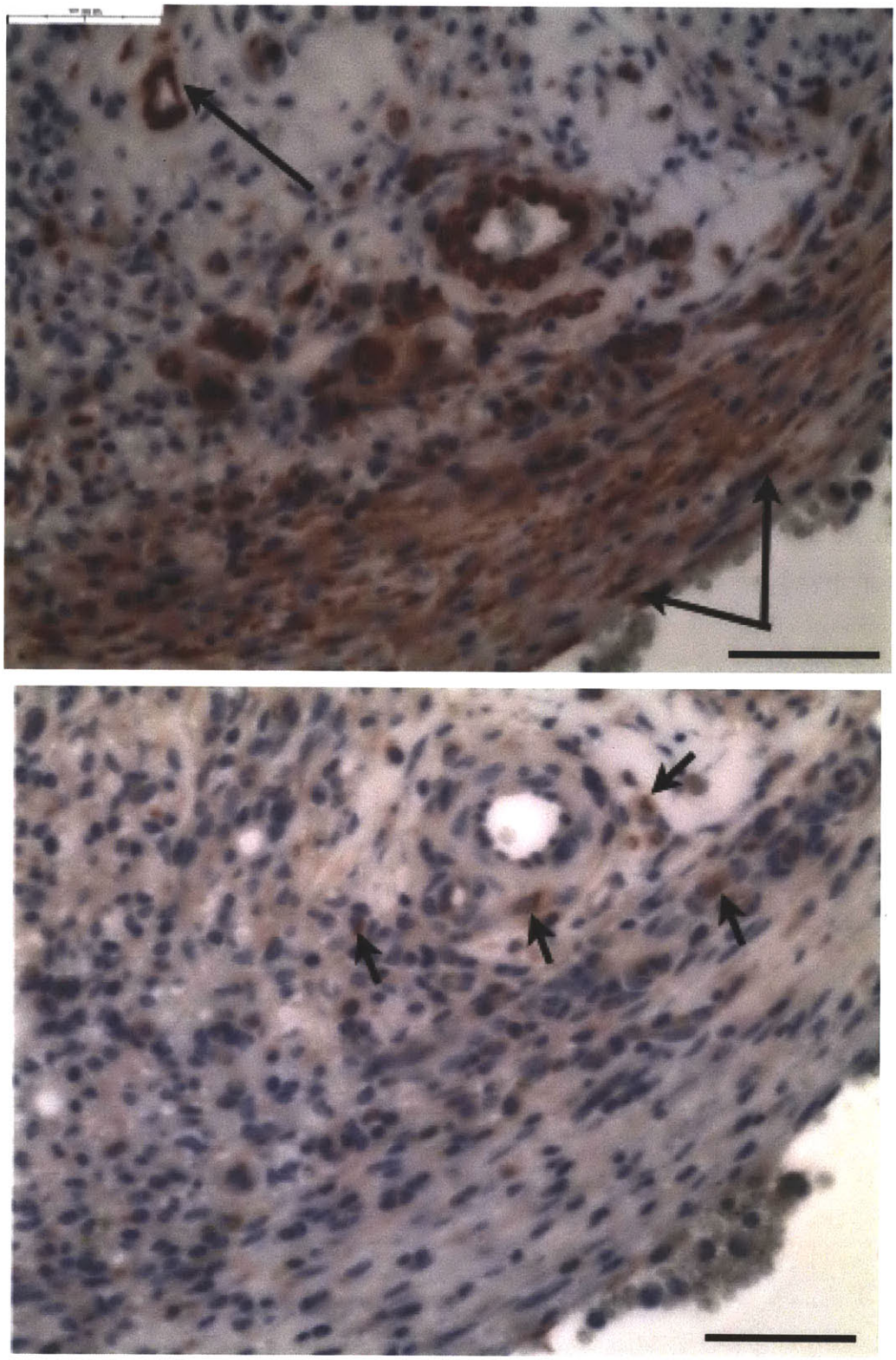

FIG. 3.6. IMMUNOHISTOCHEMICAL STAINING OF ROCK TARGETS. a) Ezrin-radixin-moesin proteins regulate cytoskeleton organization by mediating linkages between the plasma membrane and F-actin **a**) ERM staining is robust in vehicle controls, however **b**) p-ERM staining was not sensitive enough to detect significant phosphorylation of the ROCK target. Scale bars: 100 μm.

3.3.4. *Effect of Y-27632 on Tissue Cable Diameter*

Because capsule thickness was difficult to measure reliably in this pilot study, the overall diameter of the tissue cables as a function of the inhibitor dosage was measured to determine if Y-27632 had an effect on the mass of tissue formed after sciatic neurotmesis. The mean diameter of the tissue cable ranged from 1.2 to 1.6 mm at the site of transection and decreased in all experimental groups to values ranging between 0.8 mm and 1 mm at a location 2 mm distal from the site of transection. The inner diameter of the silicone tube was 1.7 mm, suggesting that the tissue cables virtually filled the inner lumen of the T tubes near the proximal site of transection, 2 weeks post-neurotmesis. This finding is reinforced by gross observations of the proximal stump, which appear to be compressed by the presence of the "T tube". Higher dosages of Y-27632 (10 μg and 100 μg) appeared to yield slightly higher mean diameters at the site of transection and 1 mm from the transection site, however at 2 mm distally all groups had mean diameters that did not appear to be different.

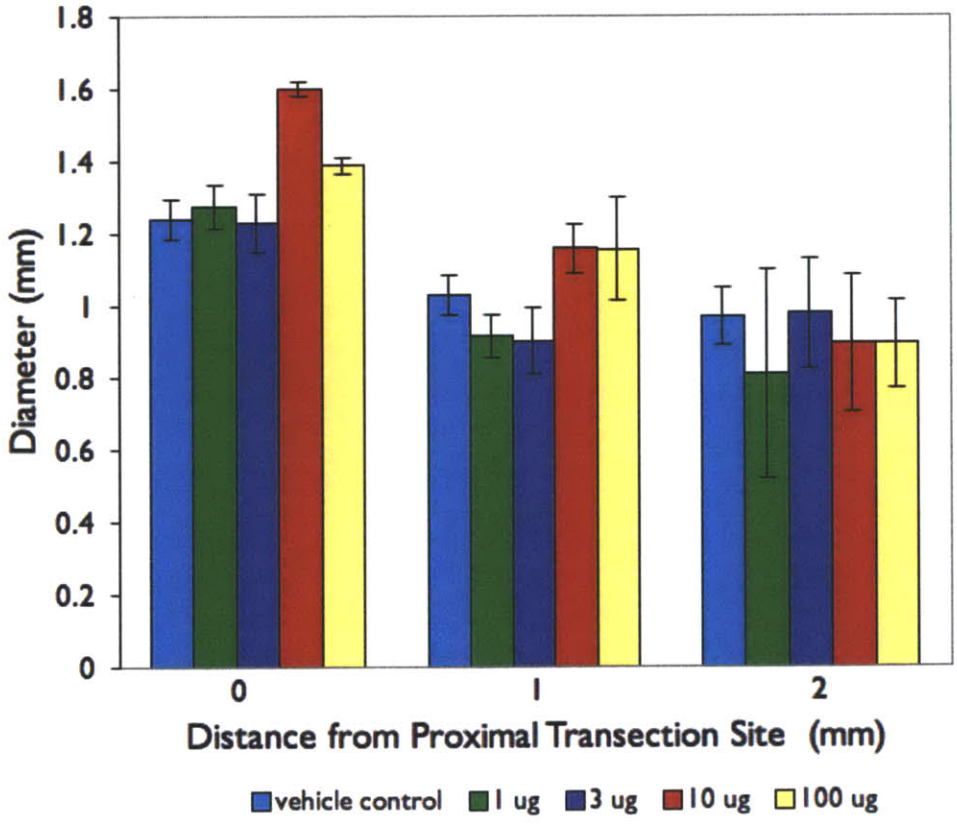

FIG. 3.5: GROSS DIAMETER OF NERVE REGENERATE AT SPECIFIED DISTANCES from Proximal Site of Transection for Various Y-27632 Dosages ± SEM

3.4. Discussion & Conclusions

In the current pilot study the effect of the small-molecule Y-27632, a soluble inhibitor of actomyosin contractility, on MFB capsule formation was investigated at 2 weeks post-sciatic neurotmesis. At the dosages tested in this study (1 μg – 100 μg of Y-27632 in 200 μL, delivered over 2 weeks), the inhibitor did not appear to abolish the formation of circumferentially oriented cells at the periphery of the newly-formed tissue cables nor did the inhibitor abolish the staining of these cells for the contractile α-SMA isoform. Myofibroblasts, identified by their positive expression of a-SMA (+), and fibroblastic appearance, were present in a capsular arrangement at the circumferential portion of the tissue in all dosage groups and the vehicle control group. In addition, blood vessels of the endoneurium as well as fibroblastic-like cells in the endoneurium exhibited (+) α-SMA staining.

In the current study capsules were difficult to segment from the endoneurium using the α-SMA stain, which also labeled numerous fibroblastic cells in the center of the tissue section. One reason for this is the early time point (2 weeks) which is known to coincide with high activity of numerous cell types in the nerve chamber model (Williams, Longo et al. 1983). At post-operative day 14 the relatively immature tissue cable was difficult to distinguish from the capsule. Evaluating the capsule at later time points (e.g. 4 weeks) may permit easier segmentation of the capsule from the newly formed nervous tissue using the techniques in chapter 2 (co-staining for myelin and F-actin).

The 15 mm gap in a silicone tube is expected to have a 0% chance of reconnection. It was selected as a strong negative control for regeneration and positive control for capsule formation. At the early time point of two weeks it is difficult to assess the % reconnection because significant axonal elongation has not yet occurred. It is possible that the demanding model of peripheral nerve regeneration obscured the clinical benefit of Y-27632. A quality of regeneration assay in future studies with longitudinally oriented sections of the tissue cables which are double-stained immunofluorescently for axons (neurofilament protein) and Schwann cells (glial fibrillary acidic protein) as described previously (Kemp, Syed et al. 2009). Such a technique may be used to aid in segmentation of capsule from regenerating axons, and

aid the investigators in measuring the effect of capsule thickness or of inhibitor dosage on the progression of linear columns of Schwann cells into the gap and the degree of axon-ScC association. Studies of capsular formation in early tissue cables would be aided by a staining technique that allows segmentation of regenerative cells and structures from the contractile capsule.

Confirmation of Y-27632 action in the current study was attempted using an immunohistochemical detection technique for the phosphorylation of ROCK target ERM. While robust ERM staining was detected in capsular cells, negligible p-ERM was detected in these cells. The results suggest that the technique was not sensitive enough to detect the phosphorylated ROCK target under these conditions. A lighter fixation protocol (such as that used in Chapter 2) and OCT-embedding of the tissue cables in lieu of paraffin embedding would ease the detection of phosphorylated targets of ROCK and be well-suited to any immunofluorescent studies of regeneration quality that might be used in the future. There is a trade off between structural integrity of the section (paraffin) and signal strength of the section (OCT) that must be weighed carefully by the investigator.

Future work using Y-27632 should include a more robust technique for verification of target inhibition. This may be accomplished by using a separate set of animals with identical dosage schedules but whose regenerates are digested enzymatically and tested for the phosphorylation of specific ROCK targets (p-MLC, p-ERM, etc) using a more sensitive technique for protein quantitation such as a Western Blot. Detection of diminished expression of the phosphorylated target in the presence of Y-27632 dosages will help the investigator conduct a dose-ranging study for the molecule and identify a therapeutic dosage.

At the dosages investigated in this study, Y-27632 did not have a measurable effect on the size of the tissue cable that formed at 2 weeks in biodurable silicone nerve guides with an inter-stump gap of 15 mm. The diameter of the tissue cables that formed in the first 2 mm measured distally from the point of transection was no different for the experimental groups.

Taken together, the results do not indicate that use of Y-27632 was a successful contraction-blocking strategy for MFB capsule formation in a silicone tube with a 15 mm inter-stump gap. This conclusion was reached following study of Y factor effects at

2 weeks post-sciatic neurotmesis. A possible explanation for this negative result is that Y-27632 was not delivered at a dosage that was sufficient to accomplish this inhibition.

In our work a novel drug delivery method was developed and verified for studying diffusible factors on nerve regeneration in a biodurable nerve guide. The system could be particularly useful for the study of contraction-blocking reagents, as the silicone nerve guide is known to illicit a thick capsule of myofibroblasts after sciatic nerve transection.

Future work with Y-27632 or other inhibitors of cellular contraction in a nerve chamber model should include several modifications to the methodology of this pilot study including a reliable technique for verification of target inhibition, a quality of regeneration assay suitable for early time points, and a suitable imaging or staining method for separating out the capsule from regenerating structures/cell types.

Portions of the introductory text of this chapter were originally published in (Soller, 2005).

3.5 Literature Cited

Amano, M., K. Chihara, et al. (1997). "Formation of actin stress fibers and focal adhesions enhanced by Rho-kinase." Science **275**(5304): 1308-1311.

Arber, S., F. A. Barbayannis, et al. (1998). "Regulation of actin dynamics through phosphorylation of cofilin by LIM-kinase." Nature **393**(6687): 805-809.

Burridge, K. and M. Chrzanowska-Wodnicka (1996). "Focal adhesions, contractility, and signaling." Annu Rev Cell Dev Biol **12**: 463-518.

Carr, M. M., T. J. Best, et al. (1992). "Strain differences in autotomy in rats undergoing sciatic nerve transection or repair." Ann Plast Surg **28**(6): 538-544.

Carragher, N. O. and M. C. Frame (2004). "Focal adhesion and actin dynamics: a place where kinases and proteases meet to promote invasion." Trends Cell Biol **14**(5): 241-249.

Chamberlain, L. J., I. V. Yannas, et al. (1998). "Early peripheral nerve healing in collagen and silicone tube implants: myofibroblasts and the cellular response." Biomaterials **19**(15): 1393-1403.

Chamberlain, L. J., I. V. Yannas, et al. (2000). "Connective tissue response to tubular implants for peripheral nerve regeneration: the role of myofibroblasts." J Comp Neurol **417**(4): 415-430.

Chamberlain, L. J., I. V. Yannas, et al. (1998). "Collagen-GAG substrate enhances the quality of nerve regeneration through collagen tubes up to level of autograft." Exp Neurol **154**(2): 315-329.

Chamberlain, L. J., I. V. Yannas, et al. (2000). "Near-terminus axonal structure and function following rat sciatic nerve regeneration through a collagen-GAG matrix in a ten-millimeter gap." J Neurosci Res **60**(5): 666-677.

Chrzanowska-Wodnicka, M. and K. Burridge (1992). "Rho, rac and the actin cytoskeleton." Bioessays **14**(11): 777-778.

Chrzanowska-Wodnicka, M. and K. Burridge (1996). "Rho-stimulated contractility drives the formation of stress fibers and focal adhesions." J Cell Biol **133**(6): 1403-1415.

Dugina, V., L. Fontao, et al. (2001). "Focal adhesion features during myofibroblastic differentiation are controlled by intracellular and extracellular factors." J Cell Sci **114**(Pt 18): 3285-3296.

Hall, A. (1998). "Rho GTPases and the actin cytoskeleton." Science **279**(5350): 509-514.

Harley, B. A., M. H. Spilker, et al. (2004). "Optimal degradation rate for collagen chambers used for regeneration of peripheral nerves over long gaps." Cells Tissues Organs **176**(1-3): 153-165.

Hinz, B. and G. Gabbiani (2003). "Mechanisms of force generation and transmission by myofibroblasts." Curr Opin Biotechnol **14**(5): 538-546.

Itoh, K., K. Yoshioka, et al. (1999). "An essential part for Rho-associated kinase in the transcellular invasion of tumor cells." Nat Med **5**(2): 221-225.

Kaibuchi, K., S. Kuroda, et al. (1999). "Regulation of the cytoskeleton and cell adhesion by the Rho family GTPases in mammalian cells." Annu Rev Biochem **68**: 459-486.

Katoh, K., Y. Kano, et al. (2001). "Stress fiber organization regulated by MLCK and Rho-kinase in cultured human fibroblasts." Am J Physiol Cell Physiol **280**(6): C1669-1679.

Katoh, K., Y. Kano, et al. (2001). "Rho-kinase--mediated contraction of isolated stress fibers." J Cell Biol **153**(3): 569-584.

Kawano, Y., Y. Fukata, et al. (1999). "Phosphorylation of myosin-binding subunit (MBS) of myosin phosphatase by Rho-kinase in vivo." J Cell Biol **147**(5): 1023-1038.

Kemp, S. W., S. Syed, et al. (2009). "Collagen nerve conduits promote enhanced axonal regeneration, schwann cell association, and neovascularization compared to silicone conduits." Tissue Eng Part A **15**(8): 1975-1988.

Kemp, S. W., S. K. Walsh, et al. (2007). "A novel method for establishing daily in vivo concentration gradients of soluble nerve growth factor (NGF)." J Neurosci Methods **165**(1): 83-88.

Kimura, K., M. Ito, et al. (1996). "Regulation of myosin phosphatase by Rho and Rho-associated kinase (Rho-kinase)." Science **273**(5272): 245-248.

Komatsu, S., T. Yano, et al. (2000). "Effects of the regulatory light chain phosphorylation of myosin II on mitosis and cytokinesis of mammalian cells." J Biol Chem **275**(44): 34512-34520.

Maekawa, M., T. Ishizaki, et al. (1999). "Signaling from Rho to the actin cytoskeleton through protein kinases ROCK and LIM-kinase." Science **285**(5429): 895-898.

Masamune, A., K. Kikuta, et al. (2003). "Rho kinase inhibitors block activation of pancreatic stellate cells." Br J Pharmacol **140**(7): 1292-1302.

McDonald, D. S. and D. W. Zochodne (2003). "An injectable nerve regeneration chamber for studies of unstable soluble growth factors." J Neurosci Methods **122**(2): 171-178.

Murata, T., S. Arii, et al. (2003). "Therapeutic significance of Y-27632, a Rho-kinase inhibitor, on the established liver fibrosis." J Surg Res **114**(1): 64-71.

Narumiya, S., T. Ishizaki, et al. (2000). "Use and properties of ROCK-specific inhibitor Y-27632." Methods Enzymol **325**: 273-284.

Parizi, M., E. W. Howard, et al. (2000). "Regulation of LPA-promoted myofibroblast contraction: role of Rho, myosin light chain kinase, and myosin light chain phosphatase." Exp Cell Res **254**(2): 210-220.

Patel, K., P. Harding, et al. (2003). "Regulation of the mesangial cell myofibroblast phenotype by actin polymerization." J Cell Physiol **195**(3): 435-445.

Rekhter, M., K. Chandrasekhar, et al. (2007). "Immunohistochemical analysis of target proteins of Rho-kinase in a mouse model of accelerated atherosclerosis." Exp Clin Cardiol **12**(4): 169-174.

Riento, K. and A. J. Ridley (2003). "Rocks: multifunctional kinases in cell behaviour." Nat Rev Mol Cell Biol **4**(6): 446-456.

Sato, N., N. Funayama, et al. (1992). "A gene family consisting of ezrin, radixin and moesin. Its specific localization at actin filament/plasma membrane association sites." Journal of Cell Science **103 (Pt 1)**: 131-143.

Serini, G., M. L. Bochaton-Piallat, et al. (1998). "The fibronectin domain ED-A is crucial for myofibroblastic phenotype induction by transforming growth factor-beta1." J Cell Biol **142**(3): 873-881.

Soller, E. (2005). In Vitro Pharmacological Inhibition of Myofibroblast Differentiation in a Collagen-GAG Matrix. Cambridge, MA, MIT. **S.M.M.E.**

Soller, E. C. (2005). In vitro pharmacological inhibition of myofibroblast differentiation and force generation in a collagen-GAG matrix. Cambridge, MA, Massachusetts Institute of Technology. **S.M.M.E.**

Spilker, M. H. (2000). Peripheral nerve regeneration through tubular devices. . Cambridge, MA., Massachusetts Institute of Technology, . **Ph.D.**

Tada, S., H. Iwamoto, et al. (2001). "A selective ROCK inhibitor, Y27632, prevents dimethylnitrosamine-induced hepatic fibrosis in rats." J Hepatol **34**(4): 529-536.

Tangkijvanich, P., A. C. Melton, et al. (2003). "Rho and p38 MAP kinase signaling pathways mediate LPA-stimulated hepatic myofibroblast migration." J Biomed Sci **10**(3): 352-358.

Tomasek, J. J., G. Gabbiani, et al. (2002). "Myofibroblasts and mechano-regulation of connective tissue remodelling." Nat Rev Mol Cell Biol **3**(5): 349-363.

Uehata, M., T. Ishizaki, et al. (1997). "Calcium sensitization of smooth muscle mediated by a Rho-associated protein kinase in hypertension." Nature **389**(6654): 990-994.

Van Aelst, L. and C. D'Souza-Schorey (1997). "Rho GTPases and signaling networks." Genes Dev **11**(18): 2295-2322.

Vishwanath, M., L. Ma, et al. (2003). "Modulation of corneal fibroblast contractility within fibrillar collagen matrices." Invest Ophthalmol Vis Sci **44**(11): 4724-4735.

Webb, R. C. (2003). "Smooth muscle contraction and relaxation." Adv Physiol Educ **27**(1-4): 201-206.

Williams, L. R., F. M. Longo, et al. (1983). "Spatial-temporal progress of peripheral nerve regeneration within a silicone chamber: parameters for a bioassay." J Comp Neurol **218**(4): 460-470.

Yee, H. F., Jr., A. C. Melton, et al. (2001). "RhoA/rho-associated kinase mediates fibroblast contractile force generation." Biochem Biophys Res Commun **280**(5): 1340-1345.

Zheng, Y., H. Bando, et al. (2004). "Involvement of rho-kinase pathway in contractile activity of rabbit RPE cells in vivo and in vitro." Invest Ophthalmol Vis Sci **45**(2): 668-674.

4

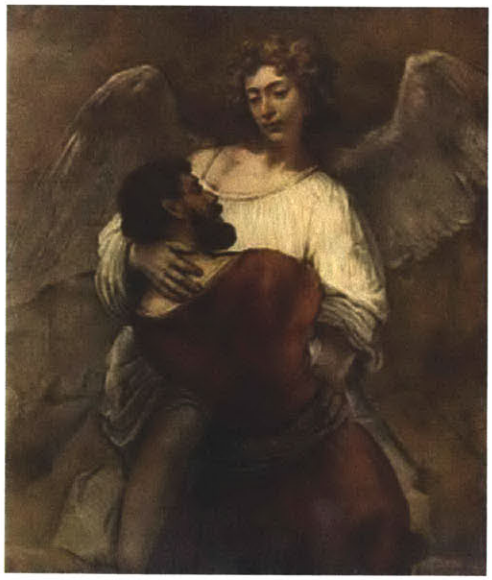

Jacob struggles with the angel
Rembrandt (Gemäldegalerie, Berlin), 1659

This page intentionally left blank.

4

Conclusions

4.1 Novel Contributions and Major Findings

In this work, an experimental study was undertaken to evaluate the relationship between cell-mediated contraction and the quality of induced axonal regeneration in a neurotmesis model of the adult rat with a 15 mm interstump gap length. The novel contributions and major findings of this work are as follows:

4.1.1. A Negative Association between Capsule Thickness δ, and Quality of Regeneration, Q.

A statistically significant, negative association was observed between the contractile capsule thickness, δ, and the quality of axonal regeneration, Q, (consisting of measures of regenerate area, the number of myelinated fibers, and the number of large-diameter fibers) at 9 weeks post-sciatic neurotmesis (Chapter 2).

4.1.2. Degradation Rate Mediates Contraction-blocking and Regenerative Activity of Collagen Scaffolds

Experimental data show that type I collagen devices of intermediate degradation rate minimized δ and maximized Q at 9 weeks post-neurotmesis.

4.1.3. Contractile Cell Permeability is a possible mechanism of scaffold regenerative activity

Reduction in δ coincided with histological observation (at 1 and 9 weeks) of contractile cell presence inside scaffolds that were moderately cross-linked and

consequently degraded at an intermediate rate, but not in highly cross-linked scaffolds that degraded at very low rate.

4.1.4. Novel Methodology to Study Soluble Factors in Biodurable Nerve Guide

Novel methodology was developed in this work to study continuously-delivered soluble factors in the nerve chamber model (Chapter 3). The Rho Kinase inhibitor Y-27632 did not show an effect on MFB formation 2 weeks post-neurotmesis in silicone nerve guides in a pilot study (Chapter 3).

This constitutes the strongest evidence to date that capsules of contractile MFB antagonize induced regeneration of severely injured peripheral nerves in the adult mammal. Speculatively, the data support the hypothesis of MFB cell escape from the wound (making use of the permeability of the scaffold) as a mechanism for scaffold regenerative activity.

Future efforts in biomaterial design for peripheral nerve regeneration should focus on minimizing capsular formation as a strategy to maximize axonal regeneration. The values of specific structural determinants of scaffold regenerative activity (those that reduce or delay formation of the MFB capsule) at early time points (1-2 weeks) warrants further study.

The role that cell permeability plays in the regenerative activity of the collagen scaffolds following neurotmesis may be probed further by using a homologous series of type I collagen devices with identical chemical composition and solids content but different average pore size in the same injury model (Appendix A.1). More numerous, smaller pores in the collagen device could lead to more cell-scaffold interactions and may lead to the discovery of an improved device that reduces capsule formation to unprecedented levels and maximizes axonal regeneration by increasing cell traffic in the scaffold.

4.2 Similarities between Induced Regeneration of Skin and Peripheral Nerves

4.2.1 Prevalence of Spontaneous Cell-mediated Contraction of Skin and Nerve Wounds

The spontaneous healing of severe wounds in both skin and nerves is characterized by the formation of a cohesive capsule of contractile cells (MFB) that originates at the wound edges in both organs during the first 1-2 weeks after severe injury. In skin wounds the MFBs pull from the edges of the full-thickness defect in the plane of the skin along a major axis (**Fig. 4.1a**). In nerve wounds, MFB form circumferentially oriented, cohesive capsules around the outer perimeter of the nerve stump and exert a hoop stress that compresses the nerve along its radial axis (**Fig. 4.1c**) consistent with the pressure cuff theory.

4.2.2. Cell-mediated Contraction Antagonizes Scaffold-Induced Regeneration

Cell-mediated contraction represents a mechanical barrier to organ regeneration and its detrimental effects are as follows: cell-mediated contraction reduces the original volume of the organ defect before significant regeneration occurs, limiting the available space in which the newly regenerated organ may form and ultimately leading to a smaller regenerate volume. As spontaneous wound healing proceeds, contractile capsules are remodeled into non-physiological fibrous scar tissue, which persists long after the injury has closed. Scar tissue lacks the function of the original organ and also reduces the final volume of the regenerate that forms in the defect volume. Speculatively, the stresses exerted by MFB capsules may also have an inhibitory mechanotransductive effect on cells involved in the regenerative response in both skin and nerves.

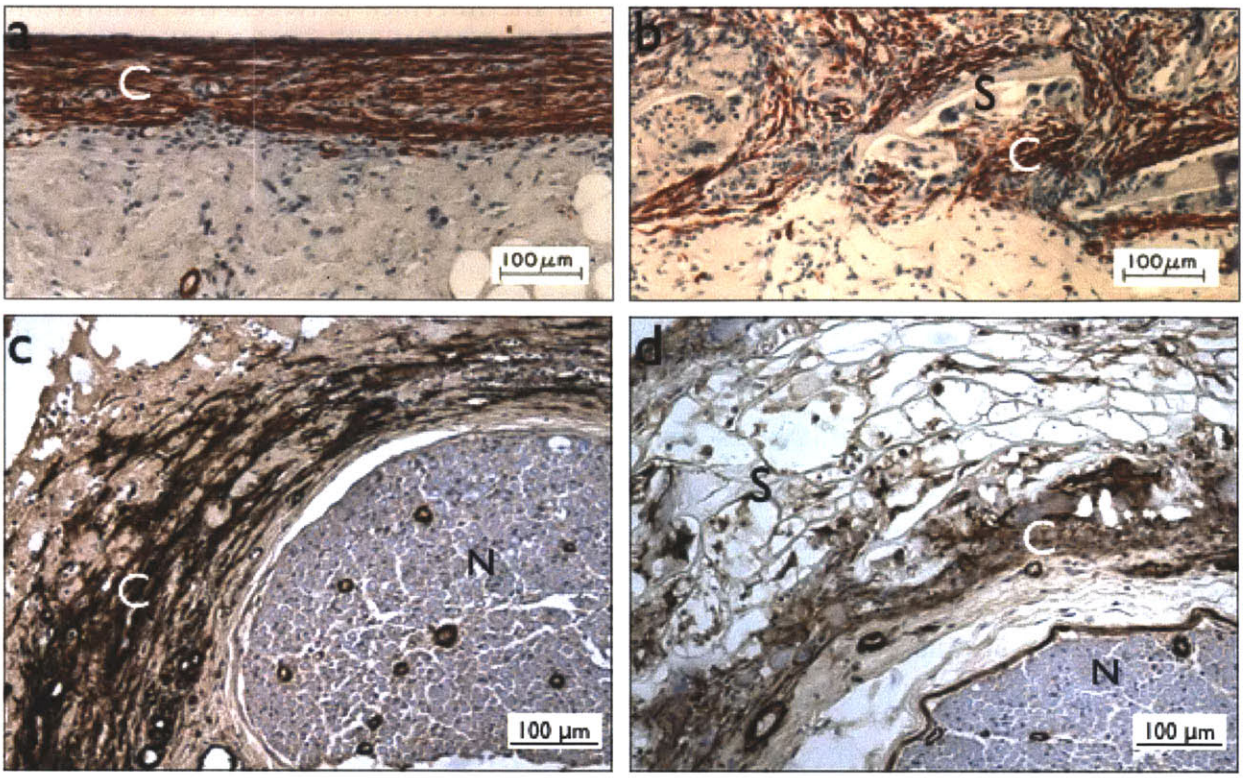

FIG. 4.1 REGENERATIVELY-ACTIVE SCAFFOLDS IN SKIN AND PERIPHERAL NERVES DISRUPT THE SPONTANEOUS MFB CAPSULE THAT FORMS DURING WOUND HEALING IN BOTH ORGANS. *SKIN:* (a) an ungrafted, full-thickness skin wound in the adult guinea pig is vigorously contracting 10 days after injury via a thick, cohesive capsular layer of MFB (C, red, alpha-SMA) oriented in the plane of the defect. (b) MFB infiltrate an "active" porous collagen scaffold (S), disrupting the MFB capsule through apparent randomization and reduction of MFB, and reducing macroscopic contraction of the wound. *NERVE*: (c) a non-crosslinked collagen scaffold (Device A) has been degraded at 7 days and has done very little to thwart a thick, cohesive MFB capsule (brown, α-SMA) that is oriented around the circumference of the transected nerve stump (N) and vigorously contracting the nerve stump. The rapid degradation of this device is similar to an ungrafted wound. (d) Numerous capsular MFB have infiltrated the pores of an intermediately-crosslinked scaffold (Device D, S) which is still intact at 7 days post-neurotmesis, similarly disrupting the MFB capsule (C) through apparent randomization and reduction of MFB, reducing macroscopic contraction of the injured organ (N). Scale bars 100 microns Skin (a, b) Troxel, K PhD Thesis, 1993.

4.2.3. Biomaterials that Minimize Contraction Maximally Induce Regeneration

Induced regeneration studies of skin and peripheral nerve have used a plethora of biomaterials with highly variable structural and chemical compositions. One trend emerges from the available data: biomaterials that are the most effective at inducing regeneration of both organs are those that are also the most effective at reducing or delaying the cell-mediated contraction of the wound by capsules of myofibroblasts (MFB) (Yannas et al, 1989; Chamberlain, Yannas et al 1998; Harley, Spilker et al, 2004; Soller 2011, Troxel PhD Thesis, 1993). In both skin and nerve wounds, the thickness and

composition of the MFB capsule that forms in the interface between the wound and biomaterial is minimized and/or disrupted by porous scaffolds with optimal structural parameters (**Fig. 4.1c,d**).

4.2.6. Implications for Future Design of Biomaterials to Induce Regeneration

These observations motivate the design of biomaterials that maximize contractile cell-scaffold interactions at the periphery of the organ defect (site of MFB origin) via structural and chemical parameters that enhance cell permeability in the early (1-4 weeks) wound healing response. Success in two organs that are distinct in structure and function (skin and nerves) suggest that the following strategy could enhance regeneration in any organ.

The biomaterials researcher may identify the spatial origin of MFB in the organ defect of interest and to establish the kinetics of the spontaneous MFB-mediated contractile response. Which cells become MFBs, and where do they come from? How long must the biomaterial remain in the defect to combat the spontaneous MFB response? Optimization of a porous biomaterial's properties (surface chemistry, average pore size, stiffness, etc) will maximize contractile cell-scaffold interactions at the periphery of the wound during the duration of the spontaneous contractile response. A useful tool for the biomaterials researcher is a homologous series of scaffolds in which one structural or chemical parameter is varied while all other parameters are held essentially constant (Yannas, 1989; Harley, Spilker et al, 2004; Soller, 2011). Measurement of the MFB capsule thickness, δ, and organization across the homologous series at early time points will provide useful information on the contraction-blocking influence of the dependent variable.

The capsule is not the whole story, but it does play a significant role in the regenerative outcome and should not be overlooked when designing biomaterials. Future biomaterials could conceivably have two parts: an inner part of the construct whose properties are designed to mimic the stem cell niche of the organ of interest and/or proliferation of seeded cells and an outer portion with properties that are designed to promote favorable contractile cell-scaffold interactions.

A.

Appendix 1: Synthesis of Type I Collagen Nerve Guides With Variable Pore Size

---

The goal of this project was the synthesis of a homologous series of tubular type I collagen devices identical in chemical composition and crosslinking treatment but varying in average pore size. The fabrication methods used in Chapter 2 to create a homologous series of type I collagen devices varying in degradation rate were utilized here with slight modifications. The independent variable used to create this series was the freezing temperature of the collagen slurry (-20°C, -40°C, -70°C and -196°C), which was held constant in Chapter 2. All devices were subjected to a standard crosslinking treatment (dehydrothermal treatment, 48 hrs, 120°C). The homogeneity and pore size of the devices were investigated qualitatively using scanning electron microscopy. Overall, average pore size was seen to decrease as the lypholization temperature decreased.

Type I collagen scaffold/tubes are fabricated as follows. A high-solids content (5% w/w) collagen dispersion is prepared by mixing type I microfibrillar bovine tendon collagen (Integra LifeSciences Corporation, Plainsboro, NJ)) with 0.5M acetic acid using a plasticating extruder and then swelling of the collagen fibers for 3 hours at room temperature. The mixture is degassed by centrifugation (60 min at 4500g) and is then injected into a mold for freeze-drying. When assembled, the two halves of the tube mold form a series of cylindrical Teflon channels surrounded by an aluminum frame but when split open each half contains semicylindrical channels through the Teflon. The highly viscous collagen suspension is directly injected into each cylindrical channel and a mandrel, fabricated from stainless steel wire surrounded by Teflon, is inserted into the center of each channel in order to form the tubular geometry of the implant. Teflon spacers inserted into the ends of the channel holds mandrels in place along the channel center axis. The collagen suspension that was injected into the mold is then frozen and

the liquid content is removed by lyophilization (freeze-drying). Molds are placed in a freeze-dryer (VirTis, Gardiner, NY). The pore structure of the tubes is controlled in a manner described in the next section. The solidified collagen suspension is removed from the mold after freezing is completed and the ice content is sublimated in a manner previously described for the production of highly porous collagen-GAG matrices (Temperature = 0°C, Pressure < 200 mTorr, 17 hours) (Dagalakis et al., 1880; Harley et al., 2004). After sublimation, the Teflon-coated mandrel can be easily removed, leaving a porous collagen tube. Detailed descriptions with diagrams have been also published (Chamberlain and Yannas, 1998; Harley et al., 2004). The final dimensions of the tubes will be O.D. 2.8 mm and I.D. 1.5 mm.

Control of average pore size of collagen scaffolds. Average pore size of the tubular scaffolds will be controlled in the approximate range 1 μm to 500 μm without significant change in the % pore volume by adjusting the freezing conditions of the collagen suspension (i.e., rate of supercooling, final temperature of freezing). The theory and practice of the basic heat transfer aspects for this process have been worked out extensively (Loree et al., 1989; O'Brien et al., 2004; O'Brien et al., 2005). Low freezing temperatures (supercooling) and a rapid rate of freezing lead to nucleation of small ice dendrites that are eventually sublimed to leave behind a pore channel with relatively small diameter while the inverse leads to scaffolds with a relatively large diameter. Detailed protocols have been published (Dagalakis et al., 1980; Yannas et al., 1989; Chamberlain and Yannas, 1998; O'Brien et al., 2004; O'Brien et al., 2005).

Tubes were investigated with scanning electron microscopy to confirm qualitative differences in average pore size. Qualitatively, average pore size appeared to vary between 5 μm to 100 μm across the range of freezing temperatures investigated (Fig. A.1)

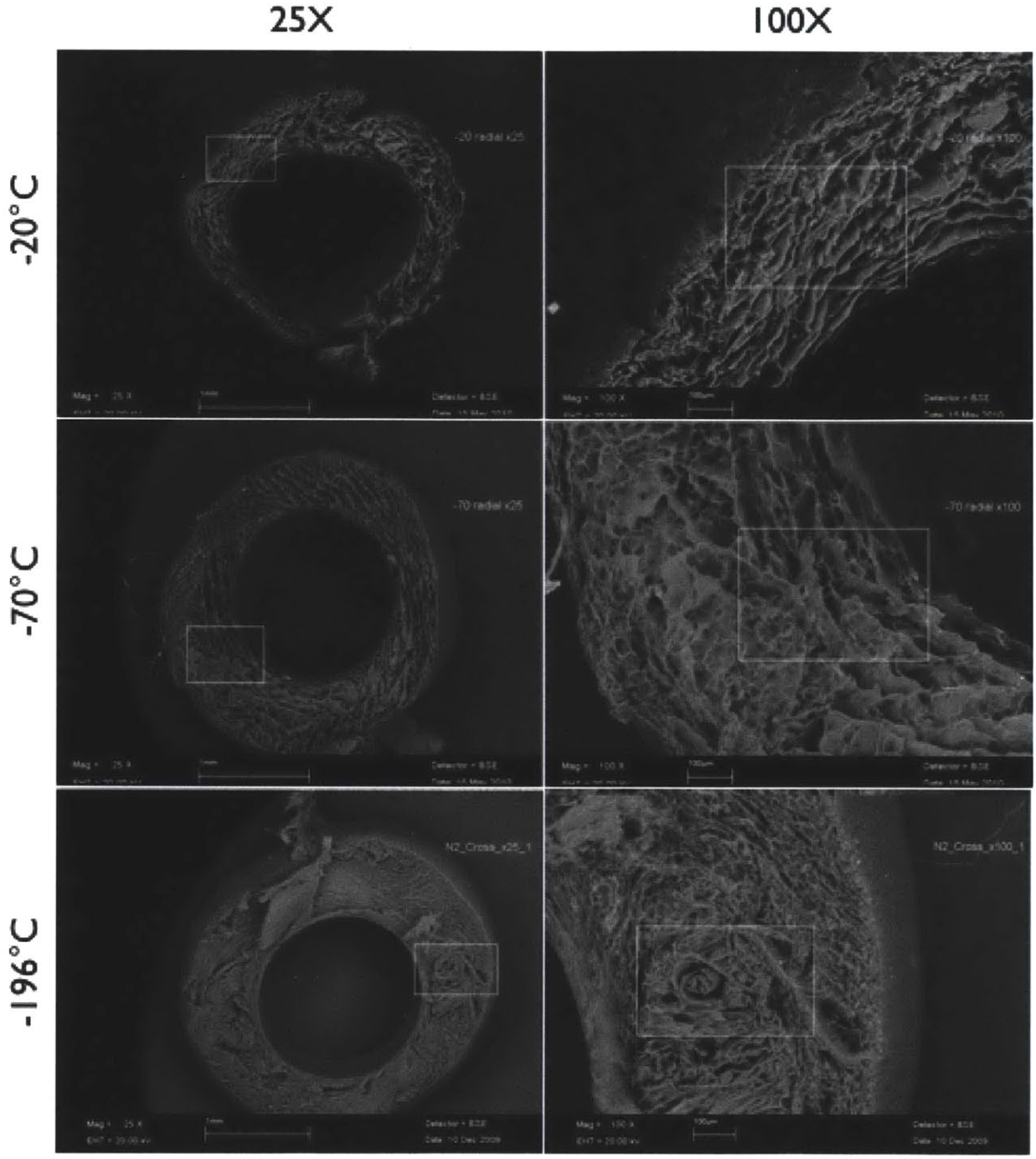

FIG. A.1 FINAL FREEZING TEMPERATURE MEDIATES PORE SIZE OF TYPE I COLLAGEN NERVE GUIDES. Scanning electron micrographs of radial pore structure of type I collagen nerve guides with freezing temperatures of -20° C, -70° C, and -196° C. Lower freezing temperatures

B.1 5% Collagen Tube Fabrication Protocol

adapted from Harley, 2000

SUPPLIES

0.25 g Type I Collagen (Integra) % 150 $L Glacial Acetic Acid (GAA, Mallinckrodt)

22 Gauge Needle (Cat. No. 309574, Becton Dickinson)

10 mL Syringes (Cat. No. 309604, Becton Dickinson)

Female-female Luer Lock Assembly (Stainless steel Luer Lock tube fitting, female luer, Cat. No. 5194k12, McMaster-Carr)

Stainless Steel Wire (0.032" D., Cat. No. GWXX-320-30, Small Parts)

Teflon Tubing, O.D. 0.056", I.D. 0.032" (PTFE Tubing, Cat. No. 06417-31, Cole-Parmer)

Teflon Tubing, O.D. 0.125", I.D. 0.065" (PTFE Tubing, Cat. No. 06407-42, Cole-Parmer)

Two Teflon and Aluminum Molds (see Figure B.1 and Figure B.2)

SOLUTIONS

Acetic Acid, 3.0 M: 300 μL glacial acetic acid, 1.7 mL distilled water

EQUIPMENT

Centrifuge (Heraeus Labofuge 400R) % Lyophilizer (VirTis Genesis EL or LE)

PROCEDURE

1. Assemble mandrels using a stainless steel wire core surrounded by Teflon tubing (O.D. 0.056", I.D. 0.032"). The length of the mandrel should be several mm larger than the length of the mold.

2. Spacers, to be used at the ends of mandrels, are made out of Teflon tubing (O.D. 0.125", I.D. 0.065") and are on the order of 5-10 mm long.

3. Autoclave mandrels and spacers before use.

4. Clean two Teflon and aluminum molds with acetic acid. Per the protocol to follow, approximately 12 tubes (6 tubes per mold) can be made.

5. Fill two 15 mL Falcon tubes with approximately 5 mL of distilled water. Leave both tubes uncapped and centrifuge at 4500 rpm for 10-15 minutes to degas.

6. Draw 3.0 M acetic acid into 3 mL syringe with 22 gauge needle 86% Weigh 0.25 g Type I Collagen (Integra Life Sciences, San Diego, CA). Place collagen into 10 mL syringe that has Parafilm covering luer-lock end. Add 4 mL degassed, distilled water and mix thoroughly with forceps.

7. Insert plunger into syringe and invert syringe, allowing collagen mixture to fall away from the syringe tip. Remove Parafilm and mix collagen slurry by moving stopper up and down. Purge air out from tip, bringing plunger up so that slurry comes up to the tip.

8. Slowly inject 1 mL 3.0 M acetic acid into collagen, placing the needle from the 3 mL syringe through the tip of the 10 mL syringe with collagen-water suspension. Add the 1 mL acetic acid slowly while mixing with needle tip and pulling back on the 10 mL syringe plunger.

9. Blend slurry well until a homogenous mixture is achieved. Attach 10 mL syringe with collagen slurry to another 10 mL syringe with a female-female Luer Lock assembly and mix by injecting collagen slurry from one syringe to another. Mix back and forth 10-15x, until collagen fibers begin to hydrate and solution appears uniform.

10. Try to make sure as much of the collagen slurry is in only one of the 10 mL syringes. Remove empty syringe and Luer Lock fitting. Seal the tip of the full syringe with multiple layers of Parafilm to ensure that the collagen does not escape during centrifugation.

11. Do not remove plunger. Let slurry mixture sit for 3 hours at room temperature to allow for the collagen fibers to swell.

12. After 3 hours, remove plunger, but keep Parafilm over syringe tip. Cut a small notch in on the side of the black rubber material using a razor.
13. Set lyophilizer to -40°C (it takes ~ 30 min for chamber to reach set temperature).

14. Centrifuge the collagen slurry in the syringe in order to degas the collagen so that it homogenizes without any macroscopic air bubbles. Place the syringe into a 50 mL Falcon tube, using a moist, folded paper towel to brace the syringe along the central axis of the conical tube.

15. Mass the Falcon tube-syringe system and make the counterweight of the same mass using a Falcon tube filled with water.

16. Centrifuge the Falcon tubes at 4500 rpm (3940xG) at 25°C for 30 minutes. Check to make sure that the syringe is still centrally aligned in the Falcon tube; if not, make the appropriate adjustments. Return the Falcon tube-syringe system to the centrifuge and spin at 4500 rpm (3940xG) at 25°C for 30 minutes.

17. Take the molds and align the top and bottom. Close molds using screw mechanism or 4 c-clamps.

18. Remove the syringe from the centrifuge. Slowly return the plunger to the syringe while removing the parafilm seal.

19. Slowly inject the centrifuged slurry (~0.25 mL per tube) into closed molds until slurry is apparent on other side. Insert mandrel into slurry, rotating mandrel during insertion so as to keep the mandrel centered and to maintain a uniform deposition of collagen throughout the mold. Cap the free ends of the mandrel with the spacers after the mandrel is fully inserted. Repeat step, filling as many holes possible of each mold.

20. Place molds in lyophilizer for 1 hour. Depending on the shelf height, the molds will be placed horizontally or vertically on the shelf. Be sure to note which orientation was used.

21. After freezing, remove the molds from the lyophilizer and split them. Gently remove the tubes using clean forceps and a razor. Keep the mandrels inside the tubes. Place tubes with mandrels back into the lyophilizer (at -40&C).

22. Pull vacuum in lyophilizer until both readouts are below 200 mTorr.

23. Raise temperature to 0°C and leave overnight under vacuum in lyophilizer (17 hours).

24. Raise temperature to 20°C and release vacuum. % Create aluminum foil packet by tearing a large sheet of aluminum foil and folding it in half once in one direction, and once in half in the other direction. The walls of the packet should now be two sheets thick. For two of the three open edges, fold over the sheet twice approximately 8 mm each time to create a durable closure.

25. The open edge is for deposition of the collagen tube. Using a lab marker, label the package with the following information:

Collagen I Nerve Tubes Tf = -40°C Investigator Name, Date of Fabrication

26. Remove tubes (Figure B.3. for final dimensions) with mandrels from lyophilizer and place into aluminum foil packets. Close the open edge by folding it over twice. Store packets in dessicator with DrieRite Absorbent (VWR International)

ASSOCIATED FIGURES

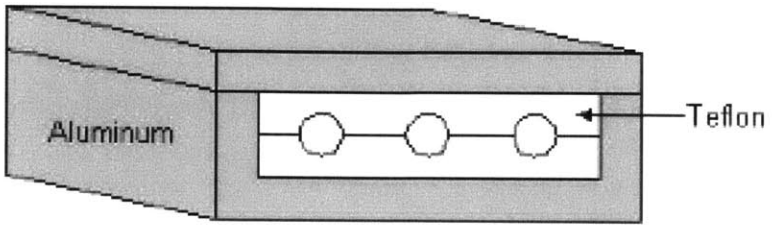

Figure B.1. Teflon and aluminum mold schematic

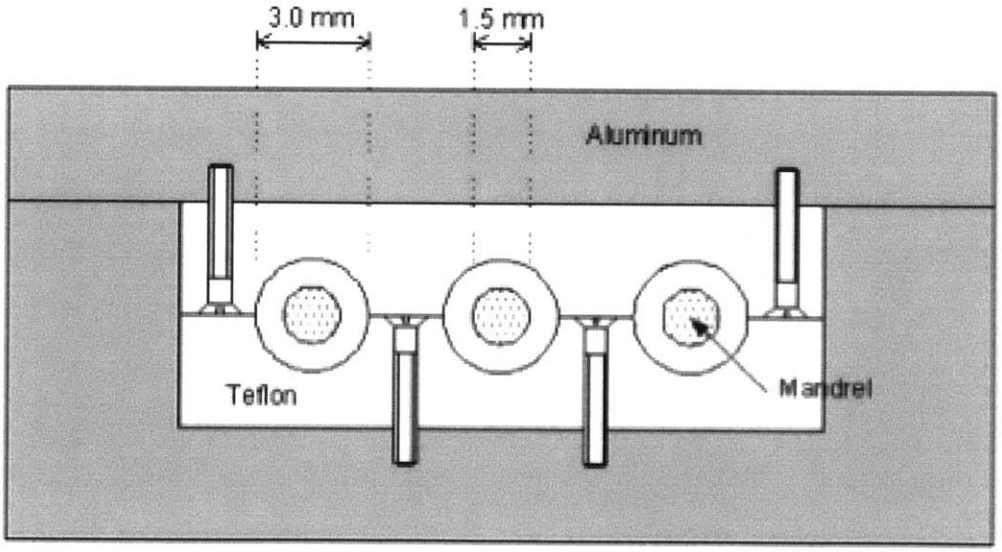

Figure B.2. Teflon and aluminum mold (side view) with inserted mandrels

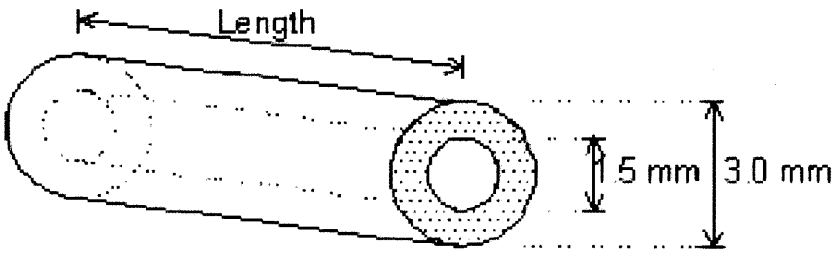

Figure B.3. Collagen nerve tube produced from Teflon and aluminum mold

B.2 Cross-linking Treatment of Collagen Tubes

adapted from Harley, 2000

Dehydrothermal (DHT) Cross-linking
PROCEDURE

1. Place collagen material in aluminum foil packet. Leave packet open at top.

2. Place packet in vacuum oven (Isotemp Model 201, Fisher Scientific, Boston, MA) at established set temperature. The following settings are for 5% collagen tubes (multiple settings possible).

Set Temperature
90°C, 120°C

ExposureTime
24 hours, 48 hours

3. Turn on vacuum. The vacuum oven should reach a final pressure of approximately -29.7 mmHg.

4. At the end of the exposure period, turn off the vacuum and cent the chamber. Open the vacuum door and immediately seal the aluminum foil bags. The matrix is now cross-linked and considered sterile, so the matrix should only be handled under sterile conditions from now on.

5. Store the matrix in a dessicator. Cross-linked matrices can remain indefinitely in a dessicator prior to testing or use.

EDAC Cross-linking

SUPPLIES

0.276g EDAC, [1 ethyl 3-(3dimenthyl aminopropyl)carbodiimide]

0.064 g NHS [N-Hydroxysuccinimide]

SOLUTIONS

2X Solution: 0.276g EDAC , (Catalog # E-7550, Sigma-Aldrich, St. Louis, MO)

0.064g NHS (Catalog # H-7377, Sigma-Aldrich)

5 mL distilled, deionized H_2O (ddH_2O)

PROCEDURE

1. Sterile filter EDAC solution using 0.2 mm filter (Cat. # 4192, Pall Gelman, Ann Arbor, MI) attached to a 10 mL syringe.

2. Incubate collagen materials in 5 mL sterile ddH_2O for 15 min to hydrate the material.

3. Add 5 mL 2X EDAC solution and incubate for 3.5 hours at room temperature.

4. Rinse matrix 1X in sterile PBS (Cat # P-2813, Sigma Aldrich) and incubate in fresh, sterile PBS for three hours at room temperature.

5. Rinse matrix twice in sterile ddH_2O.

Note: EDAC is hazardous waste and must be disposed of using appropriate waste bottle in fume hood. Handle EDAC in fume hood only.

B.3 *In Vitro* Characterization of Collagen Tubes

PRINCIPLE:
Collagen + H2O Collagenase> Peptides
CONDITIONS: T = 37°C, pH = 7.4, A570nm, Light path = 1 cm
METHOD: Colorimetric

REAGENTS:

A. 50 mM TES Buffer with 0.36 mM Calcium Chloride, pH 7.4 at 37°C (Prepare 1000 ml in deionized water using TES Free Acid, Sigma Prod. No. T-1375, and Calcium Chloride, Dihydrate, Sigma Prod. No. C-3881. Adjust the pH to 7.4 at 37°C with 1 M NaOH.)

B. Collagen Type I (Use Collagen, Type I, Sigma Prod. No. C-9879. Different lots of collagen will produce varying amounts of enzyme activity when used as a substrate for collagenase.)

C. Collagenase Enzyme Solution (Immediately before use, prepare a solution containing 0.05 - 0.1 mg/ml Collagenase in Buffer A.)

D. Ethylene Glycol Monoethyl Ether (Use Ethylene Glycol Monoethyl Ether, Sigma Prod. No. E-2632.)

E. 4% (w/v) Ninhydrin Solution (Prepare 100 ml in Reagent D, using Ninhydrin, Sigma Prod. No. N-4876.)

F. 200 mM Citrate Buffer with 0.16% (w/v) Stannous Chloride, pH 5.0 at 25°C (Prepare 100 ml in deionized water using Citric Acid, Free Acid, Anhydrous, Sigma Prod. No. C-0759. Adjust to pH 5.0 at 25°C with 5 M NaOH; then add the Stannous Chloride, Anhydrous, Sigma Prod. No. S-2752.)

G. 50% (v/v) Isopropanol Solution (Isopropanol)
(Prepare 100 ml in deionized water using Isopropanol, Anhydrous, Sigma Stock No. 405-7.)
H. Ninhydrin Color Reagent (NCR) (Immediately before use, combine equal volumes of Reagent E and Reagent F.)
I. 10 mM Hydrochloric Acid Solution (Prepare 50 ml in deionized water using Hydrochloric Acid, Sigma Prod. No. H-7020.)
K. 4.0 mM L-Leucine Standard Solution (Std Soln) (Prepare 20 ml in Reagent I using L-Leucine, Sigma Prod. No. L-8000. **PREPARE FRESH**.)

PROCEDURE:
1. Weigh the following reagent into suitable containers:
Reagent B (Collagen) TEST: 25.00 mg BLANK: 25.00 mg

2. Then add (in milliliters) the following reagent:
Reagent A (Buffer) TEST: 5.00 mL, BLANK: 5.00 mL

3. Incubate the vials at 37°C until equilibrated. Then add:

Reagent A (Buffer) TEST: 0.00 mL, BLANK: 0.10 mL
Reagent C (Enzyme Solution): TEST: 0.10 mL, BLANK 0.0 mL

4. Mix well and incubate at 37°C. Swirl the containers for 10 - 15 seconds at 0.5 and 1.5 hours. After 2 hours, filter the contents of the containers through a Whatman #54 filter paper or a syringe filter into clean containers. Use the filtrates for color development.

COLOR DEVELOPMENT:

5. Standard Curve: Prepare a standard curve by pipetting the following reagents (in milliliters) into suitable containers.

	Std 1	Std 2	Std 3	Std 4	Std Blank
Rgnt K (Std Soln)	0.05	0.10	0.15	.20	0.00
Deionized Water	0.15	0.10	0.05	0.00	0.20
Reagent H (NCR)	2.00	2.00	2.00	2.00	2.00

Sample:

Pipette (in milliliters) the following reagents into suitable containers:

	Test	Blank
Test Filtrate	0.20	-----
Blank Filtrate	-----	0.20
Reagent H (NCR)	2.00	2.00

6. Mix well and place vented caps on each container. Place the containers in a boiling water bath for 30 minutes.

7. Remove the containers and allow to cool to room temperature. Add 10 ml of Reagent G (Isopropanol) to each container. Mix well and transfer the container contents to suitable cuvettes.

8. Determine the absorbance at 570 nm for each of the containers using a suitable spectrophotometer.

CALCULATIONS:

Standard Curve: ÄA570nm Standard = A570nm Standard - A570nm Standard Blank

Prepare a standard curve by plotting the ÄA570nm of the L-Leucine Standard Solution versus micromoles of L-Leucine.

Sample Determination: ÄA570nm Sample = A570nm Test - A570nm Test Blank

CALCULATIONS: (continued) Determine the ìmoles of L-Leucine equivalents liberated using the Standard curve.

REFERENCES: Moore, S. and Stein, W.H. (1948) *J. Biol. Chem.* **176**, 367-388

Mandl, I., MacLennan, J.D., Howes, E.L., DeBellis, R.H., and Sohler, A. (1953) *Journal of Clinical Investigation* **32**, 1323-1329

B.4. Animal Surgery

Adapted from Harley, 2004; Spilker 2000

SUPPLIES

1. Order animals: Adult, female Lewis rats, 150 - 175 grams, from Charles River Laboratories. Animals must arrive at least one week in advance of surgery to reduce the stress placed on the animal due to travel.

2. Sterilize the necessary items:

1 metal bowl gauze
1 surgical blade holder
1 micro-needle holder
1 micro-scissors
2 jewelers forceps
1 large forceps

3. Ready other sterile items:

1 large scissors 1 surgical (tenotomy) scissors
2 paper clip retractors 2 forceps
1 needle holder animal skin staples wooden rods (cotton swabs)
sterile table covering scalpel blades (4 #15 blade, 1 # 11 blade)
1 bottle of PBS iodine sponge sterile draping Implants)
1 bottle pentobarbital (Nembutal Sodium Solution), 50mglml
sterile pen
10-0 sutures (Ethicon)
4-0 sutures
1 ml syringes
1 bottle Lidocaine, 1%

4. Ready other non-sterile items:

surgical board
4 rubber bands
rat ear tagging tool
numbered ear tags
microsurgery glasses (loops)
hair clippers

PROCEDURE

1. Weigh animal on an appropriately sized balance. Record the weight and determine anesthetic dosage based on the pre-operative weight.

2. Anesthetize animal with injection of sodium pentobarbital (50 mg of solution per kg of animal). Allow 10-15 minutes for anesthesia to take effect. Each animal reacts differently to the anesthetic and in some cases, more time may be required.

3. Meanwhile, arrangethe surgical area so that the table is at a comfortable level for the surgeon, and the tools are conveniently located.

4. The surgeon should be sterilely dressed in scrub shirt and pants, hat and mask.

5. When ready, shave the animal using the animal hair clippers from the base of the tail up to the middle of the back. The leg receiving the prosthesis should be shaved carefully and completely.

6. Place the animal on the surgical board in the prone position and secure the fore and hind limbs to the board using rubber bands. The hind legs should be in 30" abduction. Place a piece of gauze under the appropriate thigh to elevate the leg slightly.

7. Clean the shaved portion of the animal vigorously with the iodine sponge to disinfect the area. At this point, the surgeon should put on the sterile gloves and remain sterile for the rest of the procedure. Cut a hole in the sterile draping small enough so that only

the leg is exposed. Place the draping over the animal.

8. Using the #15 scalpel, make a 4 cm incision along the leg of the animal. Separate the skin from the muscle along the incision by cutting through the connective tissue with the surgical scissors.

9. Using the surgical scissors, separate the muscles until the sciatic nerve is visible. Carefully cut back the muscle along the skin incision line exposing the sciatic nerve.

10.Place the paper clip retractors inside the muscle to separate the wound edges. Anesthetize the nerve by placing a few drops of Lidocaine directly on the area. Cut away the fascia surrounding the sciatic nerve carefully so that the nerve is free from constraint.

11. Transect the nerve midway between the proximal nerve trunk and the distal bifurcation using microscissors. Measure the prosthesis and make a mark 3 mm in on each end. Place the tube in the gap and insert the proximal nerve stump 3 mm into the tube end, as marked. Secure the nerve in place by using two 10-0 sutures which travel through the epineuriwn and then through the tube. Tie the sutures with four single knots. Insert the distal nerve end 3 mm into the other end of the tube and secure in the same manner.

12. In the case of the cross-anastomosis procedure, the sciatic nerve in the opposite hind limb is similarly exposed and transected. The two skin incisions are then joined across the rat's back using a scalpel blade.

13. The dorsal spinous processes are removed using bone rongeurs to create a trough to make space for the tube implant to be routed over the back.

14. The proximal left sciatic nerve stump is bridged to the distal right nerve stump with a tube implant over the back.

15. For both single-leg and cross-anastomosis procedures, the paper clip retractors are removed. Close the muscle using three 4-0 sutures. Close the skin using two 4-0

sutures and three skin staples.

16. Place the animals back in the cage, fit with O_2 mask, inject with 1 cc Ringer's lactated solution to hydrate (can repeat as needed) and observe frequently until they wake up.

B.5 Post-Operative Care and Supervision Protocol

Adapted from Harley, 2002

SUPPLIES

Ketofen, 0.15 mg/mL
Cefazolin, 100 mg/mL
1 mL TB Syringes

PROCEDURE

adapted from Spilker, 2000; Harley, 2002

1. Monitor rats immediately following surgery. Analgesic is to be started immediately following surgery while the rat is still under anesthesia. Inject 0.1 mL of 0.15 mg/mL Ketofen and 0.1 mL of 100 mg/mL Cefazolin subcutaneously every 24 hours for the next 72 hours. For hydration, make a one-time injection of 1 mL sterile Lactated Ringer's solution immediately following surgery.

2. Place rats into individual cages following surgery. Place food onto floor of cage for the rat immediately following surgery.

3. Continue to monitor eating and drinking and general condition of animals.

B.6 Animal Sacrifice and Tissue Processing Protocol

Adapted from Harley, 2004

EQUIPMENT

Surgical instruments 15-ml Falcon tubes (1 for each animal)
Digital camera to take gross photographs Container with ice
Insulated Container with liquid nitrogen
Rectangular R-40 Peel-A-Way(Embedding Molds (PolySciences, Inc., Warrington, PA)
Optimal Cutting Temperature (OCT) Embedding medium
Tissue marker
Freezer packs
Portable Cooler
Microforceps

SOLUTIONS

Yanoff s Fixative

Stock Solutions

Stock A:

1.67 grams Monobasic Sodium Phosphate NaH,PO,
8.95 grams Dibasic Sodium Phosphate Na,HP04
960 ml Distilled H,O
40 ml25% Glutaraldehyde

Stock B:

4.0 grams Monobasic Sodium Phosphate NaH,P04
8.95 grams Dibasic Sodium Phosphate Na_2HPO_4
900 ml Distilled H,O
100 ml 38-40% Formaldehyde

Yannoff's fixative is a 1:1 mixture of stock A and stock B.

10% Neutral Buffered Formalin

Stock B of Yanoff s Fixative is 10%Neutral Buffered Formalin.

70% EtOH

4% paraformaldehyde

Sterile PBS

30% Sucrose (0.1M sodium phosphate buffered saline)

SACRIFICE PROCEDURE

1. Sacrifice animals by placing in carbon dioxide chamber for 3-5 minutes.

2. Open the original wound with a #15 scalpel blade. The wound can be located by identifying the dermal scar or original suture marks.

3. Open the fascia and muscle to locate the tube implant and the adjacent nerve stumps.

4.Remove the entire tube implant as well as at least 10 mm of proximal and distal nerve tissue including the nerve branches at the distal end.

5. For frozen sections and immunofluorescence (chapter 2 study), cut explant in half at midpoint using # 15 scalpel. Immediately place proximal portion in 4% paraformaldehyde on ice and continue protocol with Tissue Processing Procedure (Frozen). Use distal portion for Tissue Processing (Epon or Paraffin).

TISSUE PROCESSING PROCEDURE (Epon or paraffin)

1. Place tissue into Yanoff s fixative for 24 hours at 4 deg.C.

2. Transfer tissue into 10% neutral buffered formalin solution for 24 hours at **4'C.**

3. Remove tissue from formalin and rinse 1 x in 70% EtOH.

4. Photograph the nerve to capture the gross morphology of the tissue.

5. Section the nerve into 2 mm segments.

6. Place each small nerve segment into an individual vial containing 70% EtOH. Each tissue segment will be either embedded in Epon or stored in 70% EtOH for future use.

TISSUE PROCESSING & EMBEDDING PROCEDURE (Frozen)

1. Place proximal portion of regenerate in 4% paraformaldehyde (in 0.1 M sodium phosphate buffered saline) on gentle shaker at 4 deg. C for 8 hours

2. Rinse twice in sterile PBS and place in 30% sterile-filtered sucrose solution (in 0.1 M sodium phosphate buffered saline) overnight on gentle shaker at 4 deg. C to cryoprotect.

3. The next morning, fill labeled cryomold halfway with Optimal Cutting Temperature (OCT) polymer (Electron Microscopy Sciences), gently blot cryoprotected nerve on sterile gauze to remove excess fluid and using microforceps immerse into mold with long axis of nerve perpendicular to mold face. Hold in place while filling mold with excess OCT.

4. Using forceps grip mold by edge and slowly lower into liquid N_2, be careful not to let N_2 get into mold. Wear eye protection and cryogloves.

5. When OCT has completely frozen, place mold on dry ice and continue with remaining regenerates. Store in -80 deg. C until ready for sectioning.

B.7 Epon Embedding Protocol

Adapted from Harley 2004, Spilker 2000

Cacodylate Buffer (pH 7.4)

Stock Solutions:

Stock A (0.2 M Sodium Cacodylate - mw 214):

4.28 grams Sodium Cacodylate 100 ml of Distilled Water

1.7 ml HC1 100 ml of Distilled Water

Stock B (0.2 M HC1- mw 36.46):

1.7 ml HC1

100 ml of Distilled Water

Composition of Buffer:

25 ml of Stock A + 1.4 ml of Stock B (for pH 7.4)* + 73.6 mL Distilled Water

*=Volume of Stock B changes for different pH levels

Final Molar Composition of Buffer:

0.05 M Sodium Cacodylate 0.0028 M HCl

Cacodylate Buffered Glutaraldehyde

2% Solution:

8 ml25% Glutaraldehyde

92 ml Cacodylate Buffer (pH 7.4)

Cacodylate Buffered Sucrose Solution

0.2 M Solution:

6.846 grams Sucrose - mw 342.3

100 ml Distilled Water

Osmium Tetroxide (CatalogNo. 251755, Sigma-Aldrich, St. Louis, MO)

1% Solution:

2 mL 4% Osmium Tetroxide

6 ml Distilled Water

Poly/Bed 812 Embedding Kit (Catalog No. 08792, Polysciences, Inc., Warrington, PA)

Half Portion:

	Catalog #	Standard Formula	Slightly Harder
Poly/Bed 812	08791	24 ml	23.5 ml
DDSA	00563	15.5 ml	14.3 ml
NMA	00886	10.5 ml	12.0 ml
DMP-30*	00553	1.0 ml	1.0 ml

DMP-30* : hardener coml onent. Added just before use in final stages (step 9 and 10) only,

not for initial infiltration stages.

EMBEDDING PROCEDURE

1. Soak nerves in 2% cacodylate buffered glutaraldehyde overnight at **4OC.**
2. Soak nerves in 0.2 M cacodylate buffered sucrose solution overnight at 4OC.
3. Rinse nerve 1 time in cacodylate buffer for 10 minutes at 4OC.
4. Fix in 1% osmium tetroxide for two hours at room temperature (in the hood).
5. Dehydrate nerves in EtOH:

30% 5 minutes

50% 5 minutes

70% 5 minutes

80% 5 minutes

90% 7 minutes

95% 10 minutes

100% 10 minutes

100% 10 minutes

100% 10 minutes

6. Clear nerves in acetonitrile 2 times, 5 minutes for first exposure, 10 minutes for second. BEWARE: Use fresh acetonitrile for procedure. Acetonitrile tends to pick up water overtime, resulting in the formation of micro-pockets of water along surface of nerve, impeding Epon infiltration.

7. Infiltrate in 1:1 acetone/Epon* mixture overnight at room temperature

8. Place extra Epon at 4degC overnight for storage and reuse for Step 8 only. Remove Epon from refrigerator and warm in hands before opening to minimize potential condensation problems leading to addition of water to the Epon. Remake Epon for Steps 9 and 10 with the hardener.

9. Infiltrate in 1:3 acetone/Epon* mixture for 5 hours at room temperature.

10. Infiltrate in 100%Epon with hardener overnight at rom temperature.

11. Embed with fresh 100% Epon with hardener in TEM molds. Make all labels on computer.

12. Let cure 24 hours at 60°C in vacuum oven (standard pressure). * = During infiltration, the Epon mixture should NOT contain the hardener.

B.8 Paraffin Embedding Protocol

Adapted from Chamberlain, 1998, Miu, 2008

Materials

Specimen Containers (Cat. No. 17000, Kendall)
TRUFLOW Tissue Cassettes (Cat. No. 15-200-403E, Fisher Scientific)
Biopsy Foam Pads (Cat. No. 22038221, Fisher Scientific)
Microscope Slides (Superfrost Gold Plus, 15-188-48, Fisher Scientific)
Ethyl Alcohol EtOH (Histoprep)
Xylene (Histoprep)
Paraffin (Cat. No. 23-021-401, Fisher Scientific)

Equipment

Tissue Processor (TP1020, Leica)
Embedding Center (Shandon Histocentre 2, Thermo Fisher Scientific, Inc.)

PROCEDURE

1. Put nerves in tissue cassettes, sandwiched by two biopsy foam pads, and label the cassettes with sample information, date, and investigator name in pencil. Keep the tissue cassettes in 70% EtOH.

2. Dehydrate and paraffinize nerves by placing the cassettes into the tissue processor with the following program:

Reagent	Vacuum	Duration (min)	Temperature
EtOH, 70%	No	10	RT
EtOH, 80%	No	90	RT
EtOH, 95%	No	90	RT
EtOH, 95%	No	90	RT
EtOH, 100%	No	90	RT
EtOH, 100%	No	90	RT
EtOH, 100%	Yes	90	RT
Xylene	No	90	RT
Xylene	No	90	RT
Xylene	No	90	RT
Paraffin	Yes	180	58°C
Paraffin	Yes	180	58°C

3. Remove cassettes from tissue processor and place them in warm paraffin in paraffin machine.

4. Remove tissues from cassettes and section tissue in five 3-4 mm segments (record stump location and lengths of segments).

5. Place segment distal end down in embedding mold such that cross-sectional sections will be later made with the microtome. Embed segment in paraffin. On top of the warm paraffin, quickly add the cassette with the sample information written on it. Add more warm paraffin on top of the cassette so that it will be attached to the sample.

6. Cool embedded segment on cold plate for an hour before moving to -20°C freezer. After at least 24 hours, pop the paraffin-embedded sample from the mold. Remove any excess paraffin from the cassette and return to -20°C freezer.

SECTIONING

7. Section paraffin embedded sample with a microtome at 6um slices. Make a ribbon of several sections.

8. Place ribbon of sections on surface of water bath. Separate sections in duplicates or triplicates. Position microscope slide underneath the sections and retrieve the sections using a pencil as a guide.

9. Shake off excess water from the microscope slide. Let air dry for 1 hour.

10. Transfer slide to slide warmer for 1 hour. Store in slide box.

B.9 Toluidine Blue Staining

Adapted from Harley 2002

SOLUTIONS

Toluidine Blue Solution (Cat. No. BP107-10, Fisher Scientific, Boston, MA)

1% Solution:

1 gram, Toluidine Blue Powder

1 gram, Sodium Borate Powder 100 ml, distilled, deionized water

Solution should be filtered and stored in a bottle

PROCEDURE

1. Have Epon blocks cut by Keck Microscopy Facility (Whitehead Institute) to 1-3 micron thickness.

2. Heat the epon semithin plastic sections on slides on the hot plate to 60 - 80°C (setting about 4.5 on blue VWR 320 plates).

3. Stain with Toluidine Blue Solution for 30 - 60 seconds. Thicker sections will take less time. Use a l0ml syringe (Cat. No. 309604, Becton Dickinson & Co., Franklin Lakes, NJ) with a 0.2pm Acrodisk filter (Cat. No. 4192, Pall Gelman Laboratories, Ann Arbor, MI) to deliver stain onto the slide.

4. Rinse slides in distilled water and allow to dry on hot plate for 2 - 3 minutes. Let slide cool

5. Mount slides using Permount mounting medium (Cat. No. SP15-100, Fisher Scientific, Boston, MA) and let dry overnight.

B.10 Immunostaining

B.10.1 Gomori Trichrome AB (Sigma Aldrich)

PROCEDURE:

1. Allow slides to air dry for 30 minutes before beginning.

2. 3 X 5 min TBS wash to remove OCT

3. Weigert's Iron Hematoxylin for 5 min.

4. Wash well in running tap water (10 min)

5. Gomori Trichrome Solution for 10 min

6. 0.5% Acetic Acid for 2 min to differentiate (2.5 ml glacial acetic acid in 500 mL ddH-2O)

7. 50% EtOH 1 X 3 min

8. 80% EtOH 1 X 3 min

9. 95% EtOH 2 X 3 min

10. 100% EtOH 2 X 3 min

11. Xylenes 2 X 3 min

12. Mount in Permount and coverslip.

B.10.2 Immunofluorescence (myelin, nuclei, F-actin)

REAGENTS:

DAPI: 5 mg/ml stock (14.2 mM) is made by dissolving DAPI in 2 mL H20, store at -20 deg.C

IF Working solution is made as follows:
15 μL rhodamine phalloidin (Invitrogen)
2 μL FluoroMyelin 488 (Invitrogen)
583 μL DAPI working solution (1 μL 5 mg/ml stock in 50 mL TBS)

PROCEDURE:

1. Allow slides to dry at room temperature for 30 min.

2. Rehydrate in TBST 2 X 10 min.

3. Outline sections in Immedge Pen (Vector Labs), forming hydrophobic barrier.

4. Turn off lights. Flood sections with IF working solution (use ~ 300 μL per slide) and incubate in the dark for 20 minutes.

5. Rinse 3 X 10 minutes in TBS solution.

6. Mount in FluoroGel (Vector Labs) and cover-slip.

7. Seal cover-slip with clear nail polish and store at 4 deg C protected from light.

B.10.3 α-smooth muscle actin (α-SMA) staining

Note: for frozen sections, the initial deparaffinization/rehydration steps are not required.

IHC Autostaining

As an internal control use at least 1 slide as a positive and negative control. This will ensure to asses the technical quality of the stain. Fix tissue as little as possible e.g 3h 4% paraformaldehyde.

SOLUTIONS:

Tris-Buffred Saline(TBS) Stored at RT in packets 1 package(Dako, S3001) to 1L dH2O. Stored at 4 deg.C in soln. 1 package (Dako, S1968) to 5L dH2O Used for Diluting the antibody/horse serum/ and rinsing the slides before putting them onto the autostainer

Wash Buffer with Tween 20 Stored at 4 deg. C (Dako Cytomation, S3006, 1000ml) 500ml of x10 in 4500ml dH2O Used for washing the slides in the Autostainer. If you do no t use wash buffer with Tween your slides will not get washed properly and will show a very high background stain.

0.1% (w/v) Protease XIV

10mg Protease (Sigma P5174) 10 ml TBS

Peroxidase Blocking Reagent

(Dako, S2001) Read-to-Use 11ml/vial

Primary Antibody (monoclonal mouse anti-alpha smooth muscle Actin) IgG2a, Clone (Sigma A5228) Use frozen Aliquots (10µl) and make a **1:400** dilution in 6ml Dako Universal AB Dilutent

Secondary reagent Stored at 4 deg C DakoCytomation LSAB2® System-HRP (K0675) Biotinylated Link, (Cocktail of Goat-anti mouse and Goat-anti Rabbit IgG) Yellow liquid, ready to use

Tertiary reagent

DakoCytomation LSAB2® System-HRP (K0675) Streptavidin-HRP Red liquid, ready to use

Substrate

AEC Substrate Chromogen (Dako, K3464) Ready to use

Counter stain

Mayer's Hematoxylin (Filter before use) (Sigma: MHS 16-500ML) Tap Water

Setting up the autostainer

1. Switch on computer

2. On the Desktop click on "DAKO Autostainer"

3. Login: Dong; password: Dong

4. Select "Program" on Main Menu

5. Click on "File", in the pull down menu click on "Open" and choose "Coll X temp"

6. The template will show you two slides: #1 for the positive Coll X- staining and #2 for the negative control stain

7. To ad slides click on " Slides" and type in the number of slides you want to stain including all controls.

8. Copy and past the staining protocol by first clicking on "copy" than on the slide you want

Single steps performed by autostainer

- Rinse (TBS+Tween)
- Add 0.1% Protease - 60 min.
- Rinse with (TBS+Tween)
- End. Enyme Block: H_2O_2 - Peroxidase blocking solution - 10 min.
- Rinse (TBS+Tween)
- Primary antibody or negative mouse control - 60 min
- Rinse (TBS+Tween)
- Second. Reagent: Biotinylated link + HRP - 15 min.
- Rinse (TBS+Tween)
- Tertiary Reagent: Streptavidin- HRP - 15 min.
- Rinse (TBS+Tween)
- Switch
- Substrate: AEC 10 – 10 min

9. Click on "Next"

The Program will now show the "Program Slides" Screen Standard setting will use 150µl per treated section of each slide. The standard setup of the machine will treat the lower 2/3 of the slide (marked yellow). If you want to change this:

10. Click on the slide while holding "ctrl" Or clicking on the slide in the top left corner. This will change all slides the same way.

11. Click on "Next"

The Program will show you how much Washing Buffer is needed to run the program. Check bottle in cupboard under Autostainer. If necessary make some new Wash Buffer, then click on "OK"

Solutions

The "Load Reagents" Screen will show amount and the location in rack #1 of any

reagent used in the protocol.

Pretreatment of the slides

14. Deparaffinize and rehydrate via the following

- Xylene(or substitute) 2×5 min
- 100% EtOH - 2×3 min
- 95% EtOH 2×2 min
- 80% EtOH 1 min
- TBS 2x2 min

15. Load slides on coverplate (Make sure to keep slides wet with TBS)

16. click on "Next" after loading slides

17. Click on Prime Pump (Buffer) and Prime Pump (Water) and check if it is really running!

18. Click on "Start Run"

Counter staining and Mounting

19. After running the program, immediately remove slides and put into TBS to keep wet

20. Counter-stain with Mayers Hematoxylin for 1.5 min

21. Rinse in running tap water for 3 min.

22. Transfer "Slideholder" into a container with tap water and immediately

23. Coverslip with Aqueous Mounting Media (Faramount, Dako S3025) **Don´t use** Cytoseal for mounting as this will take your AEC Staining of!

C.1 Procedures for Image Acquisition and Analysis

Adapted from Harley, 2000

SUPPLIES

100x Objective (Nikon E-800, Whitehead Keck Microscopy Center)
Immersion Oil (Nikon Immersion Oil, MVI, Inc, Avon, MA)
70% Ethanol

PROCEDURE

1. Bring the 100x objective, immersion oil, 70% ethanol,, and the sample slides to the Whitehead Keck Center (Nicki Watson)

2. Open OpenLab program on computer attached to the microscope.

3. Put the sample slide on microscope stage and focus with eyepiece. If the image is blurry, adjust the microscope focus until it becomes clear.

4. Pick a sample on the slide with the smallest number of wrinkles and tears and is vertically or horizontally oriented on the slide (the orientation will help in the later steps, but is not absolutely necessary). Circle the sample with a water resistant marker on the back of the slide.

5. Use the function keys and the up and down arrow keys on the keyboard to adjust the quality of the image such as sharpness, brightness and contrast. If the image is too bright decrease the light intensity on the microscope.

6. Take a low magnification image of the whole nerve trunk (usually at 4x or 10 x objective) in order to determine the fascicle area of the chosen sample. If the nerve cable is much larger than the fascicle, choose the highest magnification that includes all fascicles. However, if the nerve cable area is not significantly larger than the fascicle

area, incorporate the whole nerve cable in the image.

7. Click on capture to capture the image. The captured image is then shown on the computer screen.

8. Open ImageJ (NIH). Use the low magnification image taken in step 7 and the procedures in the Image Analysis protocol to determine the area of the fascicle. In some cases the boundary of the fascicle is readily visible from the image. For samples with more than one fascicle, each fascicle should be circled, and the sum total of all fascicles calculated.

9. Determine how many images are necessary to adequately sample the nerve (Table C. 1).

Fascicle Area Range [mm^2]	Fascicle Area Range [μm^2]	Number of Images Necessary	Image Area Divided by Total Fascicle Area
A < 0.25	A < 250,000	3	≥10%
0.25 < A < 0.4167	250,000 < A < 416,700	5	10% - 16%
0.4167 < A < 0.75	416,700 < A < 750,000	9	10% - 18%
0.75 < A < 1.08	750,000 < A < 1,080,000	13	10% - 14%
1.08 < A < 1.417	1,080,000 < A < 1,417,000	17	10% - 13%
1.417 < A < 1.75	1,417,000 < A < 1,750,000	21	10% - 12%
A > 1.75	A > 1,750,000	21	<10%

Table C.1 Number of images necessary to describe nerve trunks of different cross-sectional area. Capturing the appropriate number of images results in sampling of at least 10% of the total tissue area, except when the area is larger than 1.75 mm^2. If tissue filled the entire inside diameter of the implant tubes, the area would be 1.77 mm^2; therefore, in the majority of cases sampling is greater than 10%.

10. Place a drop of immersion oil on the slide above the selected section, then move the focus in and out a little so that the oil is completely spread between the lens and the sample. Position the sample so that the long axis of the nerve is along the Y-axis.

11. Divide the nerve into four quadrants (see Figure C.1). Count the number of full-

screen imagesfromthetop-centerofthenervetrunktothebottom-centerofthetrunk(Y-Length). Count the number of full-screen images from the left-center of the nerve trunk to the right-center (X-Length).

12. Begin imaging the cross-section using the chart in Figure C.1. as a guide. Begin with image 5, the geometric center of the image. Capture all images from Quadrant 1, and then Quadrant 2, etc. Use the values of X-Length and Y-Length calculated in Step 1 to locate the position for each image. For example, Image5is 1/2*(Y-Length) down from the top-center or 1/2*(X-Length) to the right of the left-center of the nerve trunk; Image 11 is 1/4*(Y-Length) down from the top- center and 1/4 *(X-Length) to the left.

13. Capture the appropriate number of images. Refer to Table C.2. to determine images to be taken and Figure C .1. to determine the location of images.

Number of Images to be Taken	Image Location
1	5
3	5, 11, 41
5	5, 11, 21, 31, 41
9	5, 11, 12, 21, 22, 31, 32, 41, 42
13	5, 11, 12, 13, 21, 22, 23, 31, 32, 33, 41, 42, 43
17	5, 11, 12, 13, 14, 21, 22, 23, 24, 31, 32, 33, 34, 41, 42, 43, 44
21	5, 11, 12, 13, 14, 15, 21, 22, 23, 24, 25, 31, 32, 33, 34, 35, 41, 42, 43, 44, 45

Table C.2. Images to be taken for each combination of number of required images.

14. When more than one fascicle is present in the nerve, divide the quadrants between the fascicles in proportion to the area of each fascicle. Redistribute the image capturing to reflect the fasciclular size and orientation.

15. Clean the emergent oil on the **100x** objective and the sample slide using 70% ethanol. Return the objective and the emergent oil to 3-333.

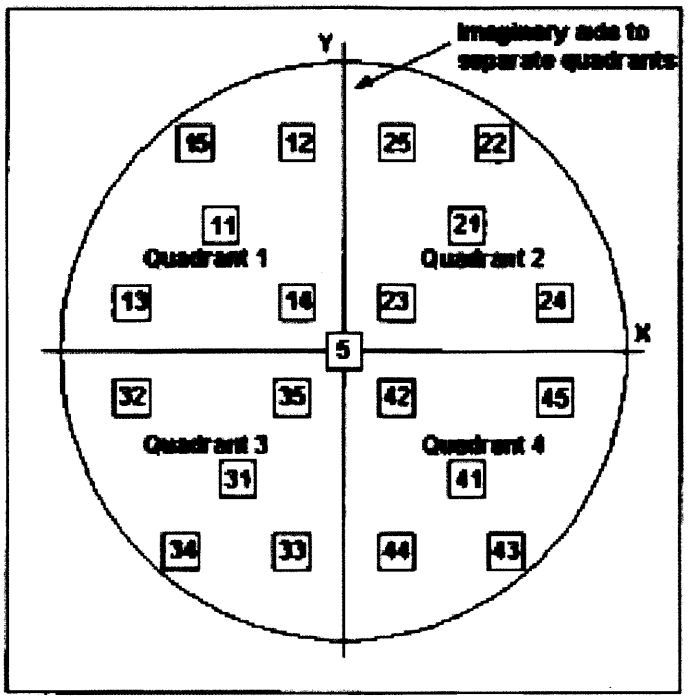

Figure C.1. Schematic showing the location of images around the nerve section

PROCEDURE

1. Open ImageJ.

2. Open image file.

3. Go to the ***Analyze*** menu and select ***SetScale.*** Select the appropriate unit of measure for the magnification of the image ***(i.e.,*** millimeters for low magnification images and micrometers for high magnification images).

4. Use ***Smooth*** andlor ***Sharpen*** from the ***Enhance*** menu to improve the quality of the image if needed. If you do not like the effect of these, choose ***Undo*** from the ***Edit*** menu before doing anything else.

5.From the ***Enhance*** menu, choose ***Arithmetic, Subtract.*** Subtract ***3.*** 6.From the ***Options*** menu, select ***Threshold.*** Threshold all the way to black so that no red is

showing in the image.

6. Select the pencil from the toolbar. Move the cursor over the red portion of the color scale and choose red as the color. (The paintbrush will appear red when the appropriate color has been selected).

8. Circle the axons with the pencil on the OUTSIDE perimeter of the myelin sheath.

9. When all axons have been circled, go to the ***Analyze*** menu and select ***Set Measurements.*** Choose ***Area, Perirneter, Length, Include Interior Holes,*** and ***Show Outlines.***

10. Save the image **as** an edited file.
11. In the ***Analyze*** menu choose ***Analyze Particles.*** Enter the following: Minimum particle size: 1 micron Ignore particles touching edge, Include Interior Holes, Reset Measurement Counter

12. Each axon will become darkened and numbered as it is counted. Make sure that all axons are filled in. If an axon is not darkened, part of the perimeter is not complete, therefore, it has been measured inappropriately. Fix and repeat step 11.

13. Choose Show ***Results*** from the ***Analyze*** menu. Copy the results (keystroke: Control-C) and paste them directly into Excel for analysis (keystroke: Control-V).

14. Close the image. Do not save the changes to your edited file.

Nerve Data Analysis Protocol

Adapted from Chamberlain 1998, Harley 2000

The following is a stepwise procedure for analyzing the data obtained via image analysis. The protocol for obtaining images and the basic image analysis technique was outlined in section C.7. This section details how the numerical values were calculated from the raw data.

1. Measure the tissue area *(A)* and capture the appropriate number of images as described.

2. Use image analysis program (NIH ImageJ) to count the number of myelinated axons per image and measure the diameters. For each axon, the program will determine the area of the axon and the perimeter. Paste the raw data for all of the axons into a Microsoft Excel spreadsheet (as described).

3. Calculate the diameter of each myelinated fiber using the following formula:

$$D=P/\pi$$

where D is the fiber diameter and P is the perimeter.

4.Calculate a diameter histogram for the axons of each image using Microsoft Excel. Highlight the column containing the fiber diameters. Select *DataAnalysis* from the *Tools* menu. Select *Histogram* from the list of data analysis tools. Enter the *Input Range, Bin Range, and Output Range.* The *Bin Range* should be a separate column from the data and should contain integers from 1-12. Excel will output the number of axons in each diameter bin in the *Output Range* location.

5. Repeat steps 2 through 4 for all images captured for the nerve (from **3** - 2 1 images).
6. Once **all** images have been analyzed, calculate the myelinated axon density using the following

formula:

$$AxonDensity = \frac{\sum_{i=1}^{N} (\#axons)_i}{N * Area_{Image}}$$

where *N* is the total number of images, *(#axons)*, is the number of axons in image i, and *Area* is the area of each digitized image.

7. Calculate the total number of myelinated axons per nerve using the following formula:

$$\frac{Axons}{Nerve} = AxonDensity * A_{Tissue}$$

where AxonDensity is as calculated in step 6 and Atissue is the total tissue area measured in step 1

8. Determine the percentage of axons in the 12 size bins using the following formula for each bin:

$$Perventage_x = \frac{\sum_{i=1}^{N} (\#axons_x)_i}{\frac{Axons}{Nerve}}$$

where (#axonsx)I is the number of axons in size bin X for image I, N is the total number of images and Axons/Nerve is as calculated in step 7.

9. Calculate the total number of large diameter myelinated fibers (D $\geq$ 6 microns) using the following formula:

$$\frac{LgAxons}{Nerve} = \left(\sum_{x=6}^{12+} Percentage_x \right) * \frac{Axons}{Nerve}$$

10. To calculate a diameter distribution, multiply each Percentagex by the Axons/Nerve to obtain values for each bin.

11. Measurements of contractile capsule thickness are made at 5 locations around the perimetry of the nerve, perpendicular to the circumference. These values are averaged and reported as a mean for each slide.